Results in Chemistry 27 (2026) 103414

Contents lists available at ScienceDirect

Results in Chemistry

journal homepage: www.sciencedirect.com/journal/results-in-chemistry

Broad-spectrum antiviral activity of benzothiazole-acrylamide hybrids against Zika, Dengue, Chikungunya, and Sindbis viruses

Wadja Feitosa dos Santos Silva [a,1], Shweta Choudhary [b,1], Isadora Hart Cavalcante [c,1], Tanuj Handa [b,1], Leandro Rocha Silva [a], Manuele Figueiredo da Silva [a], Mirely Vitória Farias da Silva [a], Rayane Martins Botelho [c], Peng Zhan [d], Franciso Jaime Bezerra Mendonça-Junior [e], João Xavier Araújo-Júnior [a,f], Tanja Schirmeister [g], Alexandre Urban Borbely [c,*], Shailly Tomar [b,*], Edeildo Ferreira da Silva-Júnior [a,*]

[a] Research Group on Biological and Molecular Chemistry, Institute of Chemistry and Biotechnology, Federal University of Alagoas, Lourival Melo Mota Avenue, AC. Simões Campus, 57072-970, Alagoas, Maceió, Brazil
[b] Department of Biosciences and Bioengineering, Indian Institute of Technology Roorkee, Roorkee 247667, Uttarakhand, India
[c] Cell Biology Laboratory, Institute of Health and Biological Sciences, Federal University of Alagoas, Maceio, Brazil
[d] Key Laboratory of Chemical Biology, Department of Medicinal Chemistry, Ministry of Education, School of Pharmaceutical Sciences, Shandong University, 44 West Culture Road, 250012 Jinan, Shandong, PR China
[e] Laboratory of Synthesis and Drug Delivery, Department of Biological Sciences, State University of Paraíba, João Pessoa 58071-160, Brazil
[f] Laboratory of Medicinal Chemistry, Institute of Pharmaceutical Sciences, Federal University of Alagoas, Lourival Melo Mota Avenue, AC. Simões campus, 57072-970, Alagoas, Maceió, Brazil
[g] Institute for Pharmaceutical and Biomedical Sciences, Johannes Gutenberg-University, Staudinger Weg5, 55128 Mainz, Germany

ARTICLE INFO

Keywords:
Benzothiazole–acrylamide hybrids
Pan-antiviral agents
Zika virus
Chikungunya virus
Dengue virus
Sindbis virus
Arboviruses
Medicinal chemistry

ABSTRACT

Arboviral infections such as those caused by Zika (ZIKV), Dengue (DENV), Chikungunya (CHIKV), and Sindbis (SINV) viruses remain major global health concerns, aggravated by the absence of specific antiviral therapies. Given the overlapping endemicity and co-circulation of these pathogens, the development of pan-antiviral agents capable of simultaneously inhibiting multiple arboviruses is a pressing need. In this study, we report the rational design, synthesis, and biological evaluation of novel benzothiazole–acrylamide hybrid compounds with pharmacophores targeting both Flavivirus and Alphavirus proteases. The designed hybrids were synthesized *via* a pharmacophore-hybridization strategy combining benzothiazole and acrylamide scaffolds previously associated with anti-ZIKV/DENV and anti-CHIKV activities. Enzymatic assays revealed selective allosteric inhibition of ZIKV NS2B/NS3 protease (IC_{50} values down to 13.6 μM), with negligible effects against the homologous DENV2 enzyme. The most promising compounds exhibited submicromolar antiviral potency in plaque-reduction assays against ZIKV, CHIKV, and SINV, achieving EC_{50} values below 1.9 μM and selectivity indices above 16. Notably, compound **LQM560** demonstrated robust and balanced activity against all three viruses, as confirmed by qRT-PCR and immunofluorescence analyses, highlighting its pan-antiviral profile. Mechanistic assays indicated an allosteric mode of inhibition toward ZIKV protease, while CHIKV suppression likely involves interference with early replication stages rather than nsP2 protease inhibition. Molecular dynamics and MM/GBSA analyses supported the stability of ligand–NS2B/NS3 complexes, consistent with experimental findings. Overall, this work identifies benzothiazole–acrylamide hybrids as a new class of pan-antiviral small molecules, offering a promising chemical framework for broad-spectrum therapeutic development against emerging arboviruses of medical relevance.

* Corresponding authors.
E-mail addresses: alexandre.borbely@icbs.ufal.br (A.U. Borbely), shailly.tomar@bt.iitr.ac.in (S. Tomar), edeildo.junior@iqb.ufal.br (E.F. Silva-Júnior).
[1] The authors contributed equally.

https://doi.org/10.1016/j.rechem.2026.103414
Received 20 January 2026; Accepted 7 May 2026
Available online 10 May 2026

1. Introduction

Neglected tropical diseases (NTDs) are defined as a set of human infection diseases caused by viruses, bacteria, parasites or fungi, transmitted especially in tropical and subtropical regions/countries [1]. Amid the NTDs, arboviruses such as Dengue virus (DENV), Zika virus (ZIKV), Chikungunya virus (CHIKV), and Sindbis virus (SINV), which are transmitted by mosquitoes, are responsible for causing meaningful morbidity and mortality rates worldwide [1]. Since DENV first isolation, five different strains (DENV1–5) have been identified, antigenically and phylogenetically different from one other [2–5]. According to a report published by the Pan American Health Organization (PAHO), within the 30th epidemiological week of 2025, a total of 3,538,994 suspected DENV cases were recorded in the American continent, representing a cumulative incidence of 339 cases *per* 100,000 habitants [6]. Regarding the WHO estimation, 2.5 billion people were living in endemic areas, and 50 million of them were infected with DENV annually, resulting in 25,000 deaths. Significantly, the incidence rate increased 30-times in the past 50 years, with accelerated geographical expansion. In Americas, DENV incidence has increased 5-times in the last decade [7–9]. Regarding ZIKV, it became a major concern after 2015, when a big outbreak occurred in the Americas, leading to disturbing effects on pregnant women, as it was involved in stillbirth, abortions, and fetal neurodevelopmental alterations later characterized as the ZIKV Congenital Syndrome (ZCS). It has been declared a "*Public Health Emergency of International 2016*" by WHOA, and according to the PAHO, by the 30th epidemiological week of 2025, more than 19,000 probable cases of ZIKV have already been reported in the Americas [10]. In parallel, CHIKV, an Alphavirus belonging to *Togaviridae* family, is characterized by polyarthralgia, which may persist for years and significantly impair the life of the affected individual [11]. According to PAHO, by the 30th epidemiological week of 2025, more than 200,000 probable cases of CHIKV have already been reported in the Americas [12]. Additionally, the SINV also belongs to the *Togaviridae* family and is part of the Western equine encephalitis complex [13,14], causing debilitating and persistent arthralgia [15,16].

Many arboviral infections are frequently misdiagnosed due to the substantial overlap in their clinical signs and symptoms, which complicates accurate and timely identification. Thus, the development of novel therapeutics would be highly valuable, particularly in endemic regions where co-circulation of various arboviruses is common, and laboratory confirmation is often limited [17–19]. Then, the diagnostic challenge underscores the critical need for the development of broad-spectrum, or pan-antiviral, compounds that can target multiple arboviruses simultaneously. Both ZIKV and DENV have a single-stranded (+)-sense RNA genome, which synthesizes three structural proteins and seven non-structural (NS) proteins. Among the NS proteins, NS3 is a multidomain protein that requires a small hydrophilic proportion of NS2B protein as cofactor, which is a membrane-bound protein, and its *C*-terminal portion is responsible for increasing catalytic activity of the NS3 toward the substrate, creating one of the substrates binding pockets and stabilizing the NS3 structure. Without NS2B protein, the NS3

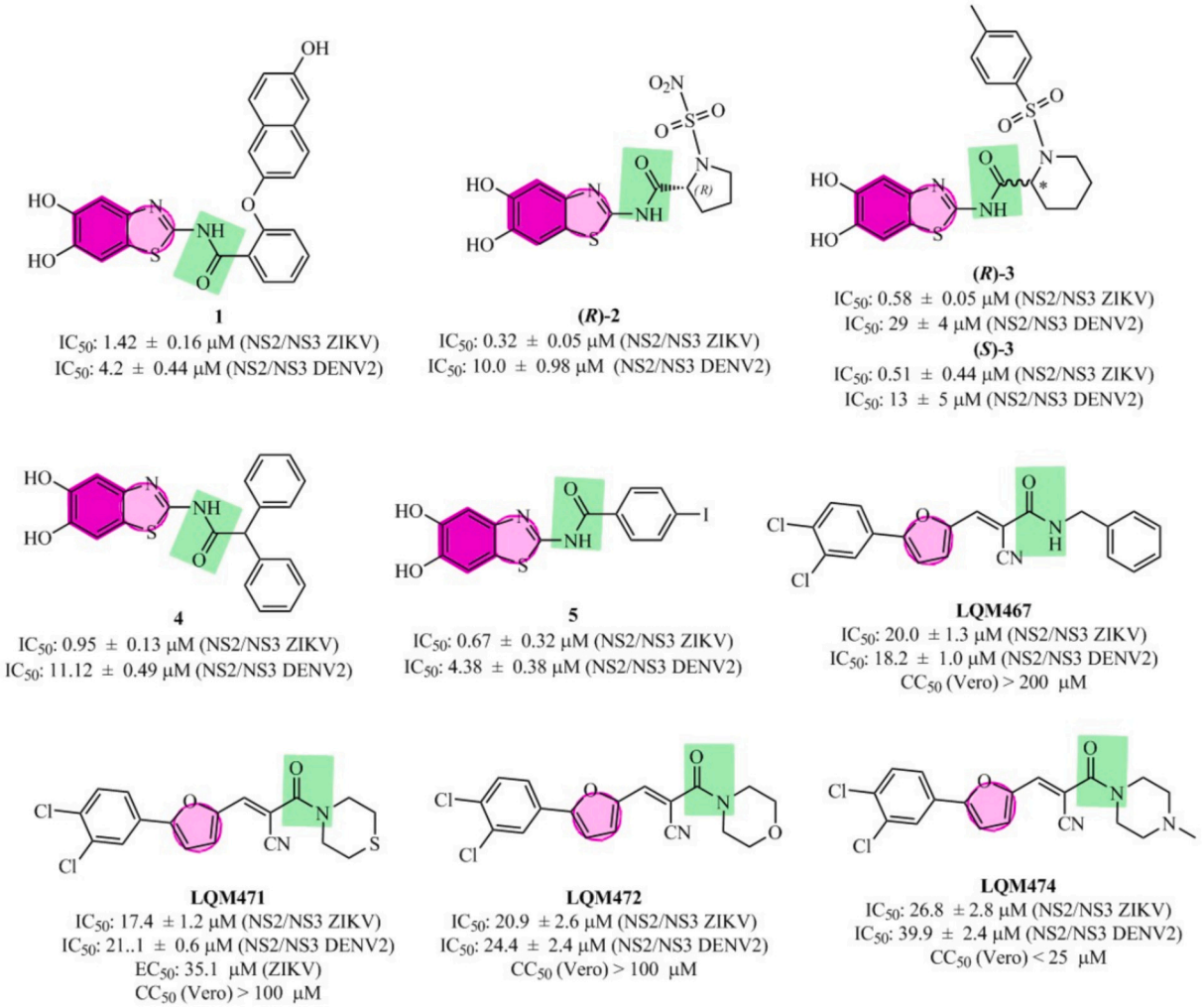

Fig. 1. Benzothiazole and cyanoacrylamide derivatives synthesized targeting NS2B/NS3 of Zika and Dengue type 2 viruses.

protease domain ($NS3^{pro}$) is inactive [20–23]. NS2B/NS3 proteases from DENV and ZIKV present high sequential (> 50% identity) and structural similarity [24]. Notwithstanding, NS2B/NS3 protease represents a promising antiviral target for developing novel drug candidates.

Our research team has devoted efforts focused on the medicinal chemistry of antivirals, including inhibitors targeting DENV2 and ZIKV NS2B/NS3 protease. We have published reviews focused on ZIKV and DENV NS5 (RNA-dependent RNA polymerase – RdRp) inhibitors [25], NS2B/NS3 inhibitors [26], including peptidomimetics [22,27], and other inhibitors targeting ZIKV [28]. Besides, we have developed several experimental studies aiming to obtain NS2B/NS3 inhibitors (Fig. 1). In this context, Wu et al. (2014) developed benzothiazole-based inhibitors of DENV2 NS2B/NS3 [29]. Compound **1** (Fig. 1), initially developed targeting DENV2 protease (IC_{50} = 4.2 ± 0.44 μM), was also active against the ZIKV protease (IC_{50} = 1.41 ± 0.16 μM), presenting a noncompetitive binding mode. However, compound **1** is poorly soluble in water due to be highly lipophilic nature [29]. Posteriorly, Millies et al. (2019) developed a series of proline-based allosteric inhibitors targeting ZIKV and DENV2 NS2B/NS3 [24]. From this work, we could identify stereoisomer compounds ***(R)*-2**, ***(R)*-3**, and ***(S)*-3** as the most potent nonpeptidic allosteric ZIKV protease inhibitors (Fig. 1). Additionally, our research team reported a series of Y-shaped and benzothiazole-based allosteric inhibitors (**4** and **5**) of NS2B/NS3 (Fig. 1), displaying submicromolar IC_{50} values [30], reported in the study performed by Maus et al. (2021). Furthermore, our research team recently demonstrated that cyanoacrylamide derivatives (**LQM467**, **471**, **472**, and **474**) could be promising inhibitors of ZIKV and DENV2 NS2B/NS3 proteases and also against ZIKV-infected cells (Fig. 1), as reported by Vilela et al. [31].

CHIKV is a positive-sense single-stranded RNA virus that contains two open-reading frames (ORFs), responsible for encoding structural and non-structural (NS) proteins. Among the structural proteins of CHIKV are E1, 6 K, E2, E3, and C, which are encoded by ORF2 at the 3′ end. On the other hand, NS proteins include nsP1, nsP2, nsP3, and nsP4, which are encoded by ORF1 at the 5′ end [32]. Among the NS proteins, nsP2 has been reported as a strategic target for the development of new therapies for this virus [33–36], as this protein is essential for viral replication, being associated with the processing of the P1234 polyprotein and having functions such as RNA helicase, RNA triphosphatase (RTPase), and nucleoside triphosphatase (NTPase) [37–40]. Similarly, SINV nsP2 is considered a key determinant of viral pathogenesis. In the SINV, this protease exerts a negative regulation on the cell response induced by infection, inhibiting the transcription of host messenger and ribosomal RNAs and, consequently, preventing the activation of genes involved in the antiviral response [41]. In this context, our research team has also devoted efforts in the development of small molecules targeting CHIKV and SINV. Initially, we synthesized acrylamides targeting CHIKV, in which we identified a 3-chlorophenyl derivative (**LQM334**) as a potential entry inhibitor (Fig. 2), probably by interacting with the E3-E2-E1 glycoprotein complex. This compounds was capable of reducing CHIKV-positive cells, 48 h post-treatment on intracellular flow cytometry staining [42]. Posteriorly, we continued to investigate this same chemical class of compounds, and then we identified four acrylamides (**LQM330**, **333**, **336**, and **338**) as potent and competitive inhibitors of CHIKV nsP2 protease, displaying IC_{50} values ranging from 20 to 0.95 μM, in which the best compound exhibited a selectivity index (SI) higher than 30 (Fig. 2). Furthermore, these compounds also demonstrated activity against SINV-infected cells, with EC_{50} values varying from 0.95 to 73.08 μM.

In the present study, we report benzothiazole-acrylamide hybrid compounds targeting ZIKV, DENV2, CHIKV, and SINV. In this context, the best compounds were investigated for cytotoxicity, protease inhibition capability, antiviral plaque reduction, viral load by RT-qPCR, immunofluorescence, isothermal titration calorimetry (ITC) as biophysical analysis; as well as, *in silico* approaches, such as molecular dynamics (MD) simulations and molecular mechanics with generalized Born surface area (MM/GBSA) calculations. Finally, we identified hybrid compounds that have pan-antiviral effects, and that could be further improved to become even more promising against these threatening arboviruses.

2. Results and discussions

2.1. Study concept and workflow

Notwithstanding that our research team has recently identified benzothiazoles and acrylamides capable of inhibiting both proteases of ZIKV/DENV2 and CHIKV [30,43,44], respectively; we decided to connect both chemical cores, assuming these structures could be pharmacophores associated with the inhibition of these viral proteases. Initially, the benzothiazole-acrylamide hybrids were designed based on the

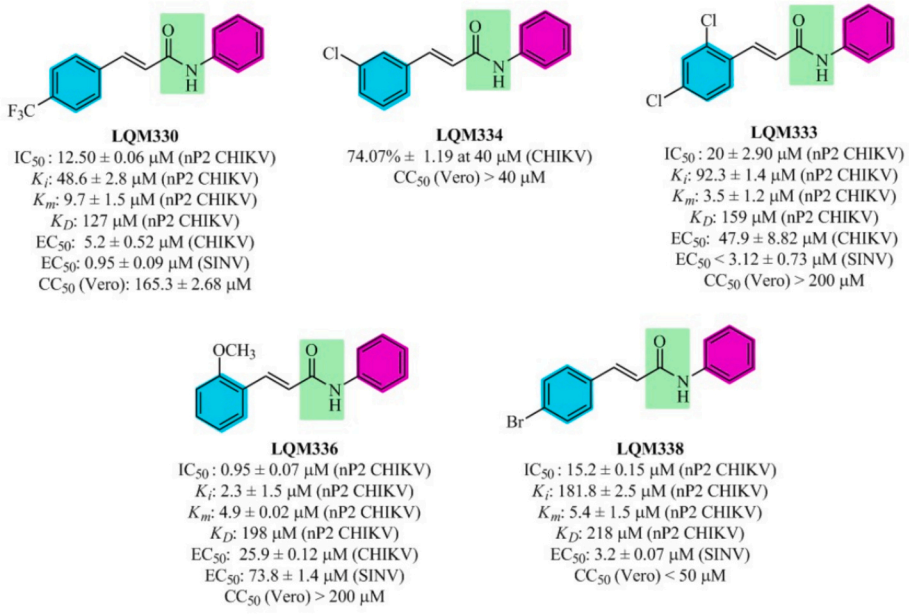

Fig. 2. Acrylamide derivatives targeting both Chikungunya and Sindbis Alphaviruses.

hybridization approach, in which their benzothiazole substituents were selected considering classic bioisosterism strategy. Thus, electron-withdrawing (EWG) and electron-donating (EDG) groups were chosen for the benzothiazole moiety, whereas the 4-*tert*-butyl (weak EDG), 4-chloro (weak EWG), and 3,3′,4-trimethoxyl (strong EDG) substituents were selected for the acrylamide moiety, which has being identified as promising group in previous studies focused on ZIKV and DENV2 [31] and CHIKV [42,44]. Additionally, the acrylamide moiety was replaced with a *trans*-phenylcyclopropane moiety to determine if the *ene* bond (C=C) of acrylamides is an essential molecular feature for their activity. Like acrylamides, this group also maintains the bond rotation restricted but it creates an even more sterically hindered region due to its cyclopropane ring. Besides, a phenylthiazole moiety was used to substitute the benzothiazole core, after identification of the most promising inhibitors. Thus, three different series of compounds were designed targeting NS2B/NS3 protease from ZIKV and DENV2. Then, all candidates were synthesized and chemically characterized by spectroscopic and spectrometric techniques. Then, these were screened in enzymatic inhibition assays involving ZIKV and DENV2 NS2B/NS3 proteases. Posteriorly, the most promising compounds were further investigated on ZIKV-infected Vero cells. Furthermore, the active compounds were screened for their antiviral effects on CHIKV- and SINV-infected Vero cells and then investigated toward CHIKV nsP2 protease by using ITC analysis. Finally, MD simulations and MM/GBSA were employed to obtain information about their ligand-target complex stabilities. In Fig. 3, the complete workflow is represented.

2.2. Chemistry

Initially, non-substituted and 4-*tert*-butyl cinnamic acids were obtained by Perkin reaction [45,46], refluxing the corresponding aldehyde, malonic acid in pyridine refluxed, and *N*-methylpiperazine as catalyst base [42], yielding the compounds with 90 and 97%, respectively. Surprisingly, halogenated benzothiazoles are poorly reactive toward cinnamic acid analogs to create amide bonds. Then, we decided to increase the reactive of cinnamic acids, by converting their acid function into their corresponding acyl chloride analogs. Thionyl chloride ($SOCl_2$) was used in DMF at room temperature, providing the corresponding acyl chlorides (55 and 99%). Still, 3,4-dimethoxyl-, and 4-*tert*-butyl-substuted 2-aminobenzo[*d*]thiazole were synthesized by using potassium thiocyanate and bromo solution in DCM, *via* Hugershoff reaction [47]. Then, the non-halogenated benzothiazole-acrylamide hybrids were obtained reacting the corresponding benzothiazole and acrylamides, in presence TBTU solubilized in DMF at room temperature, and *N,N′*-diisopropylethylamine (DIPEA) as catalyst base, as described in our previous works [24,30,31,42,43]. The corresponding final compounds were obtained in yields ranging from 48 to 99%. For the obtainment of halogenated benzothiazole-acrylamide or benzothiazole-cyclopropane hybrids, an adaptation of Schotten-Baumann reaction was used [48–50]. To obtain the hydroxylated-benzothiazole cores, their corresponding 5,6-dimethoxyl- and 6-ethoxyl-substituted cores were deprotected by using BBr_3 in DCM at −78 °C, providing the desired derivatives in 88 and 99% yield, respectively [30,43]. Posteriorly, all benzothiazole cores reacted with cinnamic acid derivatives to provide benzothiazole-acrylamide hybrids (**LQM525–583**), as well as phenyl-cyclopropane acid to yield benzothiazole-cyclopropane hybrids (**LQM584–602**). Additionally, aminophenylthiazole core was also used to produce hybrid compounds (**LQM603–606**). All spectra for intermediate and final products can be found in the Supplementary Information, whereas their description is demonstrated in the Materials and Methods section. All synthetic routes are presented in Scheme 1.

2.3. Enzymatic inhibition assays toward NS2B/NS3 proteases from Zika and Dengue viruses

In general, all synthesized compounds were evaluated for their respective potential activity against ZIKV NS2B/NS3 protease. Moreover, only compounds exhibiting ≥60% inhibition at 20 μM

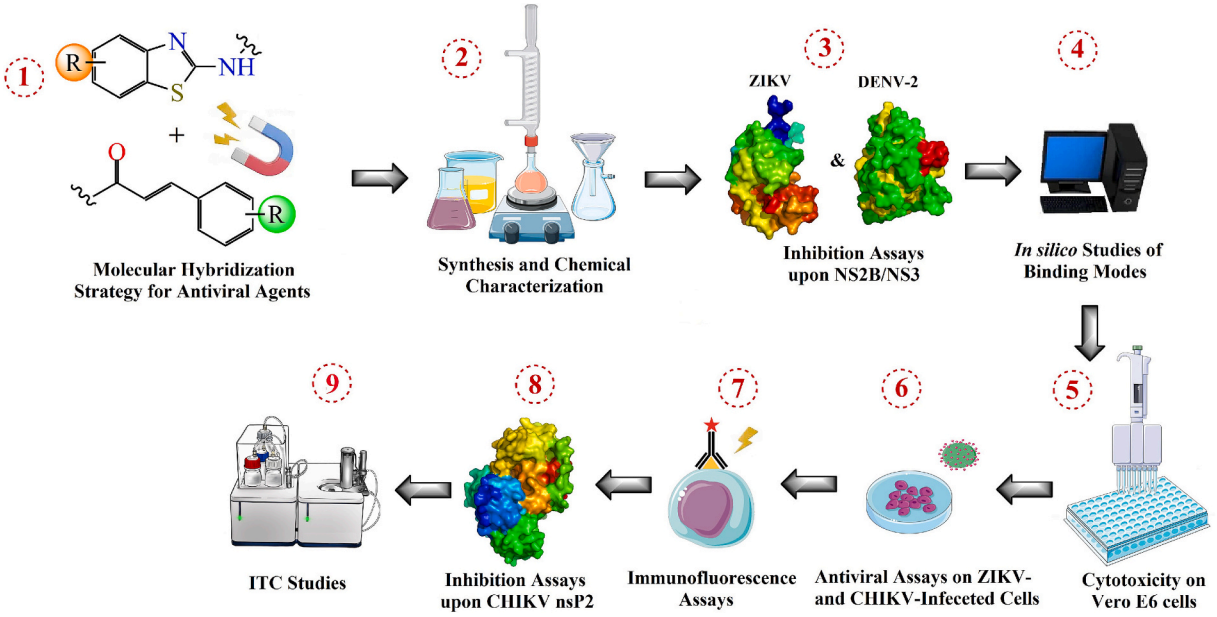

Fig. 3. Schematic workflow used in this study to obtain benzothiazole-acrylamide hybrids as pan-antivirals targeting arboviruses. *1. Initially, several benzothiazole-acrylamide hybrids were designed as potential protease inhibitors targeting both ZIKV/DENV2 and CHIKV; 2. All designed compounds were synthesized and then characterized by spectroscopic and spectrometric techniques; 3. All compounds were experimentally tested toward NS2B/NS3 protease of both ZIKV and DENV2, in which only compounds displaying ≥ 60% inhibition at 20 μM concentration were evaluated for their IC_{50} values; 4. The active compounds were investigated for their binding modes, using molecular dynamics simulations and molecular-mechanics generalized Born surface area (MM/GBSA); 5. Then, these compounds were screened for their cytotoxic effects on Vero E6 cells; 6. Non-toxic compounds were tested against ZIKV- and CHIKV-infected cells; 7. Immunofluorescence assays were performed by using DAPI and FITC staining; 8. Posteriorly to an initial FRET-based evaluation, these compounds were experimentally tested toward CHIKV nsP2; 9. To confirm if these compounds are active against nsP2, they were evaluated by using isothermal titration calorimetry (ITC) technique.*

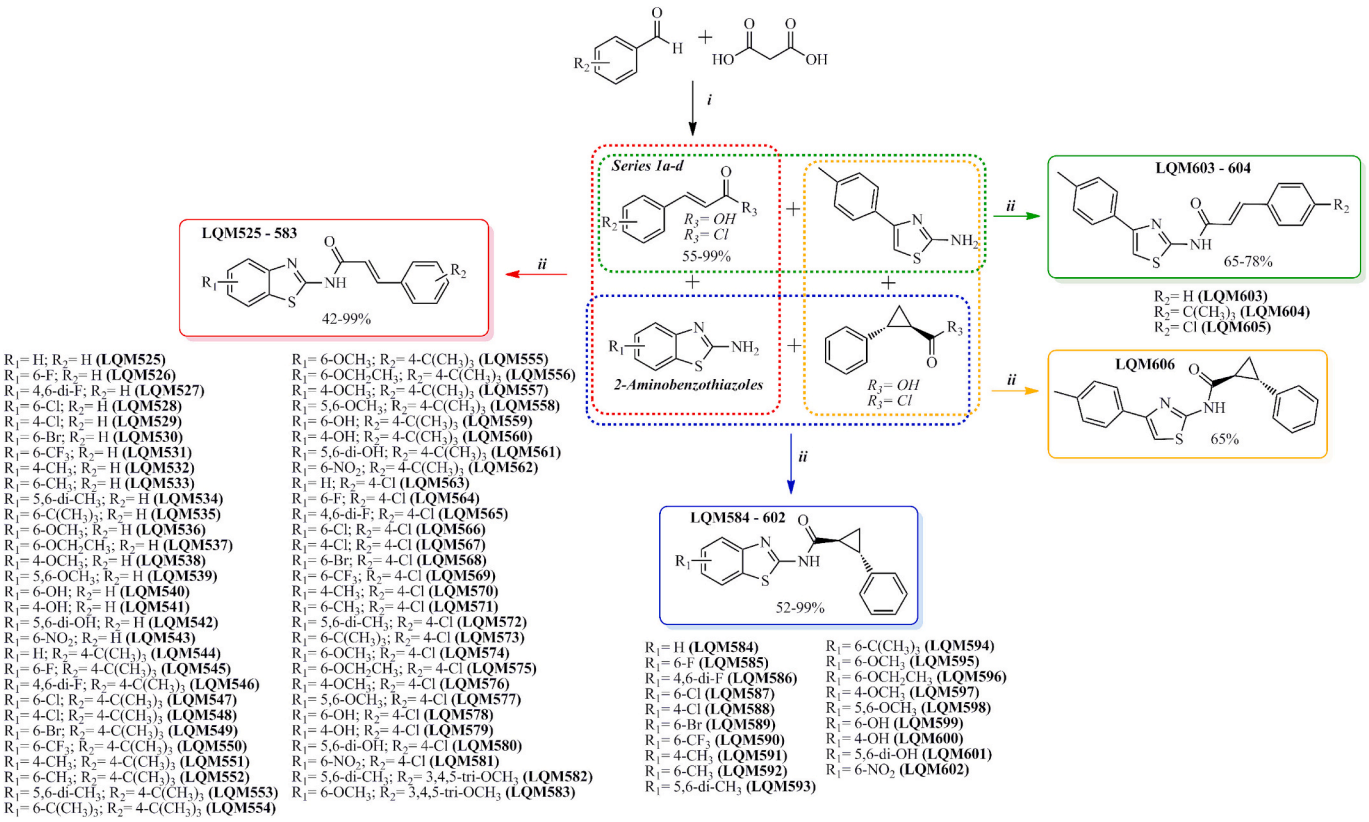

Scheme 1. Synthetic routes for the compounds in this study. Conditions: *i: Pyridine, N-methylpiperazine (10 mol%), 24 h, reflux; and ii: amines, dimethylformamide (DMF), 2-(1H-Benzotriazole-1-yl)-1,1′,3,3′-tetramethyluronium tetrafluoroborate (TBTU), diisopropylethylamine (DIPEA), 24 h, at room temperature.*

concentration had their inhibition concentration for 50% (IC_{50}) values were determined. Posteriorly, these compounds were screened toward DENV2 NS2B/NS3 protease, as well (Table 1).

Most of the synthesized compounds were found to be inactive against the NS2B/NS3 proteases from ZIKV and DENV2. Compounds having three methoxy groups (**LQM582** and **LQM583**) exhibited high fluorescence, preventing to determine their activities. Among the non-substituted acrylamide derivatives (**LQM525–543**), only **LQM537**, bearing a 6-ethoxy substituent (6-OCH_2CH_3), exhibited measurable activity against the ZIKV NS2B/NS3 protease, with an IC_{50} value of 13.6 ± 1.81 μM. However, this compound did not demonstrate significant inhibition of the DENV2 protease (%inhib.: 34.3%), suggesting selective inhibition toward the ZIKV protease. The presence of an ethoxy group at position 6 may favor interactions specific to the ZIKV protease binding site. In the series bearing a *p-tert*-butyl group on the acrylamide moiety (**LQM544–562**), some derivatives with electron-donating substituents on the benzothiazole ring showed activity. Compound **LQM560**, carrying such substituents, presented similar inhibitory activity against the ZIKV NS2B/NS3 protease, with an IC_{50} value of 15.2 ± 1.21 μM, respectively. Interestingly, **LQM560** displayed no relevant activity against DENV2 (%inhib.: 28.0%), indicating a potential role of the substituent pattern in modulating selectivity. The increased selectivity of **LQM560** toward ZIKV may be attributed to specific steric or electronic interactions. Compounds bearing a *p*-chloro substituent on the acrylamide ring (**LQM563–581**) were also examined. Among them, **LQM581**, which possesses a 6-nitro substituent on the benzothiazole scaffold, exhibited activity against the ZIKV protease (IC_{50}: 20.6 ± 2.19 μM), while showing minimal inhibition of DENV2 (%inhib.: 19.7%). This result further supports the trend of selectivity toward ZIKV observed for other active derivatives. In the phenylcyclopropane-containing series (**LQM584–602**), only **LQM601** demonstrated measurable activity, inhibiting ZIKV NS2B/NS3 with an IC_{50} value of 28.3 ± 0.8 μM, and low inhibition against DENV2 (%inhib.: 24.1%). The modest potency of this compound, coupled with its selectivity, suggests that the phenylcyclopropane motif may retain binding capability in ZIKV protease while being less compatible with the homologous pocket in DENV2. Given the encouraging selectivity profiles observed, we next evaluated whether the benzothiazole moiety is essential for activity. To explore this, four additional compounds (**LQM603–606**) were synthesized by replacing the benzothiazole ring with a phenyl-4-thiazole scaffold, increasing the distance between the two aromatic systems from 10.94 to ~12.40 Å (see Supplementary Information). These analogs were also screened against ZIKV NS2B/NS3. Notably, none of these new compounds exhibited activity against DENV2, while only **LQM604**, bearing a *p-tert*-butyl group, showed weak inhibition (%inhib.: 1.7%). Nevertheless, it retained selective inhibition toward ZIKV, with an IC_{50} value of 14.9 ± 1.14 μM, indicating that this alternative scaffold may still accommodate ZIKV allosteric binding, although with limited potency. Importantly, experimental evaluation of the binding mechanism (see Supplementary Information) revealed that these compounds act *via* an allosteric inhibition mechanism. This observation aligns with previous studies from our group, where benzothiazole-based inhibitors targeting ZIKV NS2B/NS3 were also found to function through non-competitive, allosteric binding [43]. In summary, all active compounds exhibited selective inhibition of ZIKV NS2B/NS3 protease over the homologous DENV2 enzyme. This finding is particularly noteworthy given the high sequence identity (53.45%) between the two proteases. The observed selectivity underscores the potential for rational design of ZIKV-selective allosteric inhibitors and highlights the benzothiazole scaffold as a privileged structure for further optimization.

2.4. Assessment of cell cytotoxicity on Vero cells by MTT assay

To evaluate the safety profile of our **LQM** series, we performed MTT-based viability assays on Vero cells treated with five candidate compounds over a broad concentration range (0.24–500 μM). The 50%

Table 1
Inhibition of NS2B/NS3 proteases from Zika virus (ZIKV) and Dengue virus serotype 2 (DENV2).

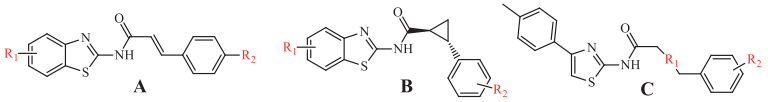

Code	Scaffold	R1	R2	IC_{50} ± SD (μM) or %Inhibition at 20 μM*	
				ZIKV	DENV2
LQM525	A	H	H	n.a.	n.d.
LQM526	A	6-F	H	n.a.	n.d.
LQM527	A	4,6-F	H	n.a.	n.d.
LQM528	A	6-Cl	H	n.a.	n.d.
LQM529	A	4-Cl	H	n.a.	n.d.
LQM530	A	6-Br	H	n.a.	n.d.
LQM531	A	6-CF_3	H	n.a.	n.d.
LQM532	A	4-CH_3	H	n.a.	n.d.
LQM533	A	6-CH_3	H	n.a.	n.d.
LQM534	A	5,6-CH_3	H	n.a.	n.d.
LQM535	A	6-$C(CH_3)_3$	H	4.3%	n.d.
LQM536	A	6-OCH_3	H	26.1%	n.d.
LQM537	A	6-OCH_2CH_3	H	**13.6 ± 1.81 μM**	34.3%
LQM538	A	4-OCH_3	H	n.a.	n.d.
LQM539	A	5,6-OCH_3	H	34.2%	n.d.
LQM540	A	6-OH	H	18.6%	n.d.
LQM541	A	4-OH	H	52.4%	n.d
LQM542	A	5,6-OH	H	29.2%	n.d.
LQM543	A	6-NO_2	H	31.5%	n.d.
LQM544	A	H	-$C(CH_3)_3$	41.6%	n.d.
LQM545	A	6-F	-$C(CH_3)_3$	n.a.	n.d.
LQM546	A	4,6-F	-$C(CH_3)_3$	40.2%	n.d.
LQM547	A	6-Cl	-$C(CH_3)_3$	11.3%	n.d.
LQM548	A	4-Cl	-$C(CH_3)_3$	n.a.	n.d.
LQM549	A	6-Br	-$C(CH_3)_3$	3.0%	n.d.
LQM550	A	6-CF_3	-$C(CH_3)_3$	n.a.	n.d.
LQM551	A	4-CH_3	-$C(CH_3)_3$	7.0%	n.d.
LQM552	A	6-CH_3	-$C(CH_3)_3$	n.a.	n.d.
LQM553	A	5,6-CH_3	-$C(CH_3)_3$	n.a.	n.d.
LQM554	A	6-$C(CH_3)_3$	-$C(CH_3)_3$	n.a.	n.d.
LQM555	A	6-OCH_3	-$C(CH_3)_3$	n.a.	n.d.
LQM556	A	6-OCH_2CH_3	-$C(CH_3)_3$	38.0%	n.d
LQM557	A	4-OCH_3	-$C(CH_3)_3$	42.4%	n.d.
LQM558	A	5,6-OCH_3	-$C(CH_3)_3$	7.0%	n.d.
LQM559	A	6-OH	-$C(CH_3)_3$	12.5%	n.d.
LQM560	A	4-OH	-$C(CH_3)_3$	**15.2 ± 1.21 μM**	28.0%
LQM561	A	5,6-OH	-$C(CH_3)_3$	53.8%	n.d.
LQM562	A	6-NO_2	-$C(CH_3)_3$	n.a.	n.d.
LQM563	A	H	-Cl	21.0%	n.d.
LQM564	A	6-F	-Cl	28.3%	n.d.
LQM565	A	4,6-F	-Cl	15.5%	n.d.
LQM566	A	6-Cl	-Cl	24.8%	n.d.
LQM567	A	4-Cl	-Cl	n.a.	n.d.
LQM568	A	6-Br	-Cl	13.8%	n.d.
LQM569	A	6-CF_3	-Cl	25.0%	n.d.
LQM570	A	4-CH_3	-Cl	25.0%	n.d.
LQM571	A	6-CH_3	-Cl	26.3%	n.d.
LQM572	A	5,6-CH_3	-Cl	19.3%	n.d.
LQM573	A	6-$C(CH_3)_3$	-Cl	9.8%	n.d.
LQM574	A	6-OCH_3	-Cl	14.2%	n.d.
LQM575	A	6-OCH_2CH_3	-Cl	47.2%	n.d.
LQM576	A	4-OCH_3	-Cl	n.a.	n.d.
LQM577	A	5,6-OCH_3	-Cl	33.4%	n.d.
LQM578	A	6-OH	-Cl	17.5%	n.d.
LQM579	A	4-OH	-Cl	52.2%	n.d.
LQM580	A	5,6-OH	-Cl	44.0%	n.d.
LQM581	A	6-NO_2	-Cl	**20.6 ± 2.19 μM**	19.7%
LQM584	B	H	H	n.a.	n.d.
LQM585	B	6-F	H	2.4%	n.d
LQM586	B	4,6-F	H	19.1%	n.d.
LQM587	B	6-Cl	H	n.a.	n.d.
LQM588	B	4-Cl	H	8.2%	n.d.
LQM589	B	6-Br	H	1.0%	n.d.
LQM590	B	6-CF_3	H	n.a.	n.d.
LQM591	B	4-CH_3	H	1.5%	n.d.
LQM592	B	6-CH_3	H	n.a.	n.d.
LQM593	B	5,6-CH_3	H	n.a.	n.d.

(*continued on next page*)

Table 1 (*continued*)

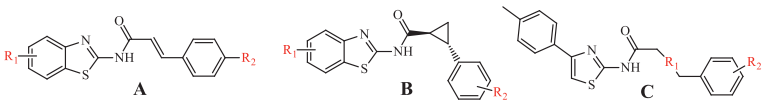

Code	Scaffold	R1	R2	IC_{50} ± SD (μM) or %Inhibition at 20 μM*	
				ZIKV	DENV2
LQM594	B	6-$C(CH_3)_3$	H	n.a.	n.d.
LQM595	B	6-OCH_3	H	3.6%	n.d.
LQM596	B	6-OCH_2CH_3	H	2.0%	n.d.
LQM597	B	4-OCH_3	H	n.a.	n.d.
LQM598	B	5,6-OCH_3	H	n.a.	n.d.
LQM599	B	6-OH	H	4.0%	n.d.
LQM600	B	4-OH	H	n.a.	n.d.
LQM601	B	5,6-OH	H	**28.3 ± 0.80 μM**	24.1%
LQM602	B	6-NO_2	H	12.2%	n.d.
LQM603	C		H	n.a.	n.d.
LQM604	C		-$C(CH_3)_3$	**14.9 ± 1.14 μM**	1.7%
LQM605	C		4-Cl	n.a.	n.d.
LQM606	C		H	12.1%	n.d.

SD: standard deviation; n.a.: not active; n.d.: not determined. Data represent the mean ± SD of three independent experiments performed in triplicate. *: Only compounds exhibiting at least 60% inhibition against at least one of the tested proteases (ZIKV or DENV2) were further evaluated for determination of their IC_{50} values.

cytotoxic concentration (CC_{50}) values derived from these curves (dashed line indicates 50% viability) reveal marked differences in cells tolerance across the series (Fig. 4). Vero cells were selected as they represent a well-established model in the field of virology, due to their high permissiveness to viral infections, which is associated with a deficiency in type I interferon production [51]. This characteristic promotes efficient replication of different viruses and allows for a more sensitive evaluation of the antiviral effects of the compounds, as the intrinsic

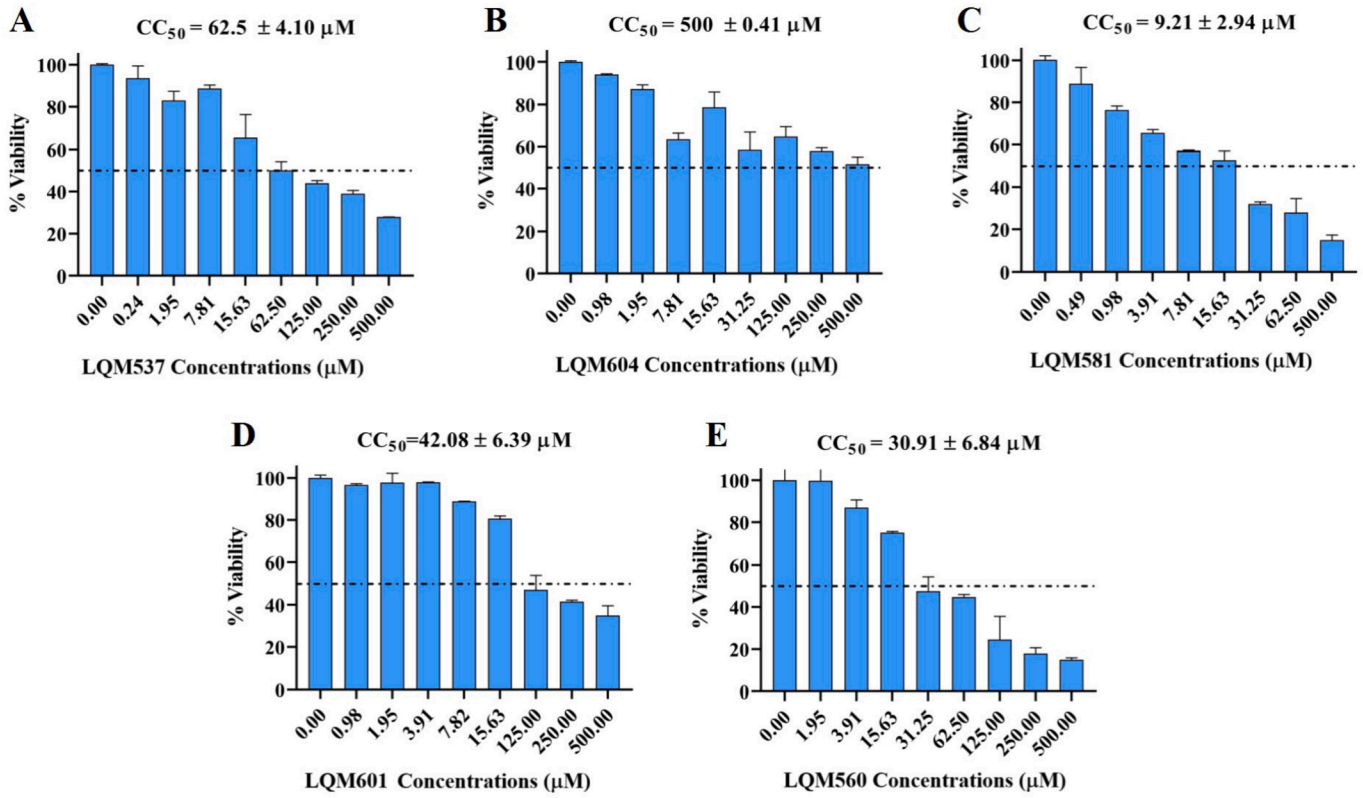

Fig. 4. Assessment of cell cytotoxicity of selected benzothiazole-2-acrylamide derivatives on Vero cells by MTT assay. *Cells were seeded in DMEM medium and exposed to compounds at concentrations ranging from 0.24 to 500 μM for 24 h. Cell viability was assessed via the MTT assay and expressed as a percentage relative to untreated controls. Data represents the mean ± SD of independent experiment performed in triplicate (n = 3).*

antiviral response of these cells is limited, thereby reducing interference from cellular immune responses in the experimental outcomes. Additionally, Vero cells were consistently used in all subsequent experiments to ensure methodological uniformity and comparability of results.

Compound **LQM581** exhibited the greatest cytotoxicity, with a CC_{50} of 9.2 ± 2.94 μM. Viability dropped below 50% at 31.2 μM and reached approximately 15% at 500 μM. Such a profile suggests that **LQM581** could compromise cell integrity if dosed above ~30 μM. **LQM537**, **LQM601**, and **LQM560** showed moderate cytotoxicity, with CC_{50} values of 62.5 ± 4.10 and 42.1 ± 6.39, and 30.91 ± 6.84 μM, respectively. These compounds maintained >50% viability up to ~15–30 μM, declining to the 20–40% range only at the highest dose (125 μM). Based on these data, the maximum non-toxic doses (MNTD), defined as those capable of maintaining ≥80% cell viability, were established as 7.8 μM for **LQM537**, 15 μM for **LQM560**, and 7.82 μM for **LQM601**. Compound **LQM604** demonstrated an CC_{50} value of 500 μM, indicating negligible cytotoxicity across the tested range. Cell viability remained above 60% even at 250 μM concentration. In general aspects, the combination of 6-NO_2 and *p*-Cl substituents in **LQM581** increases its lipophilicity leading to higher cell toxicity. Also, electron-donating groups, such as 6-OCH_2CH_3 in the benzothiazole-2-acrylamide derivative (**LQM537**) or even 5,6-di-OH in the phenylcyclopropane analog (**LQM601**) seem to contribute with their moderate cytotoxicity. Similarly, the combination of 4-OH and *p-tert*-$C(CH_3)_3$ groups in **LQM560** displayed moderate cytotoxicity. Furthermore, when the *p-tert*-$C(CH_3)_3$ group is kept and methylated benzothiazole is replaced with phenylthiazole ring (**LQM604**), its great cell viability is kept.

2.5. Antiviral plaque-reduction assays on Vero cells

To investigate the antiviral properties of novel compounds, plaque-reduction assays were performed to evaluate the inhibitory activity of these five benzothiazole-2-acrylamide derivatives against ZIKV, CHIKV, and SINV on Vero cell cultures (Table 2). This assay allowed for the quantitative assessment of viral replication by measuring the reduction in plaque numbers, providing a robust and reliable indicator of compound-mediated antiviral efficacy.

Although SINV, CHIKV, and ZIKV exhibit different replication kinetics, the 48 h time point was adopted as a standardized experimental condition to allow direct comparison between viruses and the evaluation of the antiviral activity of the tested compounds during the early stages of viral replication. Evidence from the literature indicates that, on Vero cells, the production of infectious CHIKV particles is detectable as early as 6 h post-infection and reaches its peak at approximately 36 h, corresponding to an active phase of viral replication [52]. Similarly, studies with ZIKV show that at 48 h post-infection, viral titers are elevated and plaque formation can already be observed, making this an appropriate time point for plaque assays [53,54]. Additionally, the use of this time point reduces the influence of secondary infection cycles, and late cytopathic effects, allowing for a more direct assessment of the antiviral effects of the compounds.

Table 2
Antiviral activity of benzothiazole-2-acrylamide derivatives in plaque-reduction assays against ZIKV, CHIKV, and SINV in Vero cells.

Code	CC_{50} ± SD (μM)	EC_{50} ± SD μM (SI)		
		ZIKV	CHIKV	SINV
LQM537	62.5 ± 4.10	7.2 ± 3.35 (8.7)	0.5 ± 0.22 (125.0)	n.d.
LQM560	30.9 ± 6.84	< 1.9 (> 16.3)	1.8 ± 0.18 (17.2)	0.7 ± 0.16 (44.3)
LQM581	9.2 ± 2.94	0.2 ± 0.44 (46)	n.d.	n.d.
LQM601	42.1 ± 6.39	< 1.9 (> 22.1)	n.d.	n.d.
LQM604	500.0 ± 0.41	< 1.9 (> 263.1)	n.d.	n.d.

The 50% cytotoxic concentration (CC_{50}) and EC_{50} (concentration that inhibits 50% of the virus) on Vero cells after 48h were calculated by using nonlinear regression curve fitting and the selectivity indexes were obtained for each compound using the following equation: Selectivity index (SI)= CC_{50}/EC_{50}. Finally, the mean ± standard deviation (SD) of two experiments performed in triplicate is shown. Compounds with no effects up to the concentration tested their EC_{50} values were not determined (n.d.). ZIKV: Zika virus. CHIKV: Chikungunya virus. SINV: Sindbis virus.

Plaque-reduction assays in ZIKV-infected Vero cells revealed clear differences in antiviral potency among the series of compounds, demonstrating that all these compounds are very effective against ZIKV-infected Vero cells. **LQM537** displayed an EC_{50} value of 7.2 ± 3.35 μM for the plaque formation inhibition, with a selectivity index (SI) of 8.7, being not exceptional for antiviral activity against ZIKV. Surprisingly, it presented an excellent antiviral activity against CHIKV in the plaque formation assay, having an EC_{50} value of 0.5 ± 0.22 μM and SI of 125, highlighting this compound as the most promising analog as an anti-CHIKV drug. Based on these results, **LQM537** could be more promising in a further drug development's campaign targeting CHIKV. In contrast, evaluation of **LQM537** against SINV, an Alphavirus closely related to CHIKV, revealed no inhibitory activity at the concentrations tested. These results suggest that this compound could be considered a dual-antiviral compound due to its action against both ZIKV and CHIKV. Compounds **LQM581**, **LQM601**, and **LQM604** displayed excellent results against ZIKV-infected Vero cells, in which their EC_{50} values were found to be below 1.9 μM, resulting in SI values ranging from 22.1 to >263.1, suggesting their safe therapeutic profiles. Interestingly, none of these compounds demonstrated activity against both Alphaviruses, CHIKV and SINV. Moreover, compounds **LQM560**, **LQM601**, and **LQM604** achieved more than 60% inhibition at the lowest tested concentration (1.8 μM), with EC_{50} values below this threshold and maximal inhibition plateauing near 75–80%, indicating sub-micromolar potency likely driven by enhanced cellular uptake or tighter NS2B/NS3 protease engagement, in case of ZIKV. Compounds **LQM553**, **LQM581**, **LQM601**, and **LQM604** exhibited only modest antiviral activity against CHIKV, with maximal inhibition ranging from ~30 to 50% at Maximum Non-Toxic Dose (MNTD), defined as those maintaining ≥80% cell viability (see supplementary information). Due to the limited suppression of viral replication and the absence of a consistent dose–response relationship, reliable EC_{50} values for **LQM553**, **LQM581**, **LQM601**, and **LQM604** could not be determined. Compound **LQM604** exhibited potential solubility-related limitations. Consequently, this compound was not continued further in this investigation. All plaque reduction assays were conducted under these conditions to rigorously assess the antiviral potential of the compounds while maintaining physiological relevance. The standout compound, **LQM581**, exhibited an EC_{50} value of 0.2 ± 0.44 μM and robust dose–response behavior. Finally, **LQM560** represents the best compound identified in this study, capable of inhibiting all three viruses, being identified as a pan-antiviral agent, with sub-micromolar values of EC_{50} below 1.9 μM against these pathogens and with SI values higher than 16. Collectively, the plaque assay findings validate the series of compounds as a fertile scaffold for developing potent, selective ZIKV inhibitors, as well dual or pan-antivirals. All dose-response curves are available in the supplementary material. All graphs for EC_{50} determinations can be found in Fig. 2S in the supplementary information.

2.6. Quantification of ZIKV, CHIKV, and SINV viral load by quantitative reverse transcription-polymerase chain reaction (qRT-PCR) on infected Vero cells

In this study, we evaluated the antiviral efficacy of two benzothiazole-2-acrilamide derivatives, **LQM560** and **LQM601**, against ZIKV infection *in vitro*, as measured by quantitative reverse transcription-polymerase chain reaction (qRT-PCR) (Fig. 5). Both compounds elicited dose-dependent reductions in viral load, with **LQM560**

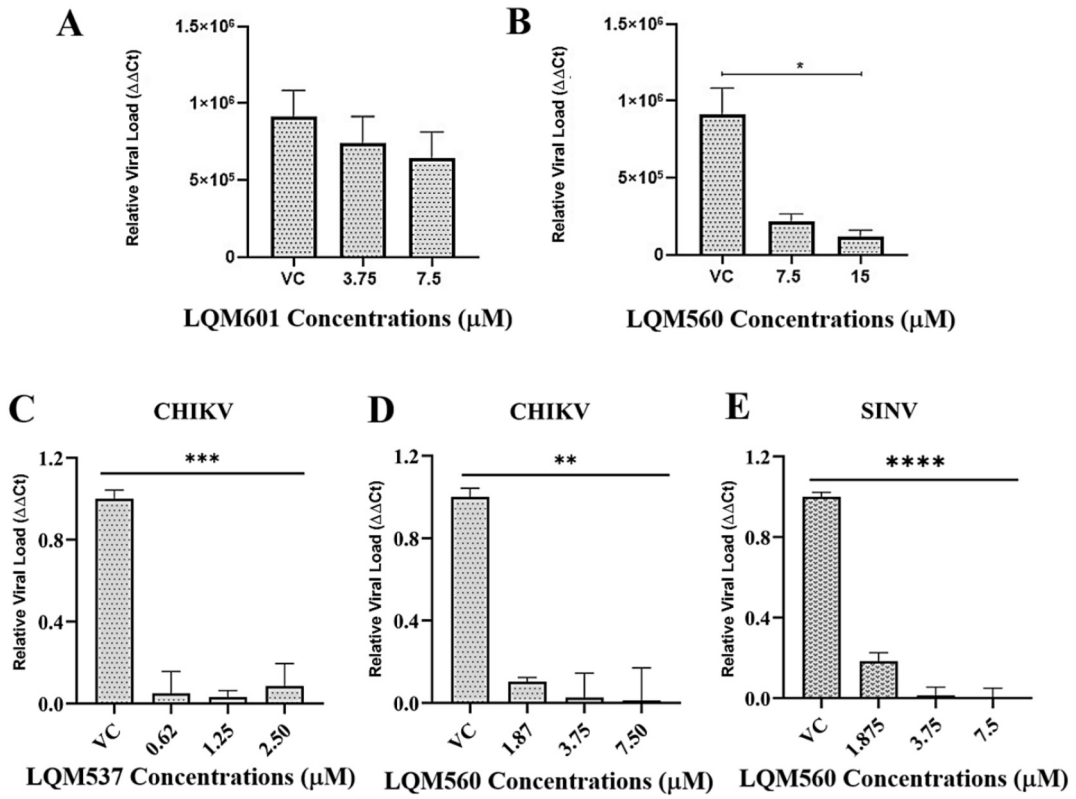

Fig. 5. Relative viral load (ΔΔCt) determined by qRT-PCR following treatment with selected compounds. *Panels A and B depict the effects of LQM560 and LQM601, respectively, on ZIKV envelope gene expression. (C-E) Broad-spectrum antiviral potential of LQM series compounds against CHIKV and SINV in cell culture as quanitified by qRT-PCR. Bar plots showing fold reduction in the abundance of viral RNA in CHIKV- or SINV-infected Vero cells treated with LQM537 and LQM560, compared to vehicle control (VC). At 24 h post-infection, total RNA was isolated and subjected to qRT-PCR to quantify the CHIKV or SINV viral RNA levels in cells. One-way ANOVA with Dunnett's multiple comparison test was used to evaluate statistical significance in intracellular viral RNA between treatment groups and the VC; ****P < 0.0001; ***P < 0.001; **P < 0.01. Values represent the mean, and error bars are the standard deviation (n = 2).*

displaying markedly greater potency than **LQM601**. For **LQM601** (Fig. 5A), treatment at 3.75 μM resulted in an approximately 25% decrease in viral RNA relative to vehicle control (VC), while 7.5 μM achieved a somewhat larger but modest reduction (~35%). Although the trend suggests dose dependence, the error bars indicate overlapping variability with VC, and no statistical annotation was provided; thus, antiviral activity of **LQM601** at these concentrations, while encouraging, appears moderate and may require higher doses or optimization of compound structure to achieve robust inhibition. Still, **LQM601** may require concentrations >10 μM to achieve comparable antiviral effect, which could raise concerns about cytotoxicity or SI. By contrast, **LQM560** (Fig. 5B) exhibited a striking and statistically significant decrease in viral RNA, in which 7.5 μM reduced viral load by nearly 80% compared to VC, and 15 μM achieved over 90% suppression ($p < 0.05$). The clear separation of error bars (statistical significance) a strong antiviral effect even at relatively low micromolar concentrations. This suggests that **LQM560** is substantially more potent than **LQM601**, and its therapeutic window appears favorable. Despite both compounds were designed to target ZIKV NS2B/NS3 protease, the enhanced activity of **LQM560** might reflect improved binding affinity, favorable polar contacts, or even off-target effects. However, its appropriate binding modes will be discussed further in this study. By analyzing the resulting qRT-PCR data against CHIKV and SINV, we were able to observe that **LQM537** and **LQM560** were able to significantly inhibit CHIKV at the tested concentrations, in which a significant reduction in fold-change was observed in viral gene expression in the treated cells in comparison to VC (Fig. 5C and D). Furthermore, the efficacy of these compounds was also evaluated using qRT-PCR assay to determine their ability to suppress SINV, in addition to the cell-based studies. The results of this experiment indicated that **LQM560** has a significant inhibitory impact on both SINV and CHIKV (Fig. 5D and E), as demonstrated by qRT-PCR analysis and plaque assay results. In contrast to that, **LQM537**, which exhibited great suppression against CHIKV (~90% at the lowest concentration), did not demonstrate a significant inhibitory impact against SINV, as indicated by the results of the qRT-PCR experiment (see supplementary information). In general, **LQM560** has great promise for being repurposed as a treatment for viral infections. Notwithstanding these results, **LQM560** emerges as the lead candidate for further *in vivo* evaluation, given its combination of potent antiviral activity and moderate cytotoxicity, as well as, its dual activity against Flavivirus (ZIKV) and Alphaviruses (CHIKV and SINV).

2.7. Immunofluorescence assays for anti-Zika virus activity on Vero cells

Immunofluorescence analysis of ZIKV-infected Vero cells treated with **LQM560** or **LQM601** provided striking visual confirmation of antiviral activity and low cytotoxicity. In vehicle-treated monolayers, ZIKV infection was evident from the intense, diffuse FITC signal throughout the cytoplasm of nearly all DAPI-stained nuclei, confirming robust viral replication and antigen accumulation (Fig. 6). When cells were treated with **LQM601** at 3.75 μM, FITC fluorescence intensity was already reduced by roughly half compared to control, with infected cells appearing as sparsely distributed puncta rather than the confluent staining seen in untreated wells; nuclei remained uniformly round and evenly stained by DAPI, indicating preserved cell viability. Raising the dose of **LQM601** to 7.5 μM further decreased FITC signal to less than 20% of control, and only rare clusters of green puncta were visible, often localized perinuclearly—suggesting interrupted polyprotein processing or impaired assembly of replication complexes—while nuclear counts and morphology were indistinguishable from mock-infected cells.

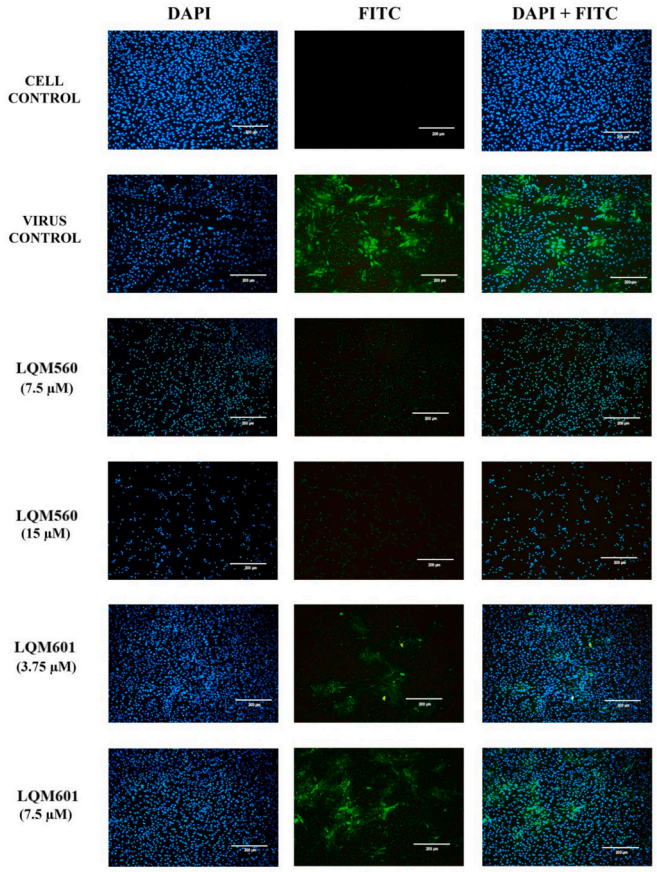

Fig. 6. Inhibition of ZIKV infection by **LQM560** and **LQM601**, as demonstrated by immunofluorescence staining. *Cells were treated with the compounds and subsequently infected with ZIKV. A marked reduction in viral signal was observed in treated samples, indicating effective antiviral activity. Images were captured at 10× magnification. Scale bar = 200 μm.*

Moreover, **LQM560** proved to be even more potent, in which at 7.5 μM concentration, FITC staining was virtually confined to individual cells at the edges of the field, amounting to roughly 10% of the fluorescence intensity in controls, and these residual viral antigens appeared as small, concentrated spots rather than the broad cytoplasmic distribution characteristic of productive infection. DAPI images again confirmed intact nuclear architecture and equivalent cell density, underscoring that the loss of FITC signal reflects antiviral efficacy rather than cytotoxicity. At 15 μM, **LQM560** abolished detectable FITC fluorescence in over 95% of cells, leaving only occasional, extremely faint puncta; the complete absence of widespread green labeling at this concentration points to near-total blockade of viral protein synthesis or trafficking. The sharper dose–response and lower residual signal for **LQM560** indicate superior cell penetration or tighter binding to NS2B/NS3, effectively halting polyprotein cleavage and downstream antigen accumulation. Throughout, DAPI-based nuclear counts remained ≥95% of control values, confirming that both compounds act selectively on the viral lifecycle without compromising the cell viability. These immunofluorescence data, taken together with PCR and plaque-reduction assays, position **LQM560** as the lead candidate for mechanistic studies, while **LQM601** shows strong, dose-dependent inhibition warranting further optimization.

2.8. Evaluation of anti-CHIKV activity by immunofluorescence assay

Immunofluorescence analysis of CHIKV-infected Vero cells treated with **LQM537** or **LQM560** offered compelling visual evidence of antiviral potency coupled with minimal cytotoxicity. In vehicle-treated controls, CHIKV infection was evident as a widespread and intense FITC signal throughout the cytoplasm of nearly all DAPI-stained nuclei, reflecting robust viral replication and structural protein accumulation (Fig. 7). Treatment with **LQM537** at 5 μM halved the overall FITC fluorescence relative to control, with green antigenic puncta appearing sparsely scattered rather than the confluent cytoplasmic staining observed in untreated monolayers; DAPI staining remained uniform and nuclear morphology intact, indicating preserved cell viability. Increasing the **LQM537** concentration to 10 μM further suppressed FITC intensity to below 25% of control levels, leaving only occasional, perinuclear clusters of viral antigens — consistent with disrupted polyprotein processing or inhibited formation of replication complexes — while nuclear counts and morphology remained indistinguishable from mock-infected cells. **LQM560** exhibited even greater efficacy: at 3.75 μM, FITC labeling was largely restricted to isolated cells at the periphery (approximately 12% of control fluorescence), and antigenic signals appeared as minute, concentrated foci instead of diffuse cytoplasmic distribution. DAPI images confirmed an intact nuclear architecture and cell density comparable to untreated wells, underscoring that FITC reduction was due to antiviral action rather than cytotoxicity. At 7.5 μM, **LQM560** eradicated detectable FITC fluorescence in over 95% of cells, with only faint, singular puncta remaining — indicative of near-complete blockade of viral protein synthesis or trafficking. The steeper dose–response and lower residual fluorescence for **LQM560** suggest superior cell permeability or even higher affinity for the CHIKV nsP2

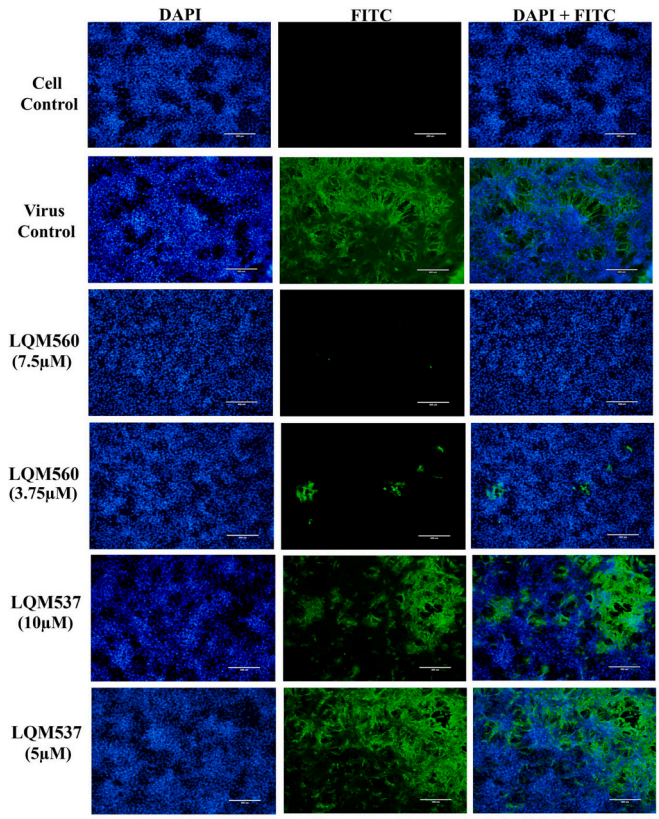

Fig. 7. Inhibition of CHIKV infection by **LQM537** and **LQM560**, as demonstrated by immunofluorescence assay. *Vero cells were infected with CHIKV (MOI 1) and exposed to LQM537 or LQM560 at indicated doses, administered pre- and post-infection. Post incubation, the cells were fixed and stained with an anti-alphavirus primary antibody and fluorescein isothiocyanate (FITC)-conjugated secondary antibody. FITC (green) denotes CHIKV-infected cells and DAPI (blue) marks cell nuclei. A marked reduction in viral signal was observed in treated samples, indicating effective antiviral activity. Scale bar = 400 μm.* (For interpretation of the references to colour in this figure legend, the reader is referred to the web version of this article.)

protease, effectively arresting polyprotein cleavage and subsequent antigen accumulation. Across all conditions, DAPI-based nuclear counts remained ≥95% of control, confirming selective inhibition of the viral lifecycle without compromising host cell viability. These immunofluorescence findings, in concert with qRT-PCR and plaque-reduction assays, highlight **LQM560** as the lead candidate for mechanistic investigations, while **LQM537** demonstrates robust, dose-dependent antiviral activity meriting further structural optimization.

2.9. Assessment of inhibition activity toward CHIKV nsP2 protease by using fluorescence resonance energy transfer (FRET) and isothermal titration calorimetry (ITC) assays

Prior to FRET-based screening of CHIKV nsP2 protease inhibitors, intrinsic fluorescence of **LQM** compounds was assessed to rule out compounds displaying intrinsic fluorescence or interference with the substrate. As observed, **LQM601** was confirmed to possess high intrinsic fluorescence with fluorescence levels in certain cases surpassing that of CHIKV nsP2 protease incubated with substrate. Owing to the potential interference of **LQM601** with the FRET-based assay, this compound was not carried forward for further studies targeting CHIKV nsP2 protease. The remaining four compounds were subsequently evaluated for inhibition of CHIKV nsP2 protease activity using FRET assay. Based on the data obtained from FRET based protease inhibition assay, none of the tested compounds exhibited any significant inhibitory effect on CHIKV nsP2 protease, even at the highest tested concentrations. This signifies that the compounds could not inhibit the CHIKV nsP2 protease. Together, these findings suggest that although **LQM537** and **LQM560** (see Fig. 1S-A and B in supplementary material) demonstrated potent antiviral activity against CHIKV, the compounds lack direct inhibitory effects against CHIKV nsP2 protease.

Encouraged by the promising anti-CHIKV activity in virus-based cell culture assays, **LQM537** and **LQM560** were further subjected to ITC studies to ascertain if these compounds show any binding affinity

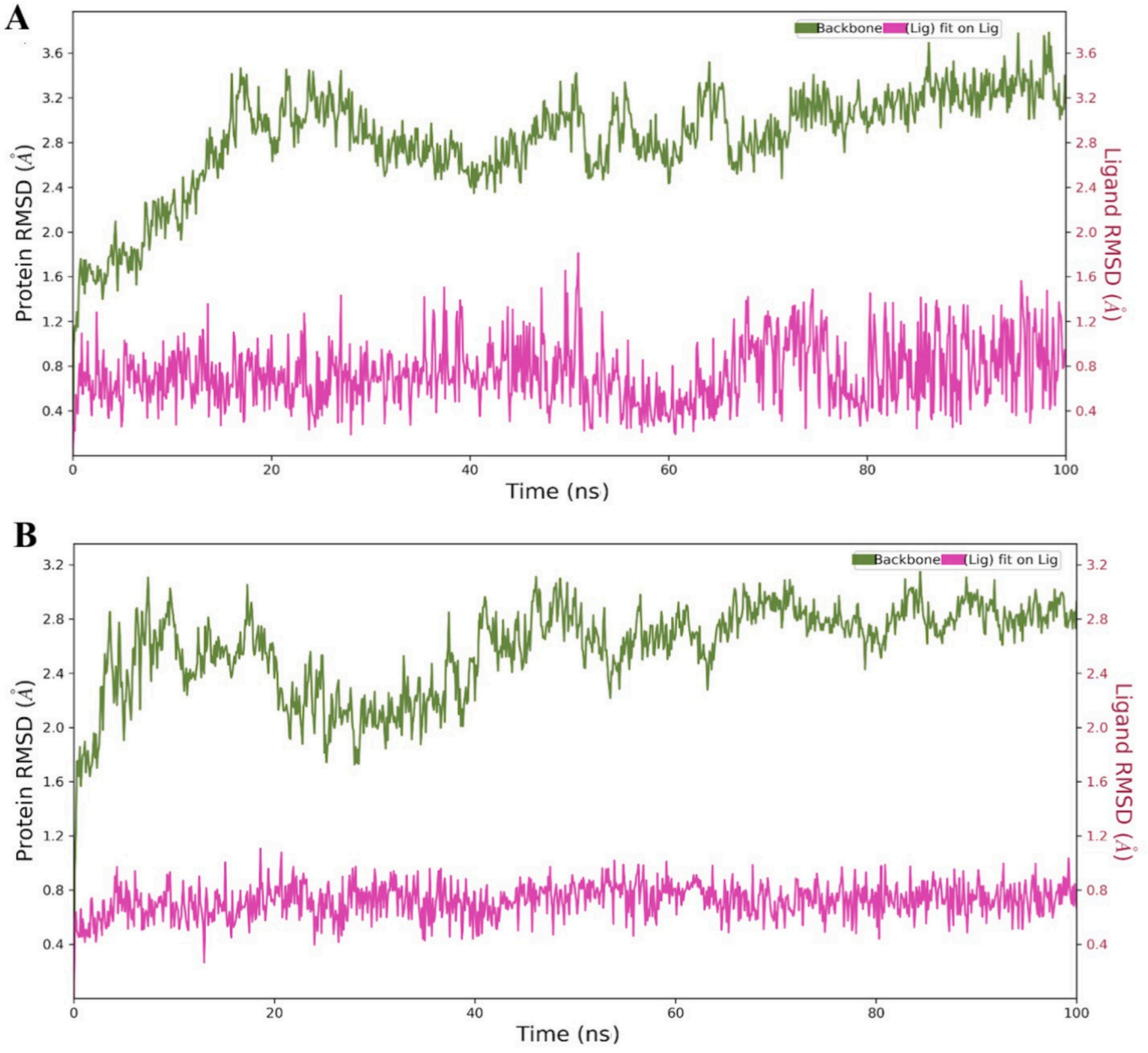

Fig. 8. Root mean square deviation (RMSD) plots for the complexes formed between the ZIKV NS2B/NS3 protease and **LQM601** (A) and **LQM560** (B), over 100 ns of molecular dynamics simulations.

toward purified CHIKV nsP2 protease. The thermodynamic data fitted into a one-site binding model revealed no binding affinity of CHIKV nsP2 protease when titrated against **LQM537** and **LQM560** (Fig. 1S-C and E in supplementary material).

2.10. *In silico binding mode studies toward ZIKA NS2B/NS3 protease*

Since **LQM560** and **LQM601** were found to be most promising analogs in this study, including their activity against NS2B/NS3 protease of ZIKV, we decided to investigate their binding modes by using different *in silico* approaches. Since these compounds did not demonstrate inhibition toward CHIKV nsP2 protease, their *in silico* evaluations were not performed. In this context, 100 ns MD simulations provided important insights into the conformational stability of the complexes formed between ZIKV NS2B/NS3 protease and **LQM560** and **LQM601**. In general, both complexes (at the allosteric pocket) exhibited an initial relaxation period during the first 20 ns, followed by relatively stable behavior, observed in the RMSD plots. In the complex formed with **LQM601** (Fig. 8A), the protein RMSD stabilized around 2.8–3.0 Å, with controlled fluctuations maintained until the end of the simulation. The ligand RMSD, in turn, consistently remained below 1.0 Å throughout the trajectory, indicating that the compound remained firmly anchored to the binding site, without significant conformational changes, suggesting good accommodation and affinity. In the complex with **LQM560** (Fig. 8B), the protein presented a similar behavior, with values around 3.2 Å throughout the simulation, indicating overall structural stability

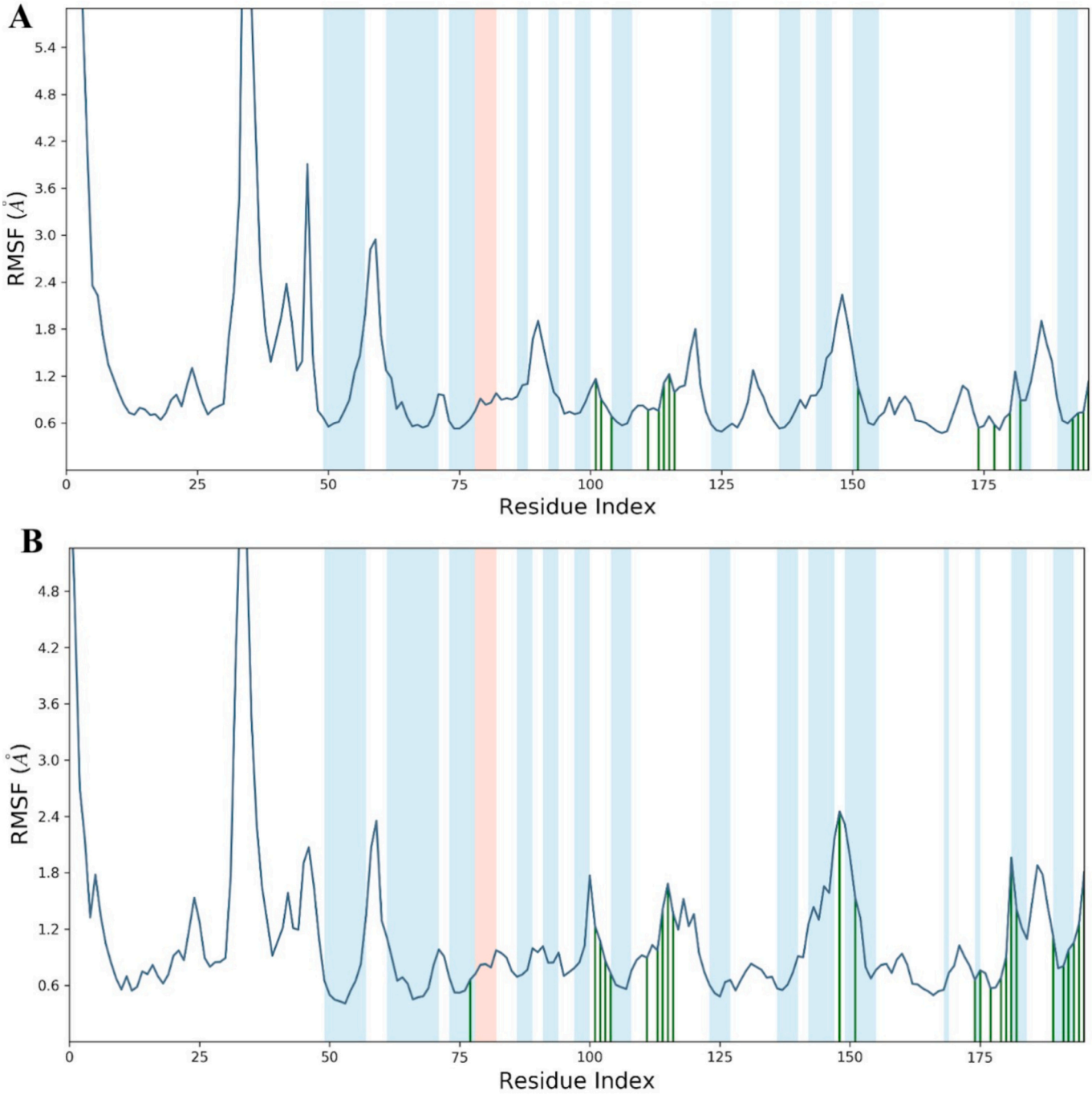

Fig. 9. Root mean square fluctuation (RMSF) plots per residue for the complexes formed between the target protein and ligands **LQM560** (A) and **LQM601** (B), over 100 ns of molecular dynamics simulations.

despite slight conformational adjustments. **LQM560** also showed excellent stability, with an average RMSD below 1.2 Å over the 100 ns, demonstrating that it remained well anchored in the binding site. Furthermore, both of these ligand-target complexes presented similar behavior than the ZIKV NS2B/NS3 apo-form in terms of RMSD values, suggesting that these compounds did not induce significant structural modifications (see Fig. 3S in the supplementary information).

The analysis of root mean square fluctuation (RMSF) reveals the most flexible residues of the proteins throughout the simulation (Fig. 9). In both complexes, it is observed that the N- and C-terminal regions exhibit the highest fluctuation peaks. RMSF values in these regions exceed 4.0 Å, reflecting high mobility. In the remaining regions, fluctuations remain below 2.0 Å, especially in areas with organized secondary structure elements, such as β-sheets (represented by blue bands in the plot) and the few α-helices (highlighted in red), which demonstrate greater rigidity and conformational stability during the simulation. In the case of the complex with **LQM601** (Fig. 9A), the residues in direct contact with the ligand (indicated by green bars) are predominantly located in regions with RMSF values below 1.5 Å, showing that the binding site remained stable. This reinforces the observation made in the RMSD analysis, indicating good ligand accommodation. For the complex with **LQM560** (Fig. 9B), although there is a pronounced RMSF peak, most residues in contact with the ligand are in moderately flexible regions, with RMSF between 0.8 and 1.6 Å. When comparing these results with the apo-form of NS2B/NS3 (see Fig. 4S in the supplementary information), it suggests that, although some mobility exists around the binding site, it does not compromise ligand stability. These findings indicate that **LQM560** and **LQM601** are associated with structurally compatible regions for stable interactions; however, **LQM601** exerts slightly less influence on the local mobility of the protein.

The analysis of intermolecular interactions in NS2B/NS3-**LQM601** complex revealed that the ligand establishes predominantly hydrophobic interactions with residues Ile^{123}, Val^{154}, Trp^{83}, Leu^{149}, Met,^{49} Leu^{76}, Ala^{164}, Ile^{165}, and Ala^{166} (Fig. 10). Relevant polar interactions were also observed with residues Asn^{167}, Thr^{120}, and Asn^{152}, as well as positive and negative electrostatic interactions with Lys^{74} and Asp^{75}, respectively. Additionally, several hydrogen bonds were formed between OH, C═O, and NH groups of the ligand and both protein residues and water molecules. In NS2B/NS3-**LQM560** complex, the ligand also exhibits a network of hydrophobic interactions with residues Leu^{85}, Val^{146}, Val^{147}, Ala^{164}, Ile^{165}, Ala^{166}, Leu^{78}, Ile^{123}, and Val^{154} (Fig. 10). A notable π–π stacking interaction was observed between the aromatic ring of the ligand and residue Trp^{83}, suggesting a favored orientation within the binding site. Residues Lys^{73} and Lys^{74} established important electrostatic contacts with the polar portion of the ligand. Furthermore, interactions with water molecules support the solubility of the hydroxylated end of the molecule and its peripheral orientation relative to the protein channel.

The MM/GBSA data analysis provided a quantitative assessment of the binding potential of the ligands to their respective targets after the 100 ns simulations. The NS2B/NS3-**LQM601** complex exhibited an average binding free energy (ΔG_{bind}) of −52.34 kcal/mol, with a standard deviation of ±7.36. The energy range varied from −61.97 to −37.69 kcal/mol, indicating moderately fluctuating energetic stability across the 10 analyzed frames. In contrast, the NS2B/NS3-**LQM560** complex showed a slightly more favorable average ΔG_{bind} value of −58.72 kcal/mol, with a standard deviation of ±5.20. The energy range spanned from −66.65 to −49.84 kcal/mol. Although it also demonstrated significant affinity, its energetic profile was slightly more favorable and more variable compared to NS2B/NS3-**LQM601** complex. These results suggest that **LQM560** displays greater stability and interaction potential with the target protein, as observed in our experimental inhibition assays.

3. Conclusions

It is undeniable that arboviruses have exerted a substantial impact on global public health, particularly the Zika and Chikungunya viruses. Given the absence of specific antiviral drugs for the treatment of these infections, and considering that certain heterocyclic-containing compounds have shown promising outcomes in previous studies — including those conducted by our research group—we herein investigated whether

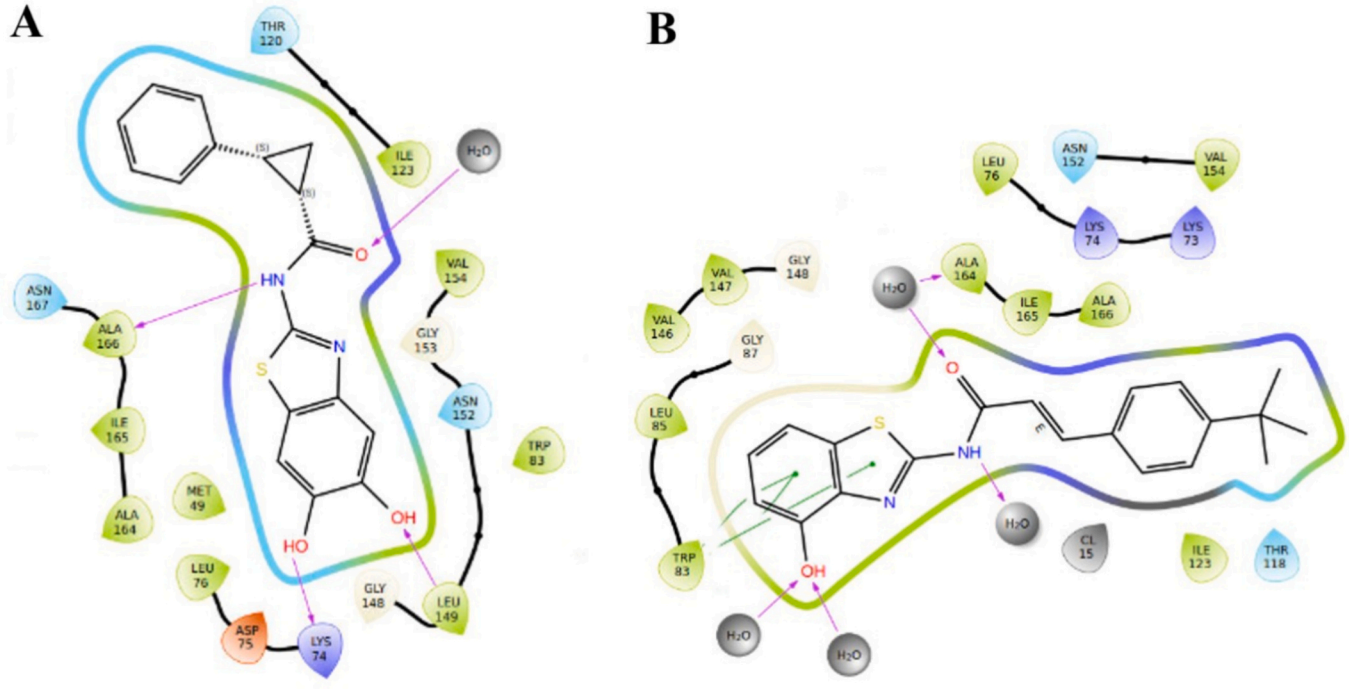

Fig. 10. 2D-diagrams of molecular interactions observed for the complexes between the NS2B/NS3-**LQM601** complex (A) and NS2B/NS3-**LQM560** complex (B) at the allosteric pocket of the protease over the course of the 100 ns simulation.

the molecular hybridization of benzothiazoles and acrylamides pharmacophores, could represent a valuable strategy to develop compounds with biological activity against more than one arbovirus, under the rationale of "*one pill, two targets*." Accordingly, a series of designed compounds bearing different electron-withdrawing (EWG) and electron-donating groups (EDG) were synthesized with satisfactory yields and subsequently characterized by various analytical techniques. Many of these compounds failed to inhibit the NS2B/NS3 proteases of ZIKV and DENV2; however, compounds **LQM537**, **560**, **581**, **601** and **604** were identified as selective allosteric inhibitors of ZIKV NS2B/NS3. Among them, **LQM581** exhibited the lowest CC_{50} values in Vero E6 cells, whereas **LQM604** showed the highest. In the antiviral plaque formation assay, unexpected but noteworthy results were observed: **LQM537** inhibited both ZIKV and CHIKV replication, while **LQM560** displayed inhibitory activity against ZIKV, CHIKV, and SINV. Within this context, **LQM537** exhibited greater selectivity toward CHIKV, whereas **LQM560** showed a preference for SINV, as further confirmed by qRT-PCR assays. Interestingly, **LQM560** and **LQM601** demonstrated the most potent inhibitory effects against ZIKV in qRT-PCR analyses. Subsequently, these four compounds were evaluated in immunofluorescence assays, where ZIKV- and CHIKV-positive cells were observed, suggesting that these molecules inhibit ZIKV replication by interfering with NS2B/NS3 protease activity. In contrast, FRET-based assays using CHIKV nsP2 revealed that **LQM537** and **LQM560** did not inhibit this protease. These findings indicate that their antiviral activity likely proceeds through an alternative mechanism, potentially acting as viral entry inhibitors, similar to compound **LQM334** previously reported by our research group. Isothermal titration calorimetry (ITC) assays corroborated this hypothesis, confirming the absence of direct interaction between these compounds and CHIKV nsP2. *In silico* studies of **LQM560** and **LQM601** against ZIKV NS2B/NS3 demonstrated that hydrophobic interactions predominated, although water-mediated hydrogen bridges — particularly involving the amide carbonyl — were also detected. MM/GBSA calculations further revealed that **LQM601** exhibits slightly higher binding affinity toward ZIKV NS2B/NS3 than **LQM560**, supporting the experimental enzymatic inhibition data. In conclusion, this study contributes substantially to the development antiviral agents and could inspire novel researches in the field to further investigate other hybrid compounds that could be promising against these virises.

4. Material and methods

4.1. Enzyme inhibition assays against ZIKV/DENV-2 N2B/NS3

The inhibitory activities of the final compounds (purity ≥95%) were determined by fluorimetric assays adapted from the literature [55]. The ZIKV and DENV2 proteases were obtained by heterologous expression in *Escherichia coli*, performed by collaborators at AK-Schirmeister. Cleavage of the fluorogenic substrate Boc-Gly-Arg-Arg-AMC (Bachem) resulted in increased fluorescence, which was monitored using a TECAN® Infinite F200 Pro microplate reader. The substrate and inhibitor dilutions were prepared as stock solutions in DMSO (20 mmol/L). Initially, biological screening was performed at 20 μM, and compounds with ≥60% inhibition were subjected to serial dilutions to determine IC_{50} values. Pure DMSO was used as a negative control. Experiments were conducted in triplicate, without pre-incubation, in white flat-bottom 96-well plates (200 μL). Each well contained 180 μL of buffer (50 mM Tris-HCl, 1 mM CHAPS, 20% glycerol, pH 9), 5 μL of protease (DENV2 at 50 nM or ZIKV at 26 nM), 10 μL of DMSO or inhibitor, and 5 μL of substrate. The amount of cleaved substrate was monitored by fluorescence (λex: 380 nm, λem: 450 nm; 25 °C; 21 cycles with 30 s intervals; gain 65; integration time 20 μs). Data were processed with GRAFIT® v.5.0.13 software. Residual enzymatic activity was calculated as a function of inhibitor concentration, and IC_{50} values were obtained by nonlinear regression using the Hill equation (1):

$$Y = \frac{Y_{max} - Y_{min}}{1 + \left(\frac{[I]}{IC_{50}}\right)} + Y_{min} \quad (1)$$

where Y *[ΔF/min]* is the substrate hydrolysis rate, Y_{max} represents the maximum value of the dose–response curve, measured at inhibitor concentrations of *[I] = 0 mM*, Y_{min} is the minimum value, obtained at high inhibitor concentrations, and s representing the Hill coefficient [56]. Finally, all these procedures are in agreement with our recent publications [24,30,31]. Buffers and substrates: DENV-2 NS2B/NS3 (250 nM enzyme) and ZIKV NS2B/NS3 (50 nM enzyme) (50 mM Tris pH 9.0, 20% (*v*/v) glycerol, 1 mM Chaps, 100 mM Boc-Gly-Arg-Arg-AMC) [57].

4.2. CHIKV nsP2 FRET protease activity assay

CHIKV nsP2 protease is purified as described in the previous studies by *Singh* et al. [58] and Souz et al. [44]. Following the purification, buffer exchange was performed in 25 mM Tris, 100 mM NaCl, pH -7.5 for doing FRET based protease inhibition assays, a well-established method for assessment of protease activity by CHIKV nsP2 protease [58]. Prior to conducting the FRET-based proteolytic assay for CHIKV nsP2 protease in presence of compounds, all **LQM** compounds were initially evaluated for intrinsic fluorescence at 360 nm excitation and 460/490 nm emission. For this purpose, the compounds were diluted to a final concentration of 200 μM in reaction buffer (20 mM Bis-Tris-Propane, pH 7.5) and were added to wells of 96-well black fluorescence assay plate. The fluorescence emission signal was monitored at 460 nm with the excitation wavelength of 360 nm using the multimode plate reader (Synergy BioTek HTX reader). Wells containing 15 μM of substrate peptide DABCYL-RAGG↓YIFS-EDANS (Biolinkk, New Delhi, India), corresponding to the nsP3/nsP4 cleavage site, served as negative control to benchmark fluorescence signals. Wells containing purified nsP2 protease (1 μM) incubated with substrate peptide were used as positive control to compare the obtained fluorescence signal. Reactions were performed in duplicates and the compounds exhibiting high intrinsic fluorescence signal were excluded from subsequent FRET-based assays. For determination of half-maximal inhibitory concentrations (IC_{50}) of **LQM** compounds, the enzymatic reactions were performed in 96-well black fluorescence assay plate containing 100 μL reaction volume in 20 mM Bis-Tris-Propane, pH 7.5 as assay buffer at 25 °C. Purified CHIKV nsP2 protease (final concentration of 1 μM) was pre-incubated for 20 min at 25 °C with compounds at different concentrations in the assay buffer. The reaction was initiated by addition of 15 μM substrate peptide DABCYL-RAGG↓YIFS-EDANS and the fluorescence readings were calculated at 360 and 460 nm excitation and emission wavelengths, respectively, using a multimode microplate reader (Synergy BioTek® HTX). Substrate incubated in assay buffer served as a negative control to eliminate all background signals and nsP2 protease incubated with substrate peptide in absence of inhibitors served as positive control to quantify percentage inhibition of nsP2 protease when incubated with inhibitors. Each reaction was set in duplicate and the results were plotted as dose-inhibition curves to calculate IC_{50} values.

4.3. Isothermal titration calorimetry assay

The thermodynamic parameters for the affinity of compounds (**LQM537** and **LQM560**) with CHIKV nsP2 protease were assessed using MicroCal ITC-200 (MicroCal, MA, USA). All samples utilized in the measurements were prepared and diluted in assay buffer containing 25 mM Tris (pH 7.5) and 250 mM NaCl, to minimize potential artifacts from buffer variability. CHIKV nsP2 protease and ligand at the respective concentrations were degassed and centrifuged to remove any precipitation. The ITC calorimetric cell was loaded with purified CHIKV nsP2 protease at 5 μM concentration. The compounds at a concentration of

500 μM to 1 mM in the syringe was programmed to titrate into the reaction cell with one injection of 0.4 μL followed by 13 injections of 3 μL at an interval of 180 s and at 25 °C. Multiple set of experiments were performed after varying the protein and ligands. Obtained ITC data was subsequently analyzed by MicroCal Origin 7.0 software from MicroCal. The ITC data was analyzed using the one-site binding model and the binding parameters (ΔH, ΔS, and K_D values) were obtained using Malvern's Origin 7.0 Microcal-ITC200 analysis software.

4.4. Cells and viruses

Vero cells (NCCS, Pune, India) were maintained in high-glucose Dulbecco's modified eagle medium (DMEM, Himedia; India) supplemented with 10% heat-inactivated fetal bovine serum (FBS, Gibco, USA), 100 units of penicillin, and 100 μg streptomycin/mL (Himedia, India). Cells were grown in a humidified atmosphere at 37 °C with 5% CO_2. Stocks of CHIKV (accession number KY057363.1; strain 119067) were maintained using standard viral adsorption technique and viral titer was determined by plaque assay prior to antiviral studies [59].

4.5. Determination of antiviral activity against CHIKV and SINV in Vero cells

To evaluate the antiviral potential of compounds, Vero cells were seeded in 24-well cell-culture plates at a density of 1×10^5 cells per well and were allowed to grow to confluency for 24 h at 37 °C and 5% CO_2. Firstly, the cytotoxicity of the compounds in Vero cells was assessed using the MTT assay [60], following the protocol established by Souza et al. [44]. The media with compound dilutions are prepared in a 96-well plate in triplicate, with compound concentrations varying from 0.24 μM to 500 μM. Following a 36-h incubation of the compound dilutions in cells, 20 μL of a 5 mg/mL MTT solution was added and incubated for an additional 4 h. Formazan crystals, generated within cells, are re-suspended in DMSO and reading were taken 560 nm using a multimode plate reader. For antiviral assessment, the cells were treated with the non-toxic concentrations of compounds for 3 h (pre-drug treatment) before virus inoculation. Post incubation, the compound-containing medium was removed and cells were subseqeuently infected with CHIKV or SINV at Multiplicity of infection (MOI) of 1 for 1.5 h. Later, the viral inoculum was removed and fresh low-serum media containing respective dilutions of compounds was added to the plate (post-treatment). Control wells, treated with an equivalent volume of DMSO and infected with respective viruses, served as virus controls. The plate was incubated for 24 h at 37 °C and 5% CO_2 and the cytopathic effect was observed. The supernatant from the plate was harvested and subjected to plaque-forming assay to quantify viral titers. The antiviral activity of compounds was also examined using indirect Immunofluorescence assay and the abundance of intracellular viral RNA was quantified using quantitative reverse transcription-polymerase chain reaction (qRT-PCR).

4.6. Plaque assay

Viral supernatants harvested from antiviral assays were subjected to plaque assay for quantification of infectious ZIKV, CHIKV or SINV titers. Briefly, Vero cells were seeded in 24-well plates at a density of 1×10^5 cells/well and cultured overnight in a humidified 5% CO_2 incubator at 37 °C. At 80–90% confluency, the cells were inoculated with ten-fold serially diluted cell-culture supernatants harvested from antiviral assay for 1.5 h. Post adsorption, the viral inoculum was removed, cells were washed with 1× PBS and were overlaid with fresh semi-solid overaly media containing 1:1 ratio of 2× MEM (Himedia, India) and carboxymethyl cellulose (2%) supplemented with 5% FBS. After 48 h of incubation, the cells were fixed with 10% solution of formaldehyde and stained with 1% crystal violet dye for visualization of plaques. The number of plaques were quantified, and PFU/mL (plaque-forming units per mL) was calculated. The EC_{50} values (concentration that inhibits 50% of the virus by the Plaque assay) on Vero cells were calculated by using nonlinear regression curve fitting and the selectivity indexes were obtained for each compound using the following equation: $SI = CC_{50}/EC_{50}$. The data represents mean and standard error from duplicate set of experiments.

4.7. RNA isolation and quantitative RT-PCR (qRT-PCR)

qRT-PCR assay was performed to quantify levels of intracellular viral RNA in cells treated with **LQM** compounds and infected with CHIKV or SINV. Using TRIzol (Invitrogen, USA) reagent, total RNA was isolated from cells as per manufacturer's instructions under RNase-free conditions. Subsequently, the viral RNA was reverse transcribed into complementary DNA using PrimeScript 1st strand cDNA Synthesis Kit (Takara Bio, USA) according to manufacturer's protocols. qRT-PCR was performed targeting the envelope gene of CHIKV and SINV using KAPA SYBR fast universal qPCR kit (Sigma-Aldrich, USA) on QuantStudio real-time PCR system (Applied Biosystems, CA). $\Delta\Delta Ct$ method was used to calculate the relative gene expression levels of viral RNA and β-actin was used as an endogenous control. The reactions were performed in duplicate and statistical significance in intracellular viral RNA between treatment groups and the *VC* was calculated using One-way ANOVA with Dunnett's multiple comparison test.

4.8. Immunofluoresence assays targeting Chikungunya and Zika viruses

Immunofluorescence assay was performed to verify the reduction of CHIKV load in cell-culture based studies. In a 6-well plate, subconfluent monolayers of Vero cells were subjected to compound treatments (pre- and post-infection) and infected with CHIKV at MOI of 1 for 1.5 h. After an incubation period of 36 h, the supernatant was removed and the cells were fixed using 500 μL of fixing reagent (Methanol: Acetone, 1:1 ratio). Post incubation period of 2 h, 0.1% of Triton X (diluted in 1× PBS) was added to each well and incubated for 7 min at room temperature to facilitate permeabilization of the cells. The plate was washed three times with 1× PBS and then 100 μL of 1:250 dilution of primary anti-alphavirus antibody (Santa Cruz Biotechnology Inc.) specific to the envelope protein of Alphavirus was added to each well at followed by an incubation period of 1 h. The cells were then gently washed three times with 1× PBS and then incubated with 100 μL of fluorescein isothiocyanate (FITC)-conjugated anti-mouse secondary antibody (1:500; Sigma) for 1 h. The cells were washed again with 1× PBS and were counterstained with 4′, 6-diamidino-2-phenylindole (DAPI; Himedia, India) for 15 min for localization of nucleus and then observed under EVOS FL Auto Imaging System (Thermo Fisher Scientific) using FITC and DAPI channels.

Regarding the assays involving ZIKV, all culture groups were fixed with 4% paraformaldehyde (PFA) in phosphate-buffered saline (PBS) for 15 min at room temperature. The fixative was then removed, and the samples were washed three times with PBS. Cell permeabilization was performed using 0.1% Triton X-100 (Sigma-Aldrich) in PBS for 10 min, followed by blocking of nonspecific antigenic sites with 0.05% fish skin gelatin (Merck/Sigma-Aldrich, Germany) in PBS for 30 min. Autofluorescence was subsequently quenched by incubation in PBS containing 3% glycine for 30 min. Next, samples were incubated overnight at 4 °C with a mouse-derived primary antibody against ZIKV NS1 (1:100, *v*/v in fish skin gelatin; clone E107, MA5–24585, Invitrogen, UK). After PBS washes, incubation with a tetramethylrhodamine isothiocyanate (TRITC)-conjugated anti-mouse secondary antibody (1:50, v/v in fish skin gelatin; Sigma-Aldrich) was carried out for 1 h at room temperature, followed by additional PBS washes. Mounting was performed using a PBS/glycerol mixture (1:3, *v*/v) under glass coverslips. Fluorescence imaging was conducted using a Nikon DS-Ri1 fluorescence microscope (Nikon, Japan), and image acquisition was performed with the DP2-BSW software (Nikon).

4.9. Liquid chromatography coupled to mass spectrometry (LC-MS)

The purity of the final compounds was determined using a HEWLETT PACKARD® 1100 series liquid chromatograph with a C18 column (75 mm × 2.0 mm, 1.6 μM, AGILENT® InfinityLab Poroshell 120 SB), using methanol ≥99% (HPLC grade) as the mobile phase. The analytical parameters were: sample concentration (1 mg/mL), flow rate (0.7 mL/min), run time (8 min), and injection volume (2 μL). Retention times (RT) were recorded in minutes and absorbance in mAU [61]. A LRMS AGILENT® 1100 mass spectrometer (positive ions trap mode) was coupled to the system to determine molecular masses (in Dalton – Da) by the *m/z* ratio, after ionization by electrospray (ESI). The monoisotopic mass was obtained through detection of pseudomolecular ions. These, in turn, correspond to the masses of the final compounds increased by 1 (one) Dalton ([M + H^+]), as well as by 23 (twenty-three) Daltons ([M + Na^+]).

4.10. Melting point

The melting points (°C) of the final compounds were determined using a digital device from A. KRÜSS OPTRONIC®, with a capacity of up to 360 °C, employing glass capillaries containing the solid samples. The measurement started at 40 °C, with a gradual increase until complete melting of the substance. The values obtained present a range of up to 2 °C [62].

4.11. Infrared spectrophotometry (FT-IR)

Infrared spectra were obtained using a THERMO SCIENTIFIC NICOLET® *Avatar 330 FT-IR* spectrophotometer, employing the attenuated total reflectance (ATR) method, in the range of 4000 to 600 cm^{-1} [63,64]. The analyses were performed using the OMNIC® 6.2 software (1992–2003), by Thermo Electron Corporation. The stretching vibrations (ν) and/or angular deformations (δ) of the main functional groups were recorded in transmittance by wavenumber (cm^{-1}), being classified, in some cases, according to symmetry: symmetric (*s*) or asymmetric (*as*) [65].

4.12. Nuclear magnetic resonance (NMR) of hydrogen (^1H) and carbon-13 (^{13}C)

The ^1H and ^{13}C NMR spectra were obtained using a BRUKER® UltraShield 300 MHz instrument, with DMSO-d_6 as the analytical solvent. For both intermediate and final compounds, a total number of scans (ns) of 32 and 4096 were used for ^1H and ^{13}C, respectively. Chemical shifts were recorded in parts per million (ppm), while coupling constants (*J*) were expressed in Hz. Signal multiplicities were classified as: singlet (s), broad singlet (br s), doublet (d), double doublet (*dd*), triplet of doublets (*td*), quartet (q), and multiplet (*m*) [66,67]. The analyses and spectral illustrations were performed using the TopSpin® 3.5 pl 7 software (2018–2019), from BRUKER® BioSpin GmbH.

4.13. Reaction procedures

4.13.1. Synthesis of cinnamic acid and (E)-3-(4-(tert-butyl)phenyl)acrylic acid

In a 250 mL round-bottom flask, 20 mL of pyridine and 6 g of the corresponding aldehyde (1 eq.) were added. Next, acetic anhydride (1.1 eq.) was added. The mixture was heated under reflux for 15 min, then *N*-methylpiperazine (10 mol%) was added as a catalytic base. The reaction was kept under reflux for 24 h. After monitoring by TLC, 20 mL of distilled H_2O were added, forming a white precipitate. The mixture was cooled (2 °C) for 30 min, stirred, and acidified with concentrated HCl (37%) to pH 1.0. The solid was filtered and washed with distilled H_2O (2 × 50 mL), yielding the product. Methodology adapted from Luo and collaborators (2015) [68].

Cinnamic acid – Yield: 97%; Aspect: white amorphous powder; ART-FTIR (Transmittance/cm^{-1}): 2830 δ(C—O); 1671 ν(C=O); 1627 ν(C=C_{ene}); 1074 ν(C_{Ar}=C_{Ar}). ^1H NMR (300 MHz, DMSO-d_6, ppm) δ 6.52 (d, 1H, J = 16.0 Hz, CH_{ene}); 7.39–7.41 (*m*, 3H, CH_{Ar}); 7.59 (d, 1H, J = 16.1 Hz, CH_{ene}); 7.65–7,68 (*m*, 2H, CH_{Ar}); 12.38 (br s, 1H, OH). ^{13}C NMR (75 MHz, DMSO-d_6, ppm) δ 119.68 (C_{ene}); 128.62 (C_{Ar}–C_{Ar}); 129.34 (C_{Ar}–C_{Ar}); 130.65 (C_{Ar}); 134.69 (C_q); 144.37 (C_{ene}); 168.01 (C=O).

(E)-3-(4-(tert-Butyl)phenyl)acrylic acid – Yield: 97%; Aspect: yellow crystalline powder; ART-FTIR (Transmittance/cm^{-1}): 2949 δ(C—O); 1668 ν(C=O); 1621 ν(C=C_{ene}); 1110 ν(C_{Ar}=C_{Ar}). ^1H NMR (300 MHz, DMSO-d_6, ppm) δ 1.26 (s, 9H, CH_3); 6.46 (d, 1H, J = 16.0 Hz, CH_{ene}); 7.41 (d, 2H, J = 8.4 Hz, CH_{Ar}); 7.55 (d, 1H, J = 16.1 Hz, CH_{ene}); 7.59 (d, 2H, J = 4.6 Hz, CH_{Ar}); 12.32 (br s, 1H, OH). ^{13}C NMR (75 MHz, DMSO-d_6, ppm) δ 31.35 ((CH_3)$_3$); 35.00 (C_{tert}); 118.76 (C_{ene}); 126.15 (C_{Ar}–C_{Ar}); 128.46 (C_{Ar}–C_{Ar}); 131.97 (C_q); 144.24 (C_{ene}); 153.55 (C_q); 168.11 (C=O).

4.13.2. Synthesis of acyl chlorides

In a 50 mL round-bottom flask, 6 mL of DMF were added under an inert argon atmosphere, followed by 500 mg of the corresponding cinnamic acid and then 2 eq. of thionyl chloride ($SOCl_2$). The mixture was stirred for 24 h at room temperature. After completion of the reaction, the crude mixture was slowly transferred to a saturated and cooled $NaHCO_3$ solution (10 mL), which was stirred, forming a precipitate after 10 min. The solid was filtered and washed with $NaHCO_3$ solution (3 × 10 mL) and distilled H_2O (2 × 20 mL), yielding the crude product. This was purified by recrystallization in acetone/H_2O (1:2).

Cinnamoyl chloride – Yield: 90%; Aspect: yellow amorphous powder. ART-FTIR (Transmittance/cm^{-1}): 1676 ν(C=O); 1627 ν(C=C_{ene}); 1066 ν(C_{Ar}=C_{Ar}). ^1H NMR (300 MHz, DMSO-d_6, ppm) δ 7.34 (d, 1H, J = 15.8 Hz, CH_{ene}); 7.44–7.49 (*m*, 3H, CH_{Ar}); 7.81 (d, 1H, J = 15.8 Hz, CH_{ene}); 7.83–7.86 (*m*, 2H, CH_{Ar}). ^{13}C NMR (75 MHz, DMSO-d_6, ppm) δ 117.35 (C_{ene}); 122.75 (C_{Ar}); 129.55 (C_{Ar}); 131.88 (C_{Ar}–C_{Ar}); 133.94 (C_{Ar}); 134.05 (C_q); 144.53 (C_{ene}); 163.17 (C=O).

(E)-3-(4-(tert-Butyl)phenyl)acryloyl chloride – Yield: 55%; Aspect: white amorphous powder. ART-FTIR (Transmittance/cm^{-1}): 1758 ν(C=O); 1707 ν(C=C_{ene}); 1071 ν(C_{Ar}=C_{Ar}). ^1H NMR (300 MHz, DMSO-d_6, ppm) δ 1.29 (s, 9H, CH_3); 6.76 (d, 1H, J = 15.9 Hz, CH_{ene}); 7.48 (d, 2H, J = 8.4 Hz, CH_{Ar}); 7.73 (d, 2H, J = 8.4 Hz, CH_{Ar}); 7.87 (d, 1H, J = 15.9 Hz, CH_{ene}). ^{13}C NMR (75 MHz, DMSO-d_6, ppm) δ 31.31 (($\underline{C}H_3$)$_3$); 35.20 (C_{terc}); 116.44 (C_{ene}); 126.35 (C_{Ar}–C_{Ar}); 129.35 (C_{Ar}–C_{Ar}); 131.39 (C_q); 148.94 (C_{ene}); 154.95 (C_q); 163.31 (C=O).

4.13.3. Synthesis of 2-amino-5,6-dimethoxybenzo[d]thiazole

In a 250 mL round-bottom flask, 100 mL of acetic acid, 5 g of 3,4-diethoxyaniline or 3,4-dimethoxyaniline (1 eq.), and 2.2 eq. of potassium isothiocyanate were added. The mixture was cooled in an ice bath, and bromine (1 eq.) was added dropwise. After reaching room temperature, the reaction was maintained for 24 h, forming a dark brown precipitate. The solid was filtered and subjected to reflux with concentrated HCl (37%) for 2 h. After this period, a filtration was carried out, and the liquid fraction was neutralized with potassium hydroxide (KOH) pellets in an ice bath (exothermic reaction). Finally, the precipitate was filtered and washed with distilled H_2O (2 × 50 mL), yielding the pure product.

2-Amino-5,6-dimethoxybenzo[d]thiazole **(43)** – Yield: 99%; Aspect: brown amorphous powder. ART-FTIR (Transmittance/cm^{-1}): 3370 ν(N—H)$_{as}$; 3350 ν(N—H)$_s$; 1053 ν(C_{Ar}=C_{Ar}); 981 ν(S—C). ^1H NMR (300 MHz, DMSO-d_6, ppm) δ 3.72 (d, 6H, J = 7.2 Hz, (CH_3)$_2$); 6.96 (s, 1H, CH_{Ar}); 7.19 (br s, 2H, NH_2); 7.27 (s, 1H, CH_{Ar}). ^{13}C NMR (75 MHz, DMSO-d_6, ppm) δ 56.14 ($\underline{C}H_3$); 56.66 ($\underline{C}H_3$); 102.80 (C_{Ar}); 105.28 (C_{Ar}); 121.80 (C_q); 145.06 (C_q); 147.13 ($\underline{C}$—O); 148.62 ($\underline{C}$—O); 166.29 ($\underline{C}$–NH_2).

4.13.4. Synthesis of 2-amino-6-(tert-butyl)benzo[d]thiazole

The initial procedure followed the same protocol described above

(item 3.5.1.3). However, it differed in the purification method. After 24 h of reaction, a white precipitate was formed. The mixture was neutralized with concentrated ammonia solution (25%) and subjected to liquid-liquid extraction with ethyl acetate and distilled H_2O (1:3). The organic phase was rotary evaporated, yielding an impure orange powder [69]. Purification was performed by classical column chromatography using petroleum ether/ethyl acetate (7:3) as the mobile phase, affording the pure product.

***2-A*mino*-6-(tert-butyl)benzothiazole* (44) –** Yield: 65%; Aspect: orange amorphous powder. ART-FTIR (Transmittance/cm^{-1}): 3431 ν (N—H)$_{as}$; 3280 ν(N—H)$_s$; 1044 ν(C_{Ar}=C_{Ar}); 905 ν(S—C). ^{1}H NMR (300 MHz, DMSO-d_6, ppm) δ 1.27 (s, 9H, $(CH_3)_3$); 7.23 (s, 2H, CH_{Ar}); 7.32 (br s, 2H, NH_2); 7.64 (s, 1H, CH_{Ar}). ^{13}C NMR (75 MHz, DMSO-d_6, ppm) δ 31.93 (($\underline{C}H_3)_3$); 34.75 (C_{tert}); 117.59 (C_{Ar}); 123.19 (C_{Ar}); 131.33 (C_q); 144.02 (C_{Ar}); 150.98 (C_q); 166.96 ($\underline{C}$–C_{terc}); 172.48 ($\underline{C}$–NH_2).

4.13.5. Coupling of 2-aminobenzo[d]thiazoles to cinnamic acid derivatives and trans-phenylcyclopropanecarboxylic acid

4.13.5.1. Non-halogenated derivatives. 2-Aminobenzo[*d*]thiazole (1 eq.) was added to a 25 mL flask containing 5 mL of DMF. Then, the corresponding cinnamic acid (1.1 eq.) and TBTU (1 eq.) were added. The mixture was stirred at room temperature for 10 min, after which DIPEA (3 eq.) was added as a catalytic base. The reaction was stirred for 48 h at room temperature. After completion, 20 mL of saturated $NaHCO_3$ solution were added, forming a precipitate, which was stirred for 15 min. The solid was filtered, washed with saturated $NaHCO_3$ solution (3 × 10 mL) and distilled H_2O (3 × 25 mL), yielding the crude product. This was purified by recrystallization in acetone:H_2O (1:2), affording the pure product.

4.13.5.2. Halogenated derivatives. In a 25 mL round-bottom flask, 100 mg of the corresponding halogenated 2-aminobenzothiazole were added to 3 mL of anhydrous DMF under an argon atmosphere, followed by the addition of Et_3N (4 eq.). The mixture was stirred at 70 °C for 30 min. Next, a solution of the corresponding acyl chloride (1.1 eq.) in anhydrous DMF, also under an argon atmosphere, was added to the initial mixture. The reaction proceeded under the same conditions for 24 h.

***(E)-N-(Benzo[d]thiazol-2-yl)cinnamamide* (LQM525)** – Yield: 70%; Aspect: yellow amorphous powder; R_F: 0.77; R_T: 1.09 min; Purity: 99%; Mp: 211–212 °C. ART-FTIR (Transmittance/cm^{-1}): 3164 ν (N—H)$_s$; 1688 ν(C=O); 1624 ν(C=C_{ene}); 1074 ν(C_{Ar}=C_{Ar}); 988 ν(S—C). ^{1}H NMR (300 MHz, DMSO-d_6, ppm) δ 6.83 (d, 1H, J = 15.3 Hz, CH_{ene}); 7.17 (*m*, 1H, CH_{Ar}); 7.28–7.4 (*m,* 4H, CH_{Ar}); 7.51–7.54 (*m*, 2H, CH_{Ar}); 7.61 (s, 1H, CH_{Ar}); 7.66 (d, 1H, CH_{ene}); 7.86 (d, 1H, CH_{Ar}); 12.45 (br s, 1H, NH). ^{13}C NMR (75 MHz, DMSO-d_6, ppm) δ 119.88 (C_{Ar}); 121.00 (C_{ene}); 122.18 (C_{Ar}); 124.04 (C_{Ar}); 126.61 (C_{Ar}); 128.59 (C_{Ar}); 129.36 (C_q); 129.59 (C_{Ar}); 131.0 (C_{Ar}); 132.15 (C_q); 134.65 (C_{Ar}); 143.6 (C_{ene}); 149.13 (C_q); 158.54 (C_{Ar}); 164.51 (C=O); 168.01 (C=N). $C_{16}H_{12}N_2OS$: 280.07 g/mol; LRMS (ESI$^+$): *m/z* ([M + H]$^+$) 281.1 (100%); 151.2 (3.4%); 131.2 (5.6%).

***(E)-N-(6-Fluorobenzo[d]thiazol-2-yl)cinnamamide* (LQM526)** – Yield: 69%; Aspect: white amorphous powder; R_F: 0.37; R_T: 1.32 min; Purity: 96%; Mp: 298–299 °C. ART-FTIR (Transmittance/cm^{-1}): 3153 ν (N—H); 1682 ν(C=O); 1624 ν(C=C_{ene}); 1093 ν(C_{Ar}=C_{Ar}); 920 ν(S—C). ^{1}H NMR (300 MHz, DMSO-d_6, ppm) δ 6.95 (d, 1H, J = 15.6 Hz, CH_{ene}); 7.29 (*td*, 1H, J = 9.0 and 2.7 Hz, CH_{Ar}); 7.46–7.51 (*m,* 3H, CH_{Ar}); 7.65–7.68 (*m*, 2H, CH_{Ar}); 7.74–7.79 (*m,* 1H, CH_{Ar}); 7.8 (d, 1H, J = 15.6 Hz, CH_{ene}); 7.91 (d, 1H, CH_{Ar}); 12.61 (br s, 1H, NH). ^{13}C NMR (75 MHz, DMSO-d_6, ppm) δ 108.46 (C_{Ar}); 108.81 (C_{Ar}); 119.74 (C_{Ar}); 122.06 (C_{ene}); 128.61 (C_{Ar}–C_{Ar}); 129.59 (C_{Ar}–C_{Ar}); 131.03 (C_q); 133.34 (C_q); 134.63 (C_{Ar}); 143.70 (C_{ene}); 145.89 (C_q); 158.56 ($\underline{C}$—F); 164.57 (C=O); 168.63 (C=N). $C_{16}H_{11}FN_2OS$: 298.06 g/mol; LRMS (ESI$^+$): *m/z* ([M + H]$^+$) 299.1 (100%); 169.1 (1.2%); 131.2 (5.6%).

***(E)-N-(4,6-Difluorobenzo[d]thiazol-2-yl)cinnamamide* (LQM527)** – Yield: 71%; Aspect: powder white amorphous; R_F: 0.47; R_T: 1.62 min; Purity: 96%; Mp: 268–269 °C. ART-FTIR (Transmittance/cm^{-1}): 3060 ν (N—H); 1664 ν(C=O); 1614 ν(C=C_{ene}); 1020 ν(C_{Ar}=C_{Ar}); 987 ν(S—C). ^{1}H NMR (300 MHz, DMSO-d_6, ppm) δ 6.92 (d, 1H, J = 15.9 Hz, CH_{ene}); 7.32–7.4 (*m,* 1H, CH_{Ar}); 7.46–7.51 (*m,* 3H, CH_{Ar}); 7.65–7.68 (*m*, 2H, CH_{Ar}); 7.79–7.84 (*m,* 2H, CH_{Ar} and CH_{ene}); 12.79 (br s, 1H, NH). ^{13}C NMR (75 MHz, DMSO-d_6, ppm) δ 104.76 (C_{Ar}); 105.12 (C_{Ar}); 119.51 (C_{ene}); 128.64 (C_{Ar}–C_{Ar}); 129.58 (C_{Ar}–C_{Ar}); 131.10 (C_q); 134.55 (C_q); 135.31 (C_{Ar}); 135.38 (C_{ene}); 143.99 (C_q); 155.48 ($\underline{C}$—F); 158.32 ($\underline{C}$—F); 159.10 (C=O); 164.72 (C=N). $C_{16}H_{10}F_2N_2OS$: 316.05 g/mol; LRMS (ESI$^+$): *m/z* ([M + H]$^+$) 317.1 (100%); 131.2 (5.1%).

***(E)-N-(6-Chlorobenzo[d]thiazol-2-yl)cinnamamide* (LQM528)** – Yield: 61%; Aspect: white amorphous powder; R_F: 0.5; R_T: 1.86 min; Purity: 99%; Mp: 269–270 °C. ART-FTIR (Transmittance/cm^{-1}): 3064 ν (N—H); 1684 ν(C=O); 1623 ν(C=C_{ene}); 1099 ν(C_{Ar}=C_{Ar}); 988 ν(S—C). ^{1}H NMR (300 MHz, DMSO-d_6, ppm) δ 6.98 (d, 1H, J = 15.9 Hz, CH_{ene}); 7.46–7.51 (*m*, 4H, CH_{Ar}); 7.66–7.68 (*m,* 2H, CH_{Ar}); 7.75 (d, 1H, J = 8.9 Hz, CH_{Ar}); 7.8 (d, 1H, J = 15.9 Hz, CH_{ene}); 8.14 (d, 1H, J = 1.76, CH_{Ar}); 12.71 (br s, 1H, NH). ^{13}C NMR (75 MHz, DMSO-d_6, ppm) δ 119.70 (C_{Ar}); 121.91 (C_{Ar}); 122.22 (C_{ene}); 126.96 (C_{Ar}); 128.08 (C_{Ar}); 128.63 (C_{Ar}–C_{Ar}); 129.59 (C_{Ar}–C_{Ar}); 131.07 ($\underline{C}$—Cl); 133.86 (C_q); 134.61 (C_q); 143.82 (C_{ene}); 148.05 (C_q); 159.38 (C=O); 164.68 (C=N). $C_{16}H_{11}ClN_2OS$: 314.03 g/mol; LRMS (ESI$^+$): *m/z* ([M + H]$^+$) 315.1 (100%); 185.0 1.4%); 131.3 (4.6%).

***(E)-N-(4-Chlorobenzo[d]thiazol-2-yl)cinnamamide* (LQM529)** – Yield: 79%; Aspect: beige amorphous powder; R_F: 0.42; R_T: 1.75 min; Purity: 95%; Mp: 127–128 °C. ART-FTIR (Transmittance/cm^{-1}): 3111 ν (N—H); 1686 ν(C=O); 1619 ν(C=C_{ene}); 1071 ν(C_{Ar}=C_{Ar}); 981 ν(S—C). ^{1}H NMR (300 MHz, DMSO-d_6, ppm) δ 6.93 (d, 1H, J = 15.9 Hz, CH_{ene}); 7.27 (t, 1H, CH_{Ar}); 7.44–7.52 (*m,* 4H, CH_{Ar}); 7.63–7.66 (*m,* 2H, CH_{Ar}); 7.78 (d, 1H, J = 15.9 Hz, CH_{ene}); 7.98 (*dd,* 1H, J = 7.9 and 1.2 Hz, CH_{Ar}); 12.44 (br s, 1H, NH). ^{13}C NMR (75 MHz, DMSO-d_6, ppm) δ 120.68 (C_{ene}); 121.17 (C_{Ar}); 124.47 ($\underline{C}$—Cl); 124.6 (C_{Ar}); 126.47 (C_{Ar}); 128.53 (C_{Ar}–C_{Ar}); 129.55 (C_{Ar}–C_{Ar}); 130.87 (C_q); 133.92 (C_{Ar}); 134.79 (C_q); 143.24 (C_{ene}); 146.26 (C_q); 160.7 (C=O); 165.47 (C=N). $C_{16}H_{11}ClN_2OS$: 314.03 g/mol; LRMS (ESI$^+$): *m/z* ([M + H]$^+$) 315.1 (100%); 185.1 (1.4%); 131.2 (7.1%).

***(E)-N-(6-Bromobenzo[d]thiazol-2-yl)cinnamamide* (LQM530)** – Yield: 66%; Aspect: white amorphous powder; R_F: 0.62; R_T: 2.06 min; Purity: 99%; Dp: 315–316 °C. ART-FTIR (Transmittance/cm^{-1}): 3162 ν (N—H); 1684 ν(C=O); 1626 ν(C=C_{ene}); 1085 ν(C_{Ar}=C_{Ar}); 989 ν(S—C). ^{1}H NMR (300 MHz, DMSO-d_6, ppm) δ 7.12 (d, 1H, J = 15.9 Hz, CH_{ene}); 7.45–7.51 (*m*, 3H, CH_{Ar}); 7.57 (*dd,* 1H, J = 8.6 and 1.9 Hz, CH_{Ar}); 7.65–7.68 (*m*, 2H, CH_{Ar}); 7.73 (d, 1H, J = 14.4 Hz, CH_{Ar}); 7.8 (d, 1H, J = 15.9 Hz, CH_{ene}); 8.26 (d, 1H, J = 2.0 Hz, CH_{Ar}); 12.85 (br s, 1H, NH). ^{13}C NMR (75 MHz, DMSO-d_6, ppm) δ 115.94 ($\underline{C}$—Br); 119.89 (C_{Ar}); 122.63 (C_{ene}); 124.71 (C_{Ar}); 128.63 ((C_{Ar})$_3$); 129.58 (C_{Ar}–C_{Ar}); 131.04 (C_q); 134.38 (C_q); 134.66 (C_{Ar}); 143.65 (C_{ene}); 148.45 (C_q); 159.29 (C=O); 164.79 (C=N). $C_{16}H_{11}BrN_2OS$: 357.98 g/mol; LRMS (ESI$^+$): *m/z* ([M + H]$^+$) 361.0 (100%); 228.9 (1.3%); 131.2 (5.4%).

***(E)-N-(6-(Trifluoromethyl)benzo[d]thiazol-2-yl)cinnamamide* (LQM531)** – Yield: 65%; Aspect: white amorphous powder; R_F: 0.8; R_T: 2.08 min; Purity: 98%; Mp: 193–194 °C. ART-FTIR (Transmittance/cm^{-1}): 3066 ν(N—H); 1686 ν(C=O); 1628 ν(C=C_{ene}); 1055 ν(C_{Ar}=C_{Ar}); 982 ν(S—C). ^{1}H NMR (300 MHz, DMSO-d_6, ppm) δ 6.97 (d, 1H, J = 15.8 Hz, CH_{ene}); 7.46–7.53 (*m,* 4H, CH_{Ar}); 7.64–7.69 (*m,* 2H, CH_{Ar}); 7.83 (d, 1H, J = 15.8 Hz, CH_{ene}); 7.92 (d, 1H, J = 8.4 Hz, CH_{Ar}); 8.51 (s, 1H, CH_{Ar}); 12.8 Hz (br s, 1H, NH). ^{13}C NMR (75 MHz, DMSO-d_6, ppm) δ 119.56 (C_{Ar}); 121.40 (C_{ene}); 124.41 ($\underline{C}F_3$); 128.68 (C_{Ar}– C_{Ar}); 129.61 ((C_{Ar})$_3$); 131.14 (C_q); 132.71 (C_q); 134.55 (C_{Ar}); 144.15 (C_{Ar}); 146.14 (C_{ene}); 148.72 (C_q); 151.89 (C_q); 161.78 (C=O); 164.88 (C=N). $C_{17}H_{11}F_3N_2OS$: 348.05 g/mol; LRMS (ESI$^+$): *m/z* ([M + H]$^+$) 349.1 (100%); 131.3 (3.3%).

***(E)-N-(4-Methylbenzo[d]thiazol-2-yl)cinnamamide* (LQM532)** – Yield: 68%; Aspect: yellow amorphous powder; R_F: 0.4; R_T: 1.71 min; Purity: 98%; Mp: 120–121 °C. ART-FTIR (Transmittance/cm^{-1}): 3175 ν

(N—H); 1650 ν(C=O); 1616 ν(C=C_{ene}); 1078 ν(C_{Ar}=C_{Ar}); 979 ν(S—C). ^{1}H NMR (300 MHz, DMSO-d_6, ppm) δ 2.59 (s, 3H, CH_3); 6.97 (d, 1H, J = 15.8 Hz, CH_{ene}); 7.18 (m, 2H, CH_{Ar}); 7.46–7.51 (m, 3H, CH_{Ar}); 7.64–7.67 (m, 2H, CH_{Ar}); 7.76–7.81 (m, 2H, CH_{Ar} and CH_{ene}); 12.69 (br s, 1H, NH). ^{13}C NMR (75 MHz, DMSO-d_6, ppm) δ 18.43 ($\underline{C}H_3$); 119.56 (C_{Ar}); 119.90 (C_{Ar}); 124.01 (C_{ene}); 127.09 (C_{Ar}); 128.55 (C_{Ar}–C_{Ar}); 129.59 (C_{Ar}–C_{Ar}); 130.29 (C_q); 130.97 (C_q); 131.81 ($\underline{C}$–CH_3); 134.67 (C_{Ar}); 143.29 (C_{ene}); 148.23 (C_q); 157.67 (C=O); 164.43 (C=N). $C_{17}H_{14}N_2OS$: 294.08 g/mol; LRMS (ESI$^+$): m/z ([M + H]$^+$) 295.1 (100%); 165.1 (2.4%); 131.2 (1.5%).

***(E)-N-(6-Methylbenzo[d]thiazol-2-yl)cinnamamide* (LQM533)** – Yield: 80%; Aspect: yellow amorphous powder; R_F: 0.37; R_T: 1.52 min; Purity: 95%; Mp: 265–266 °C. ART-FTIR (Transmittance/cm^{-1}): 3060 ν (N—H); 1684 ν(C=O); 1625 ν(C=C_{ene}); 1069 ν(C_{Ar}=C_{Ar}); 983 ν(S—C). ^{1}H NMR (300 MHz, DMSO-d_6, ppm) δ 2.41 (s, 3H, CH_3); 6.95 (d, 1H, J = 15.8 Hz, CH_{ene}); 7.25 (dd, 1H, J = 8.1 and 1.3 Hz, CH_{Ar}); 7.45–7.52 (m, 3H, CH_{Ar}); 7.62–7.67 (m, 3H, CH_{Ar}); 7.75–7.8 (m, 2H, CH_{Ar} and CH_{ene}); 12.49 (br s, 1H, NH). ^{13}C NMR (75 MHz, DMSO-d_6, ppm) δ 21.46 ($\underline{C}H_3$); 119.97 (C_{Ar}); 120.64 (C_{Ar}); 121.75 (C_{ene}); 127.92 (C_{Ar}); 128.56 (C_{Ar}–C_{Ar}); 129.57 (C_{Ar}–C_{Ar}); 130.94 (C_q); 132.31 (C_q); 133.52 ($\underline{C}$–CH_3); 134.68 (C_{Ar}); 143.4 (C_{ene}); 147.13 (C_q); 157.66 (C=O); 164.38 (C=N). $C_{17}H_{14}N_2OS$: 294.08 g/mol; LRMS (ESI$^+$): m/z ([M + H]$^+$) 295.1 (100%); 165.1 (2.8%); 131.2 (1.3%).

***(E)-N-(5,6-Dimethylbenzo[d]thiazol-2-yl)cinnamamide* (LQM534)** – Yield: 86%; Aspect: brown amorphous powder; R_F: 0.42; R_T: 1.87 min; Purity: 95%; Mp: 219–220 °C. ART-FTIR (Transmittance/cm^{-1}): 3138 ν(N—H); 1663 ν(C=O); 1620 ν(C=C_{ene}); 1046 ν(C_{Ar}=C_{Ar}); 987 ν(S—C). ^{1}H NMR (300 MHz, DMSO-d_6, ppm) δ 2.31 (s, 6H, $(CH_3)_2$); 6.94 (d, 1H, J = 15.9 Hz, CH_{ene}); 7.45–7.49 (m, 3H, CH_{Ar}); 7.55 (s, 1H, CH_{Ar}); 7.63–7.66 (m, 2H, CH_{Ar}); 7.71 (s, 1H, CH_{Ar}); 7.76 (d, 1H, J = 15.9 Hz, CH_{ene}); 12.46 (br s, 1H, NH). ^{13}C NMR (75 MHz, DMSO-d_6, ppm) δ 20.01 ($\underline{C}H_3$); 20.16 ($\underline{C}H_3$); 120.00 (C_{Ar}); 121.36 (C_{ene}); 121.89 (C_{Ar}); 128.54 (C_{Ar}–C_{Ar}); 129.53 (C_q); 129.56 (C_{Ar}–C_{Ar}); 130.92 (C_q); 132.91 (C_{Ar}); 134.69 ($\underline{C}$–CH_3); 135.26 ($\underline{C}$–CH_3); 143.30 (C_{ene}); 147.71 (C_q); 157.58 (C=O); 164.28 (C=N). $C_{18}H_{16}N_2OS$: 308.1 g/mol; LRMS (ESI$^+$): m/z ([M + H]$^+$) 309.1 (100%); 179.1 (3.3%).

***(E)-N-(6-(tert-Butyl)benzo[d]thiazol-2-yl)cinnamamide* (LQM535)** – Yield: 57%; Aspect: yellow amorphous powder; R_F: 0.46; R_T: 1.29 min; Purity: 98%; Mp: 173–174 °C. ART-FTIR (Transmittance/cm^{-1}): 2959 ν(N—H); 1693 ν(C=O); 1616 ν(C=C_{ene}); 1084 ν(C_{Ar}=C_{Ar}); 921 ν(S—C). ^{1}H NMR (300 MHz, DMSO-d_6, ppm) δ 1.33 (s, 9H, $(CH_3)_3$); 6.96 (d, 1H, J = 15.8 Hz, CH_{ene}); 7.64–7.73 (m, 6H, CH_{Ar}); 7.78 (d, 1H, J = 15.7 Hz, CH_{ene}); 7.96 (s, 1H, CH_{Ar}); 7.99 (s, 1H, CH_{Ar}); 12.52 (br s, 1H, NH). ^{13}C NMR (75 MHz, DMSO-d_6, ppm) δ 31.88 (($\underline{C}H_3$)$_3$); 35.15 (C_{terc}); 110.03 (C_{Ar}); 118.25 (C_{ene}); 124.40 (C_{Ar}); 124.97 (C_{Ar}); 127.85 (C_{Ar}); 128.57 (C_{Ar}); 128.66 (C_{Ar}); 129.36 (C_{Ar}); 129.59 (C_{Ar}); 130.68 (C_q); 134.67 (C_q); 141.87 (C_{ene}); 143.24 ($\underline{C}$–C_{terc}); 158.06 (C_q); 164.37 (C=O); 168.03 (C=N). $C_{20}H_{20}N_2OS$: 336.13 g/mol; LRMS (ESI$^+$): m/z ([M + H]$^+$) 337.1 (100%); 207.2 (2.5%); 131.2 (5.6%).

***(E)-N-(6-Methoxybenzo[d]thiazol-2-il)cinnamamide* (LQM536)** – Yield: 80%; Aspect: yellow amorphous powder; R_F: 0.82; R_T: 1.14 min; Purity: 96%; Mp: 259–261 °C. ART-FTIR (Transmittance/cm^{-1}): 3165 ν (N—H); 1681 ν(C=O); 1621 ν(C=C_{ene}); 1058 ν(C_{Ar}=C_{Ar}); 998 ν(S—C). ^{1}H NMR (300 MHz, DMSO-d_6, ppm) δ 3.81 (s, 3H, CH_3); 6.94 (d, 1H, J = 15.8 Hz, CH_{ene}); 7.04 (dd, 1H, J = 8.8 and 2.4 Hz, CH_{Ar}); 7.46–7.5 (m, 3H, CH_{Ar}); 7.58 (d, 1H, J = 2.4 Hz, CH_{Ar}); 7.64–7.67 (m, 3H, CH_{Ar}); 7.77 (d, 1H, J = 15.8 Hz, CH_{ene}); 12.46 (br s, 1H, NH). ^{13}C NMR (75 MHz, DMSO-d_6, ppm) δ 56.11 ($\underline{C}H_3$); 105.20 (C_{Ar}); 115.41 (C_{Ar}); 119.95 (C_{Ar}); 121.62 (C_{ene}); 128.55 (C_{Ar}–C_{Ar}); 128.65 (C_q); 129.57 (C_{Ar}–C_{Ar}); 130.93 (C_q); 133.49 (C_q); 134.70 (C_{Ar}); 143.29 (C_{ene}); 156.47 ($\underline{C}$–OCH_3); 156.65 (C=O); 164.25 (C=N). $C_{17}H_{14}N_2O_2S$: 310.08 g/mol; LRMS (ESI$^+$): m/z ([M + H]$^+$) 311.1 (100%); 181.1 (4.2%); 131.2 (1.2%).

***(E)-N-(6-Ethoxybenzo[d]thiazol-2-yl)cinnamamide* (LQM537)** – Yield: 72%; Aspect: orange amorphous powder; R_F: 0.35; R_T: 1.46 min; Purity: 95%; Mp: 222–223 °C. ART-FTIR (Transmittance/cm^{-1}): 3176 ν (N—H); 1683 ν(C=O); 1623 ν(C=C_{ene}); 1061 ν(C_{Ar}=C_{Ar}); 977 ν(S—C). ^{1}H NMR (300 MHz, DMSO-d_6, ppm) δ 1.35 (t, 3H, J = 6.9 Hz, CH_3); 4.07 (q, 2H, J = 6.9 Hz, OCH_2); 6.94 (d, 1H, J = 15.8 Hz, CH_{ene}); 7.02 (dd, 1H, J = 8.6 and 2.4 Hz, CH_{Ar}); 7.45–7.47 (m, 3H, CH_{Ar}); 7.56 (d, 1H, J = 2.4 Hz, CH_{Ar}); 7.62–7.67 (m, 3H, CH_{Ar}); 7.77 (d, 1H, J = 15.8 Hz, CH_{Ar}); 12.44 (br s, 1H, NH). ^{13}C NMR (75 MHz, DMSO-d_6, ppm) δ 15.15 ($\underline{C}H_3$); 64.09 ($\underline{C}H_2$); 105.87 (C_{Ar}); 115.76 (C_{Ar}); 120.0 (C_{ene}); 121.60 (C_{Ar}); 128.54 (C_{Ar}–C_{Ar}); 129.57 (C_{Ar}–C_{Ar}); 129.63 (C_q); 130.91 (C_{Ar}); 133.48 (C_q); 133.48 (C_q); 143.26 (C_{ene}); 155.87 ($\underline{C}$–OCH_2CH_3); 156.45 (C=O); 164.24 (C=N). $C_{18}H_{16}N_2O_2S$: 324.09 g/mol; LRMS (ESI$^+$): m/z ([M + H]$^+$); 325.1 (100%); 195.1 (2.3%); 131.3 (1.3%).

***(E)-N-(4-Methoxybenzo[d]thiazol-2-yl)cinnamamide* (LQM538)** – Yield: 70%; Aspect: yellow amorphous powder; R_F: 0.65; R_T: 1.17 min; Purity: 95%; Mp: 132–134 °C. ART-FTIR (Transmittance/cm^{-1}): 3245 ν (N—H); 1670 ν(C=O); 1628 ν(C=C_{ene}); 1045 ν(C_{Ar}=$_{Ar}$); 972 ν(S—C). ^{1}H NMR (300 MHz, DMSO-d_6, ppm) δ 3.92 (s, 3H, CH_3); 6.9 (d, 1H, J = 15.7 Hz, CH_{ene}); 7.0 (d, 1H, J = 7.9 Hz, CH_{Ar}); 7.26 (t, 1H, J = 8.0 Hz, CH_{Ar}); 7.45–7.49 (m, 3H, CH_{Ar}); 7.54 (d, 1H, J = 8.0 Hz, CH_{Ar}); 7.64–7.67 (m, 2H, CH_{Ar}); 7.79 (d, 1H, J = 15.7 Hz, CH_{ene}); 12.72 (br s, 1H, NH). ^{13}C NMR (75 MHz, DMSO-d_6, ppm) δ 56.31 ($\underline{C}H_3$); 108.17 (C_{Ar}); 113.99 (C_{Ar}); 125.03 (C_{ene}); 128.57 (C_{Ar}–C_{Ar}); 129.57 (C_{Ar}–C_{Ar}); 130.97 (C_q); 133.52 (C_q); 134.64 (C_{Ar}); 139.04 (C_q); 143.46 (C_{ene}); 152.33 (C_q); 156.95 (C=O); 164.30 (C=N). $C_{17}H_{14}N_2O_2S$: 310.08 g/mol; LRMS (ESI$^+$): m/z ([M + H]$^+$) 311.1 (100%); 181.1 (4.2%); 131.2 (1.2%).

***(E)-N-(5,6-Dimethoxybenzo[d]thiazol-2-il)cinnamamide* (LQM539)** – Yield: 68%; Aspect: yellow amorphous powder; R_F: 0.42; R_T: 0.94 min; Purity: 98%; Mp: 140–141 °C. ART-FTIR (Transmittance/cm^{-1}): 3153 ν(N—H); 1679 ν(C=O); 1626 ν(C=C_{ene}); 1030 ν(C_{Ar}=C_{Ar}); 977 ν(S—C). ^{1}H NMR (300 MHz, DMSO-d_6, ppm) δ 3.82 (d, 6H, J = 5.4 Hz, CH_3); 6.96 (d, 1H, J = 15.8 Hz, CH_{ene}); 7.31 (s, 1H, CH_{Ar}); 7.45–7.51 (m, 3H, CH_{Ar}); 7.56 (s, 1H, CH_{Ar}); 7.64–7.69 (m, 2H, CH_{Ar}); 7.75 (d, 1H, J = 15.8 Hz, CH_{ene}); 12.42 (br s, 1H, NH). ^{13}C NMR (75 MHz, DMSO-d_6, ppm) δ 56.19 ($O\underline{C}H_3$); 56.42 ($O\underline{C}H_3$); 103.98 (C_{Ar}); 120.02 (C_{Ar}); 123.64 (C_{ene}); 128.52 (C_{Ar}–C_{Ar}); 129.36 (C_q); 129.57 (C_{Ar}–C_{Ar}); 130.88 (C_q); 134.68 (C_{Ar}); 143.12 (C_{ene}); 143.19 (C_q); 147.48 ($\underline{C}$–OCH_3); 149.43 ($\underline{C}$–OCH_3); 156.94 (C=O); 163.99 (C=N). $C_{18}H_{16}N_2O_3S$: 340.09 g/mol; LRMS (ESI$^+$): m/z ([M + H]$^+$) 341.1 (100%); 211.1 (1.7%).

***(E)-N-(6-Hydroxybenzo[d]thiazol-2-yl)cinnamamide* (LQM540)** – Yield: 98%; Aspect: yellow amorphous powder; R_F: 0.35; R_T: 0.73 min; Purity: 97%; Mp: 272–273 °C. ART-FTIR (Transmittance/cm^{-1}): 3320 δ(O—H); 3149 ν(N—H); 1664 ν(C=O); 1604 ν(C=C_{ene}); 1020 ν (C_{Ar}=C_{Ar}); 918 ν(S—C). ^{1}H NMR (300 MHz, DMSO-d_6, ppm) δ 6.87–6.89 (m, 1H, CH_{Ar}); 6.93 (d, 1H, J = 15.8 Hz, CH_{ene}); 7.3 (s, 1H, CH_{Ar}); 7.45–7.49 (m, 3H, CH_{Ar}); 7.55 (d, 1H, J = 8.6 Hz, CH_{Ar}); 7.62–7.68 (m, 2H, CH_{Ar}); 7.75 (d, 1H, CH_{ene}); 9.56 (br s, 1H, OH); 12.39 (br s, 1H, NH). ^{13}C NMR (75 MHz, DMSO-d_6, ppm) δ 107.24 (C_{Ar}); 116.03 (C_{Ar}); 120.30 (C_{Ar}); 121.90 (C_{ene}); 128.81 (C_{Ar}); 129.86 (C_{Ar}–C_{Ar}); 131.18 (C_{Ar}–C_{Ar}); 133.76 (C_q); 134.40 (C_q); 142.51 (C_{ene}); 143.4 (C_q); 154.97 ($\underline{C}$–OH); 155.83 ($\underline{C}$=O); 164.39 ($\underline{C}$=N). $C_{16}H_{12}N_2O_2S$: 296.06 g/mol; LRMS (ESI$^+$): m/z ([M + H]$^+$) 297.1 (100%); 167.0 (3.8%); 131.1 (4.9%).

***(E)-N-(4-Hydroxybenzo[d]thiazol-2-yl)cinnamamide* (LQM541)** – Yield: 98%; Aspect: yellow amorphous powder; R_F: 0.32; R_T: 0.84 min; Purity: 96%; Mp: 272–273 °C. ART-FTIR (Transmittance/cm^{-1}): 3324 δ(O—H); 3182 ν(N—H); 1687 ν(C=O); 1629 ν(C=C_{ene}); 1053 ν (C_{Ar}=C_{Ar}); 931 ν(S—C). ^{1}H NMR (300 MHz, DMSO-d_6, ppm) δ 6.84 (d, 1H, J = 7.9 Hz, CH_{Ar}); 6.94 (d, 1H, J = 15.8 Hz, CH_{ene}); 7.11 (t, 1H, J = 7.9 Hz, CH_{Ar}); 7.38 (d, 1H, J = 7.9 Hz, CH_{Ar}); 7.45–7.50 (m, 3H, CH_{Ar}); 7.64–7.67 (m, 2H, CH_{Ar}); 7.78 (d, 1H, J = 15.7 Hz, CH_{ene}); 9.79 (br s, 1H, OH); 12.61 (br s, 1H, NH). ^{13}C NMR (75 MHz, DMSO-d_6, ppm) δ 112.18 (C_{Ar}); 112.68 (C_{Ar}); 120.37 (C_{ene}); 125.44 (C_{Ar}); 128.94 (C_{Ar}–C_{Ar}); 129.96 (C_{Ar}–C_{Ar}); 131.33 (C_q); 134.21 (C_{Ar}); 135.07 (C_q); 138.88 (C_{ene}); 143.67 (C_q); 150.84 ($\underline{C}$–OH); 156.44 (C=O); 164.65 (C=N). $C_{16}H_{12}N_2O_2S$: 296.06 g/mol; LRMS (ESI$^+$): m/z ([M + H]$^+$) 297.1 (100%); 167.0 (3.6%); 131.1 (4.5%).

***(E)-N-(5,6-di-Hydroxybenzo[d]thiazol-2-yl)cinnamamide* (LQM542)** – Yield: 99%; Aspect: yellow amorphous powder; R_F: 0.33;

R_T: 0.64 min; Purity: 97%; Mp: 272–273 °C. ART-FTIR (Transmittance/cm^{-1}): 3177 δ(O—H); 1676 ν(C=O); 1604 ν(C=C_{ene}); 1059 ν(C_{Ar}=C_{Ar}); 943 ν(S—C). ^{1}H NMR (300 MHz, DMSO-d_6, ppm) δ 7.45 (d, 1H, J = 15.6 Hz, CH_{ene}); 7.59 (s, 1H, CH_{Ar}); 7.72 (s, 1H, CH_{Ar}); 7.89–7.92 (*m*, 3H, CH_{Ar}); 7,0.95 (br s, 1H, OH); 7.96–8.04 (*m*, 2H, CH_{Ar}); 8.09 (d, 1H, CH_{ene}); 9.23 (br s, 1H, OH); 12.68 (br s, 1H, NH). ^{13}C NMR (75 MHz, DMSO-d_6, ppm) δ 106.36 (C_{Ar}); 120.44 (C_{ene}); 122.18 (C_{Ar}); 129.18 (C_{Ar}–C_{Ar}); 129.72 (C_{Ar}–C_{Ar}); 133.27 (C_q); 134.81 (C_{Ar}); 141.03 (C_{ene}); 142.02 (C_q); 142.54 (C–OH); 143.97 (C–OH); 145.62 (C_q); 155.48 (C=O); 163.15 (C=N). $C_{16}H_{12}N_2O_3S$: 312.06 g/mol; LRMS (ESI$^+$): *m/z* ([M + H]$^+$) 313.1 (100%); 274.3 (1.2%); 208.9 (10.6%); 182.9 (3.6%); 131.1 (8.6%).

***(E)-N-(6-Nitrobenzo[d]thiazol-2-yl)cinnamamide* (LQM543)** – Yield: 70%; Aspect: yellow amorphous powder; R_F: 0.57; R_T: 1.34 min; Purity: 96%; Mp: 269–270 °C. ART-FTIR (Transmittance/cm^{-1}): 3160 ν (N—H); 1683 ν(C=O); 1598 ν(C=C_{ene}); 1051 ν(C_{Ar}=C_{Ar}); 996 ν(S—C). ^{1}H NMR (300 MHz, DMSO-d_6, ppm) δ 6.97 (d, 1H, J = 15.8 Hz, CH_{ene}); 7.47–7.48 (*m*, 3H, CH_{Ar}); 7.66–7.69 (*m*, 2H, CH_{Ar}); 7.84 (d, 1H, J = 15.8 Hz, CH_{ene}); 7.91 (d, 1H, J = 8.9 Hz, CH_{Ar}); 8.28 (*dd*, 1H, J = 8.2 and 2.3 Hz, CH_{Ar}); 9.06 (d, 1H, J = 2.3 Hz, CH_{Ar}); 12.98 (s, 1H, NH). ^{13}C NMR (75 MHz, DMSO-d_6, ppm) δ 119.37 (C_{Ar}); 119.52 (C_{ene}); 121.06 (C_{Ar}); 122.26 (C_{Ar}); 128.73 (C_{Ar}–C_{Ar}); 129.62 (C_{Ar}–C_{Ar}); 131.24 (C_{Ar}); 132.86 (C_q); 134.49 (C_q); 143.45 (C_{ene}); 144.47 (C–NO_2); 154.05 (C_q); 164.11 (C=O); 165.05 (C=N). $C_{16}H_{11}N_3O_3S$: 325.05 g/mol; LRMS (ESI$^+$): *m/z* ([M + H]$^+$) 326.0 (100%); 301.2 (2.4%); 279.1 (3.3%); 251.0 (2.8%); 217.1 (2.9%); 195.0 (2.0%); 149.2 (2.8%); 131.3 (15.5%).

***(E)-N-(Benzo[d]thiazol-2-yl)-3-(4-(tert-butyl)phenyl)acrylamide* (LQM544)** – Yield: 72%; Aspect: beige amorphous powder; R_F: 0.37; R_T: 3.12 min; Purity: 96%; Mp: 214–215 °C. ART-FTIR (Transmittance/cm^{-1}): 2954 ν(N—H); 1677 ν(C=O); 1622 ν(C=C_{ene}); 1071 ν(C_{Ar}=C_{Ar}); 985 ν(S—C). ^{1}H NMR (300 MHz, DMSO-d_6, ppm) δ 1.29 (s, 9H, $(CH_3)_3$); 6.92 (d, 1H, J = 15.7 Hz, CH_{ene}); 7.31 (t, 1H, J = 7.3 Hz, CH_{Ar}); 7.42–7.50 (*m*, 3H, CH_{Ar}); 7.58–7.60 (*m*, 2H, CH_{Ar}); 7.74–7.79 (*m*, 2H, CH_{Ar} and CH_{ene}); 7.99 (d, 1H, CH_{Ar}); 12.53 (br s, 1H, NH). ^{13}C NMR (75 MHz, DMSO-d_6, ppm) δ 31.36 (($\underline{C}H_3)_3$); 35.11(C_{terc}); 119.01 (C_{Ar}); 120.98 (C_{ene}); 122.15 (C_{Ar}); 124.00 (C_{Ar}); 126.40 (C_{Ar}–C_{Ar}); 126.48 (C_{Ar}); 128.46 (C_{Ar}–C_{Ar}); 131.97 (C_q); 132.16 (C_q); 143.46 (C_q); 149.16 (C_{ene}); 153.97 (C_q); 158.58 (C=O); 164.65 (C=N). $C_{20}H_{20}N_2OS$: 336.13 g/mol; LRMS (ESI$^+$): *m/z* ([M + H]$^+$) 337.1 (100%).

***(E)-3-(4-(tert-Butyl)phenyl)-N-(6-fluorobenzo[d]thiazol-2-yl) acrylamide* (LQM545) –** Yield: 67%; Aspect: orange amorphous powder; R_F: 0.52; R_T: 3.59 min; Purity: 95%; Mp: 240–241 °C. ART-FTIR (Transmittance/cm^{-1}): 2959 ν(N—H); 1693 ν(C=O); 1674 ν(C=C_{ene}); 1084 ν(C_{Ar}=C_{Ar}); 978 ν(S—C). ^{1}H NMR (300 MHz, DMSO-d_6, ppm) δ 1.29 (s, 9H, $(CH_3)_3$); 6.91 (d, 1H, J = 15.6 Hz, CH_{ene}); 7.29 (*td*, 1H, J = 9.0 and 2.6 Hz, CH_{Ar}); 7.48 (d, 2H, J = 8.3 Hz, CH_{Ar}); 7.59 (d, 2H, J = 8.3 Hz, CH_{Ar}); 7.74–7.79 (*m*, 2H, CH_{Ar} and CH_{ene}); 7.9 (*dd*, 1H, J = 8.7 and 2.5 Hz, CH_{Ar}); 12.65 (br s, 1H, NH). ^{13}C NMR (75 MHz, DMSO-d_6, ppm) δ 31.35 (($\underline{C}H_3)_3$); 35.12 (C_{terc}); 108.43 (C_{Ar}); 108.79 (C_{Ar}); 118.83 (C_{Ar}); 122.13 (C_{ene}); 126.40 (C_{Ar}–C_{Ar}); 128.48 (C_{Ar}–C_{Ar}); 131.93 (C_q); 133.33 (C_q); 133.48 (C_q); 145.57 (C_{ene}); 154.00 (C_q); 157.52 (C—F); 160.7 (C=O); 164.7 (C=N). $C_{20}H_{19}FN_2OS$: 354.12 g/mol; LRMS (ESI$^+$): *m/z* ([M + H]$^+$) 355.1 (100%); 131.2 (1.0%).

***(E)-3-(4-(tert-Butyl)phenyl)-N-(4,6-difluorobenzo[d]thiazol-2-yl) acrylamide* (LQM546) –** Yield: 66%; Aspect: white amorphous powder; R_F: 0.57; R_T: 1.58 min; Purity: 95%; Mp: 203–204 °C. ART-FTIR (Transmittance/cm^{-1}): 3198 ν(N—H); 1679 ν(C=O); 1623 ν(C=C_{ene}); 1021 ν(C_{Ar}=C_{Ar}); 947 ν(S—C). ^{1}H NMR (300 MHz, DMSO-d_6, ppm) δ 1.16 (s, 9H, $CH_3)_3$; 6.92 (d, 1H, J = 15.9 Hz, CH_{ene}); 7.32–7.40 (*m*, 1H, CH_{Ar}); 7.46–7.51 (*m*, 2H, CH_{Ar}); 7.65–7.68 (*m*, 2H, CH_{Ar}); 7.79–7.84 (*m*, 2H, CH_{Ar} and CH_{ene}); 12.82 (br s, 1H, NH). ^{13}C NMR (75 MHz, DMSO-d_6, ppm) δ 31.36 (($\underline{C}H_3)_3$; 35.11 (C_{terc}); 101.95 (C_{Ar}); 104.27 (C_{Ar}); 104.63 (C_q); 119.02 (C_{ene}); 128.15 (C_{Ar}–C_{Ar}); 129.09 (C_{Ar}–C_{Ar}); 130.61 (C_q); 134.60 (C_q); 134.89 (C–C_{terc}); 143.50 (C_{ene}); 155.48 (C—F); 158.32 (C—F); 158.61 (C=O); 164.23 (C=N). $C_{20}H_{18}F_2N_2OS$: 372.11 g/mol; LRMS (ESI$^+$): *m/z* ([M + H]$^+$) 373.1 (100%); 131.2 (5.1%).

***(E)-3-(4-(tert-Butyl)phenyl)-N-(6-chlorobenzo[d]thiazol-2-yl) acrylamide* (LQM547) –** Yield: 68%; Aspect: white amorphous powder; R_F: 0.55; R_T: 1.88 min; Purity: 95%; Mp: 265–266 °C. ART-FTIR (Transmittance/cm^{-1}): 3063 ν(N—H); 1677 ν(C=O); 1627 ν(C=C_{ene}); 1096 ν(C_{Ar}=C_{Ar}); 979 ν(S—C). ^{1}H NMR (300 MHz, DMSO-d_6, ppm) δ 1.29 (s, 9H, $(CH_3)_3$); 6.91 (d, 1H, J = 15.9 Hz, CH_{ene}); 7.43–7.50 (*m*, 3H, CH_{Ar}); 7.57–7.6 (*m*, 2H, CH_{Ar}); 7.73–7.79 (*m*, 2H, CH_{Ar} and CH_{ene}); 8.13 (s, 1H, CH_{Ar}); 12.60 (br s, 1H, NH). ^{13}C NMR (75 MHz, DMSO-d_6, ppm) δ 31.35 (($\underline{C}H_3)_3$); 35.12 (C_{terc}); 118.83 (C_{Ar}); 121.88 (C_{Ar}); 122.16 (C_{ene}); 126.41 (C_{Ar}–C_{Ar}); 126.91 (C_q); 128.02 (C_{Ar}); 128.49 (C_{Ar}–C_{Ar}); 131.92 (C_q); 133.88 (C_q); 143.68 (C_{ene}); 148.06 (C_q); 154.03 (C—Cl); 159.50 (C=O); 164.82 (C=N). $C_{20}H_{19}ClN_2OS$: 370.09 g/mol; LRMS (ESI$^+$): *m/z* ([M + H]$^+$) 371.1 (100%).

***(E)-3-(4-(tert-Butyl)phenyl)-N-(4-chlorobenzo[d]thiazol-2-yl) acrylamide* (LQM548) –** Yield: 86%; Aspect: beige amorphous powder; R_F: 0.52; R_T: 1.8 min; Purity: 95%; Mp: 94–95 °C. ART-FTIR (Transmittance/cm^{-1}): 3479 ν(N—H); 1676 ν(C=O); 1616 ν(C=C_{ene}); 1071 ν (C_{Ar}=C_{Ar}); 972 ν(S—C). ^{1}H NMR (300 MHz, DMSO-d_6, ppm) δ 1.29 (s, 9H, $(CH_3)_3$); 6.89 (d, 1H, J = 15.7 Hz, CH_{ene}); 7.3 (t, 1H, CH_{Ar}); 7.39–7.45 (*m*, 1H, CH_{Ar}); 7.48–7.55 (*m*, 2H, CH_{Ar}); 7.57–7.62 (*m*, 2H, CH_{Ar}); 7.78 (d, 1H, J = 15.7 Hz, CH_{ene}); 7.98 (*dd*, 1H, J = 7.8 and 0.9 Hz, CH_{Ar}); 12.98 (br s, 1H, NH). ^{13}C NMR (75 MHz, DMSO-d_6, ppm) δ 31.35 (($\underline{C}H_3)_3$); 35.14 (C_{terc}); 118.94 (C_{ene}); 121.34 (C_{Ar}); 124.75 (C_{Ar}–C_{Ar}); 126.43 (C_{Ar}–C_{Ar}); 126.64 (C—Cl); 128.49 (C_{Ar}); 131.91 (C_{Ar}); 133.78 (C_q); 143.76 (C_{ene}); 146.08 (C_q); 154.06 (C_q); 159.90 (C–C_{terc}); 164.96 (C=O); 171.14 (C=N). $C_{20}H_{19}ClN_2OS$: 370.09 g/mol; LRMS (ESI$^+$): *m/z* ([M + H]$^+$) 371.2 (100%).

***(E)-N-(6-Bromobenzo[d]thiazol-2-yl)-3-(4-(tert-butyl)phenyl) acrylamide* (LQM549)** – Yield: 72%; Aspect: orange amorphous powder; R_F: 0.31; R_T: 2.05 min; Purity: 96%; Mp: 220–221 °C. ART-FTIR (Transmittance/cm^{-1}): 3060 ν(N—H); 1678 ν(C=O); 1625 ν(C=C_{ene}); 1082 ν(C_{Ar}=C_{Ar}); 979 ν(S—C). ^{1}H NMR (300 MHz, DMSO-d_6, ppm) δ 1.29 (s, 9H, $(CH_3)_3$); 6.91 (d, 1H, J = 15.8 Hz, CH_{ene}); 7.48–7.50 (*m*, 2H, CH_{Ar}); 7.56–7.61 (*m*, 3H, CH_{Ar}); 7.69 (d, 1H, J = 8.6 Hz, CH_{Ar}); 7.77 (d, 1H, J = 15.8 Hz, CH_{ene}); 8.27 (d, 1H, J = 1.8 Hz, CH_{Ar}); 12.62 (br s, 1H, NH). ^{13}C NMR (75 MHz, DMSO-d_6, ppm) δ 31.35 (($\underline{C}H_3)_3$); 35.13 (C_{terc}); 115.93 (C_{Ar}); 118.78 (C_{Ar}); 122.58 (C_{ene}); 124.72 (C_{Ar}–C_{Ar}); 126.41 (C_{Ar}–C_{Ar}); 128.50 (C_q); 129.62 (C_{Ar}); 131.91 (C_q); 134.38 (C_q); 143.73 (C_{ene}); 148.50 (C_q); 154.06 (C—Br); 154.06 (C=O); 164.80 (C=N). $C_{20}H_{19}BrN_2OS$: 414.04 g/mol; LRMS (ESI$^+$): *m/z* ([M + H]$^+$) 417.1 (100%); 187.2 (1.7%).

***(E)-3-(4-(tert-Butyl)phenyl)-N-(6-(trifluoromethyl)benzo[d]thiazol-2-il)acrylamide* (LQM550) –** Yield: 78%; Aspect: orange amorphous powder; R_F: 0.45; R_T: 2.48 min; Purity: 99%; Mp: 235–236 °C. ART-FTIR (Transmittance/cm^{-1}): 3067 ν(N—H); 1685 ν(C=O); 1626 ν(C=C_{ene}); 1057 ν(C_{Ar}=C_{Ar}); 972 ν(S—C). ^{1}H NMR (300 MHz, DMSO-d_6, ppm) δ 1.31 (s, 9H, $(CH_3)_3$); 6.93 (d, 1H, J = 15.9 Hz, CH_{ene}); 7.49–7.52 (*m*, 3H, CH_{Ar}); 7.61 (d, 2H, J = 8.1 Hz, CH_{Ar}); 7.76–7.81 (*m*, 1H, CH_{Ar} and CH_{ene}); 8.15 (s, 1H, CH_{Ar}); 12.63 (br s, 1H, NH). ^{13}C NMR (75 MHz, DMSO-d_6, ppm) δ 31.56 (($\underline{C}H_3)_3$); 35.33 (C_{terc}); 119.04 (C_{Ar}); 119.14 (C_{ene}); 122.09 (C_{Ar}); 122.37 (C_{Ar}); 126.62 (C_{Ar}–C_{Ar}); 127.12 ($\underline{C}F_3$); 128.23 (C–CF_3); 128.70 (C_{Ar}–C_{Ar}); 132.13 (C_q); 134.09 (C_q); 143.89 (C_{ene}); 148.27 (C–C_{terc}); 154.24 (C_q); 159.71 (C=O); 165.03 (C=N). $C_{21}H_{19}F_3N_2OS$: 404.12 g/mol; LRMS (ESI$^+$): *m/z* ([M + H]$^+$) 405.1 (100%); 218.2 (2.3%); 188.3 (3.1%).

***(E)-3-(4-(tert-Butyl)phenyl)-N-(4-methylbenzo[d]thiazol-2-yl) acrylamide* (LQM551) –** Yield: 78%; Aspect: white amorphous powder; R_F: 0.35; R_T: 1.74 min; Purity: 97%; Mp: 129–130 °C. ART-FTIR (Transmittance/cm^{-1}): 2960 ν(N—H); 1651 ν(C=O); 1614 ν(C=C_{ene}); 1076 ν(C_{Ar}=C_{Ar}); 982 ν(S—C). ^{1}H NMR (300 MHz, DMSO-d_6, ppm) δ 1.29 (s, 9H, $(CH_3)_3$); 2.58 (s, 3H, CH_3); 6.93 (d, 1H, J = 15.8 Hz, CH_{ene}); 7.17–7.27 (*m*, 2H, CH_{Ar}); 7.46–7.49 (*m*, 2H, CH_{Ar}); 7.56–7.59 (*m*, 2H, CH_{Ar}); 7.75 (d, 1H, J = 15.8 Hz, CH_{ene}); 7.8 (s, 1H, CH_{Ar}); 12.62 (br s, 1H, NH). ^{13}C NMR (75 MHz, DMSO-d_6, ppm) δ 18.41 ($\underline{C}H_3$); 31.35 (($\underline{C}H_3)_3$); 35.10 (C_{terc}); 119.05 (C_{Ar}); 119.53 (C_{Ar}); 123.96 (C_{ene}); 126.39 (C_{Ar}–C_{Ar}); 127.07 (C_q); 128.41 (C_{Ar}–C_{Ar}); 130.25 (C_q); 131.81 (C_q);

131.98 (C–CH_3); 143.35 (C_{ene}); 148.24 (C_q); 153.94 (C_{Ar}); 157.70 (C=O); 164.57 (C=N). $C_{21}H_{22}N_2OS$: 350.15 g/mol; LRMS (ESI^+): *m/z* ([M + H]$^+$) 351.2 (100%).

***(E)-3-(4-(tert-Butyl)phenyl)-N-(6-methylbenzo[d]thiazol-2-yl) acrylamide* (LQM552) –** Yield: 64%; Aspect: white amorphous powder; R_F: 0.46; R_T: 4.28 min; Purity: 95%; Mp: 228–229 °C. ART-FTIR (Transmittance/cm^{-1}): 2955 *ν*(N—H); 1676 *ν*(C=O); 1621 *ν*(C=C_{ene}); 1062 *ν*(C_{Ar}=C_{Ar}); 983 *ν*(S—C). ^{1}H NMR (300 MHz, DMSO-d_6, ppm) *δ* 1.29 (s, 9H, $(CH_3)_3$); 2.41 (s, 3H, CH_3); 6.91 (d, 1H, *J* = 15.8 Hz, CH_{ene}); 7.25 (*dd*, 1H, *J* = 8.0 and 1.3 Hz, CH_{Ar}); 7.44–7.5 (*m*, 2H, CH_{Ar}); 7.57–7.65 (*m*, 3H, CH_{Ar}); 7.74 (d, 2H, CH_{Ar} and CH_{ene}); 12.41 (br s, 1H, NH). ^{13}C NMR (75 MHz, DMSO-d_6, ppm) *δ* 21.44 ($\underline{C}H_3$); 31.36 (($\underline{C}H_3$)$_3$); 35.11 (C_{terc}); 119.08 (C_{Ar}); 120.63 (C_{Ar}); 121.74 (C_{ene}); 126.39 (C_{Ar}–C_{Ar}); 127.91 (C_q); 128.44 (C_{Ar}–C_{Ar}); 131.98 (C_q); 132.31 (C_q); 133.47 (C–CH_3); 143.29 (C_{ene}); 147.14 (C_q); 153.94 (C_{Ar}); 157.70 (C=O); 164.53 (C=N). $C_{21}H_{22}N_2OS$: 350.15 g/mol; LRMS (ESI^+): *m/z* ([M + H]$^+$) 351.2 (100%).

***(E)-3-(4-(tert-Butyl)phenyl)-N-(5,6-dimethylbenzo[d]thiazol-2-yl)acrylamide* (LQM553) –** Yield: 68%; Aspect: yellow amorphous powder; R_F: 0.36; R_T: 1.86 min; Purity: 97%; Mp: 139–140 °C. ART-FTIR (Transmittance/cm^{-1}): 2963 *ν*(N—H); 1662 *ν*(C=O); 1613 *ν*(C=C_{ene}); 1048 *ν*(C_{Ar}=C_{Ar}); 979 *ν*(S—C). ^{1}H NMR (300 MHz, DMSO-d_6, ppm) *δ* 1.29 (s, 9H, $(CH_3)_3$); 2.32 (d, 6H, *J* = 2.6 Hz, $(CH_3)_2$); 6.9 (d, 1H, *J* = 15.8 Hz, CH_{ene}); 7.48 (d, 2H, *J* = 8.3 Hz, CH_{Ar}); 7.57 (t, 3H, *J* = 7.2 Hz, CH_{Ar}); 7.70–7.76 (*m*, 2H, CH_{Ar} and CH_{ene}); 12.4 (br s, 1H, NH). ^{13}C NMR (75 MHz, DMSO-d_6, ppm) *δ* 20.01 ($\underline{C}H_3$); 20.16 ($\underline{C}H_3$); 31.36 (($\underline{C}H_3$)$_3$); 35.11 (C_{terc}); 119.14 (C_{Ar}); 121.34 (C_{ene}); 121.91 (C_{Ar}); 126.40 (C_{Ar}–C_{Ar}); 128.43 (C_{Ar}–C_{Ar}); 129.52 (C_q); 131.99 (C–CH_3); 132.88 (C–CH_3); 135.26 (C_q); 143.19 (C_{ene}); 147.72 (C_q); 153.91 (C_q); 157.75 (C=O); 164.42 (C=N). $C_{22}H_{24}N_2OS$: 364.16 g/mol; LRMS (ESI^+): *m/z* ([M + H]$^+$) 365.2 (100%).

***(E)-N-(6-(tert-Butyl)benzo[d]thiazol-2-yl)-3-(4-(tert-butyl) phenyl)acrylamide* (LQM554) –** Yield: 69%; Aspect: yellow amorphous powder; R_F: 0.56; R_T: 1.19 min; Purity: 98%; Mp: 202–203 °C. ART-FTIR (Transmittance/cm^{-1}): 2960 *ν*(N—H); 1687 *ν*(C=O); 1627 *ν*(C=C_{ene}); 1108 *ν*(C_{Ar}=C_{Ar}); 905 *ν*(S—C). ^{1}H NMR (300 MHz, DMSO-d_6, ppm) *δ* 1.29 (s, 12H, $(CH_3)_6$); 1.30 (s, 6H, $(CH_3)_2$); 6.89 (d, 1H, *J* = 15.8 Hz, CH_{ene}); 7.45–7.49 (*m*, 2H, CH_{Ar}); 7.55–7.58 (*m*, 2H, CH_{Ar}); 7.61 (s, 1H, CH_{Ar}); 7.69 (d, 1H, *J* = 15.5 Hz, CH_{ene}); 7.94 (s, 1H, CH_{Ar}); 8.45 (s, 1H, CH_{Ar}); 10.12 (br s, 1H, NH). ^{13}C NMR (75 MHz, DMSO-d_6, ppm) *δ* 31.36 (($\underline{C}H_3$)$_3$); 31.90 (($\underline{C}H_3$)$_3$); 34.12 (C_{tert}); 35.12 (C_{terc}); 119.71 (C_{Ar}); 120,24 (C_{ene}); 123.68 (C_{Ar}); 124.24 (C_{Ar}); 126.37 (C_{Ar}–C_{Ar}); 128.38 (C_{Ar}–C_{Ar}); 129.36 (C_q); 132.12 (C_q); 145.74 (C_{ene}); 146.67 ($\underline{C}_q$–C_{terc}); 153.75 (C_q); 157.43 ($\underline{C}_q$–C_{terc}); 164.92 (C=O); 173.25 (C=N). $C_{24}H_{28}N_2OS$: 392.19 g/mol; LRMS (ESI^+): *m/z* ([M + H]$^+$) 393.1 (100%); 206.2 (2.6%); 188.1 (6.7%).

***(E)-3-(4-(tert-Butyl)phenyl)-N-(6-methoxybenzo[d]thiazol-2-yl) acrylamide* (LQM555) –** Yield: 73%; Aspect: orange amorphous powder; R_F: 0.36; R_T: 2.92 min; Purity: 98%; Mp: 221–222 °C. ART-FTIR (Transmittance/cm^{-1}): 2950 *ν*(N—H); 1683 *ν*(C=O); 1626 *ν*(C=C_{ene}); 1060 *ν*(C_{Ar}=C_{Ar}); 993 *ν*(S—C). ^{1}H NMR (300 MHz, DMSO-d_6, ppm) *δ* 1.29 (s, 9H, $(CH_3)_3$); 3.81 (s, 3H, CH_3); 6.9 (d, 1H, *J* = 15.7 Hz, CH_{ene}); 7.03 (*dd*, 1H, *J* = 8.8 and 2.4 Hz, CH_{Ar}); 7.47–7.50 (*m*, 2H, CH_{Ar}); 7.57–7.59 (*m*, 3H, CH_{Ar}); 7.65 (d, 1H, *J* = 8.8 Hz, CH_{Ar}); 7.74 (d, 1H, *J* = 15.7 Hz, CH_{ene}); 12.42 (br s, 1H, NH). ^{13}C NMR (75 MHz, DMSO-d_6, ppm) *δ* 31.36 (($\underline{C}H_3$)$_3$); 35.1 (C_{terc}); 56.12 ($\underline{C}H_3$); 105.21 (C_{Ar}); 115.38 (C_{Ar}); 119.09 (C_{Ar}); 121.59 (C_{ene}); 126.39 (C_{Ar}–C_{Ar}); 128.42 (C_{Ar}–C_{Ar}); 132.00 (C_q); 133.49 (C_q); 143.16 (C_q); 143.29 (C_{ene}); 153.9 (C_q); 156.53 (C–OCH_3); 156.63 (C=O); 164.39 (C=N). $C_{21}H_{22}N_2O_2S$: 366.14 g/mol; LRMS (ESI^+): *m/z* ([M + H]$^+$) 367.2 (100%).

***(E)-3-(4-(tert-Butyl)phenyl)-N-(6-ethoxybenzo[d]thiazol-2-yl) acrylamide* (LQM556) –** Yield: 86%; Aspect: brown amorphous powder; R_F: 0.4; R_T: 4.05 min; Purity: 95%; Mp: 216–217 °C. ART-FTIR (Transmittance/cm^{-1}): 2949 *ν*(N—H); 1673 *ν*(C=O); 1602 *ν*(C=C_{ene}); 1039 *ν* (C_{Ar}=C_{Ar}); 977 *ν*(S—C). ^{1}H NMR (300 MHz, DMSO-d_6, ppm) *δ* 1.29 (s, 9H, $(CH_3)_3$); 1.35 (t, 3H, *J* = 6.9 Hz, CH_3); 4.07 (q, 2H, *J* = 6.9 Hz, OCH_2); 6.9 (d, 1H, *J* = 15.7 Hz, CH_{ene}); 7.02 (*dd*, 1H, *J* = 8.8 and 2.4 Hz, CH_{Ar}); 7.44–7.49 (*m*, 2H, CH_{Ar}); 7.55–7.57 (*m*, 2H, CH_{Ar}); 7.59 (s, 1H, CH_{Ar}); 7.63 (d, 1H, *J* = 8.8 Hz, CH_{Ar}); 7.73 (d, 1H, *J* = 15.7 Hz, CH_{Ar}); 12.43 (br s, 1H, NH). ^{13}C NMR (75 MHz, DMSO-d_6, ppm) *δ* 15.15 ($\underline{C}H_3$); 31.35 (($\underline{C}H_3$)$_3$); 35.10 (C_{terc}); 64.07 ($\underline{C}H_2$); 105.84 (C_{Ar}); 115.74 (C_{Ar}); 119.7 (C_{ene}); 121.58 (C_{Ar}); 126.39 (C_{Ar}–C_{Ar}); 128.42 (C_{Ar}–C_{Ar}); 132.00 (C_q); 133.47 (C_q); 143.15 (C_{ene}); 143.20 (C_q); 153.89 (C_q); 155.84 (C–OCH_2CH_3); 156.50 (C=O); 164.38 (C=N). $C_{22}H_{24}N_2O_2S$: 380.16 g/mol; LRMS (ESI^+): *m/z* ([M + H]$^+$) 381.2 (100%).

***(E)-3-(4-(tert-Butyl)phenyl)-N-(4-methoxybenzo[d]thiazol-2-yl) acrylamide* (LQM557) –** Yield: 73%; Aspect: yellow amorphous powder; R_F: 0.83; R_T: 2.99 min; Purity: 98%; Mp: 199–200 °C. ART-FTIR (Transmittance/cm^{-1}): 2958 *ν*(N—H); 1678 *ν*(C=O); 1625 *ν*(C=C_{ene}); 1050 *ν*(C_{Ar}=C_{Ar}); 982 *ν*(S—C). ^{1}H NMR (300 MHz, DMSO-d_6, ppm) *δ* 1.28 (s, 9H, $(CH_3)_3$); 3.92 (s, 3H, CH_3); 6.86 (d, 1H, *J* = 15.8 Hz, CH_{ene}); 6.99 (d, 1H, *J* = 8.0 Hz, CH_{Ar}); 7.25 (t, 1H, *J* = 7.9 Hz, CH_{Ar}); 7.49 (t, 3H, *J* = 8.0 Hz, CH_{Ar}); 7.56 (t, 2H, *J* = 7.9 Hz, CH_{Ar}); 7.75 (d, 1H, *J* = 15.8 Hz, CH_{ene}); 12.66 (br s, 1H, NH). ^{13}C NMR (75 MHz, DMSO-d_6, ppm) *δ* 31.34 (($\underline{C}H_3$)$_3$); 35.09 (C_{terc}); 56.29 ($\underline{C}H_3$); 108.14 (C_{Ar}); 113.97 (C_{Ar}); 118.97 (C_{ene}); 124.99 (C_{Ar}); 126.38 (C_{Ar}–C_{Ar}); 128.44 (C_{Ar}–C_{Ar}); 131.94 (C_q); 133.52 (C_q); 139.04 (C_q); 143.33 (C_{ene}); 152.30 (C_q); 153.94 (C–OCH_3); 157.00 (C=O); 164.44 (C=N). $C_{21}H_{22}N_2O_2S$: 366.14 g/mol; LRMS (ESI^+): *m/z* ([M + H]$^+$) 367.2 (100%).

***(E)-3-(4-(tert-Butyl)phenyl)-N-(5,6-dimethoxybenzo[d]thiazol-2-yl)acrylamide* (LQM558) –** Yield: 70%; Aspect: yellow amorphous powder; R_F: 0.46; R_T: 0.93 min; Purity: 99%; Mp: 130–131 °C. ART-FTIR (Transmittance/cm^{-1}): 3158 *ν*(N—H); 1678 *ν*(C=O); 1628 *ν*(C=C_{ene}); 1039 *ν*(C_{Ar}=C_{Ar}); 852 *ν*(S—C). ^{1}H NMR (300 MHz, DMSO-d_6, ppm) *δ* 1.35 (s, 9H, $(CH_3)_3$); 3.88 (d, 6H, *J* = 5.6 Hz, CH_3); 6.97 (d, 1H, *J* = 15.7 Hz, CH_{ene}); 7.37 (s, 1H, CH_{Ar}); 7.46–7.55 (*m*, 2H, CH_{Ar}); 7.58–7.68 (*m*, 3H, CH_{Ar}); 7.66 (d, 1H, *J* = 15.7 Hz, CH_{ene}); 12.45 (br s, 1H, NH). ^{13}C NMR (75 MHz, DMSO-d_6, ppm) *δ* 31.36 (($\underline{C}H_3$)$_3$); 35.10 (C_{terc}); 56.19 (O$\underline{C}H_3$); 56.41 (O$\underline{C}H_3$); 103.94 (C_{Ar}); 104.16 (C_{Ar}); 119.11 (C_q); 123.64 (C_{ene}); 126.16 (C_{Ar}–C_{Ar}); 128.38 (C_{Ar}–C_{Ar}); 132.03 (C_q); 142.98 (C_{ene}); 143.19 (C_q); 147.43 (C–OCH_3); 149.39 (C–OCH_3); 156.97 (C_q); 164.11 (C=O); 168.13 (C=N). $C_{22}H_{24}N_2O_3S$: 396.15 g/mol; LRMS (ESI^+): *m/z* ([M + H]$^+$) 397.1 (100%); 211.1 (1,7%).

***(E)-3-(4-(tert-Butyl)phenyl)-N-(6-hydroxybenzo[d]thiazol-2-yl) acrylamide* (LQM559) –** Yield: 99%; Aspect: yellow amorphous powder; R_F: 0.45; R_T: 1.44 min; Purity: 95%; Mp: 168–169 °C. ART-FTIR (Transmittance/cm^{-1}): 3152 *δ*(O—H); 2960 *ν*(N—H); 1682 *ν*(C=O); 1603 *ν*(C=C_{ene}); 1090 *ν*(C_{Ar}=C_{Ar}); 916 *ν*(S—C). ^{1}H NMR (300 MHz, DMSO-d_6, ppm) *δ* 1.28 (s, 9H, $(CH_3)_3$); 6.87–6.92 (*m*, 2H, CH_{Ar} and CH_{ene}); 7.3 (d, 1H, *J* = 2.2 Hz, CH_{Ar}); 7.47 (d, 2H, *J* = 8.3 Hz, CH_{Ar}); 7.54–7.59 (*m*, 3H, CH_{Ar}); 7.72 (d, 1H, *J* = 15.8 Hz, CH_{ene}); 9.55 (br s, 1H, OH); 12.35 (br s, 1H, NH). ^{13}C NMR (75 MHz, DMSO-d_6, ppm) *δ* 31.35 (($\underline{C}H_3$)$_3$); 35.10 (C_{terc}); 106.94 (C_{Ar}); 115.72 (C_{Ar}); 119.13 (C_{Ar}); 121.58 (C_{ene}); 126.38 (C_{Ar}–C_{Ar}); 128.39 (C_{Ar}–C_{Ar}); 132.01 (C_q); 133.48 (C_q); 142.22 (C_{ene}); 142.99 (C_q); 153.83 (C–C_{terc}); 154.66 (C–OH); 155.59 (C=O); 164.24 (C=N). $C_{20}H_{20}N_2O_2S$: 352.12 g/mol; LRMS (ESI^+): *m/z* ([M + H]$^+$) 353.1 (100%).

***(E)-3-(4-(tert-Butyl)phenyl)-N-(4-hydroxybenzo[d]thiazol-2-yl) acrylamide* (LQM560) –** Yield: 98%; Aspect: yellow amorphous powder; R_F: 0.4; R_T: 2.1 min; Purity: 99%; Mp: 168–169 °C. ART-FTIR (Transmittance/cm^{-1}): 3320 *δ*(O—H); 2962 *ν*(N—H); 1660 *ν*(C=O); 1618 *ν* (C=C_{ene}); 1021 *ν*(C_{Ar}=C_{Ar}); 948 *ν*(S—C). ^{1}H NMR (300 MHz, DMSO-d_6, ppm) *δ* 1.16 (s, 9H, $(CH_3)_3$); 6.71 (d, 1H, *J* = 7.7 Hz, CH_{Ar}); 6.77 (d, 1H, *J* = 15.8 Hz, CH_{ene}); 6.98 (t, 1H, *J* = 7.9 Hz, CH_{Ar}); 7.25 (d, 1H, *J* = 7.8 Hz, CH_{Ar}); 7.34–7.40 (*m*, 2H, CH_{Ar}); 7.44–7.47 (*m*, 2H, CH_{Ar}); 7.62 (d, 1H, *J* = 15.8 Hz, CH_{ene}); 9.68 (br s, 1H, OH); 12.44 (br s, 1H, NH). ^{13}C NMR (75 MHz, DMSO-d_6, ppm) *δ* 31.36 $(CH_3)_3$; 35.11 (C_{terc}); 111.78 (C_{Ar}); 112.29 (C_{Ar}); 118.94 (C_{ene}); 125.02 (C_{Ar}); 126.40 (C_{Ar}–C_{Ar}); 128.42 (C_{Ar}–C_{Ar}); 131.99 (C_q); 133.82 (C_q); 138.50 (C_{ene}); 143.18 (C_q); 150.43 (C–C_{terc}); 153.89 (C–OH); 156.08 (C=O); 164.40 (C=N). $C_{20}H_{20}N_2O_2S$: 352.12 g/mol; LRMS (ESI^+): *m/z* ([M + H]$^+$) 353.2 (100%); 187.1 (1.5%).

***(E)-3-(4-(tert-Butyl)phenyl)-N-(5,6-di-hydroxybenzo[d]thiazol-2-yl)acrylamida* (LQM561) –** Yield: 99%; Aspect: brown amorphous powder; R_F: 0.38; R_T: 1.14 min; Purity: 98%; Mp: 183–184 °C. ART-FTIR (Transmittance/cm^{-1}): 3191 δ(O—H); 1680 ν(C=O); 1621 ν(C=C_{ene}); 1106 ν(C_{Ar}=C_{Ar}); 985 ν(S—C). ^{1}H NMR (300 MHz, DMSO-d_6, ppm) δ 1.61 (s, 9H, $(CH_3)_3$); 7.2 (d, 2H, J = 15.8 Hz, CH_{ene}); 7.42 (s, 1H, CH_{Ar}); 7.56 (s, 1H, CH_{Ar}); 7.75–7.81 (*m*, 2H, CH_{Ar}); 7.87–7.87 (*m*, 2H, CH_{Ar}); 8.02 (d, 1H, J = 15.8 Hz, CH_{ene}); 12.62 (br s, 1H, NH). ^{13}C NMR (75 MHz, DMSO-d_6, ppm) δ 31.60 ($\underline{C}H_3)_3$); 35.34 (C_{terc}); 107.08 (C_{Ar}); 119.45 (C_{ene}); 122.81 (C_{Ar}); 126.41 (C_{Ar}); 126.62 (C_{Ar}); 128.59 (C_{Ar}); 128.73 (C_{Ar}); 132.29 (C_q); 142.64 (C–OH); 143.02 (C–OH); 144.60 (C_{ene}); 154.01 (C_q); 156.28 (C–C_{terc}); 164.16 (C=O); 168.37 (C=N). $C_{20}H_{20}N_2O_3S$: 368.12 g/mol; LRMS (ESI^+): *m/z* ([M + H]$^+$) 369.1 (100%); 131.0 (1.1%).

***(E)-3-(4-(tert-Butyl)phenyl)-N-(6-nitrobenzo[d]thiazol-2-yl) acrylamide* (LQM562)** – Yield: 68%; Aspect: yellow amorphous powder; R_F: 0.38; R_T: 3.74 min; Purity: 95%; Mp: 185–186 °C. ART-FTIR (Transmittance/cm^{-1}): 2954 ν(N—H)$_s$; 1678 ν(C=O); 1605 ν(C=C_{ene}); 1048 ν(C_{Ar}=C_{Ar}); 992 ν(S—C). ^{1}H NMR (300 MHz, DMSO-d_6, ppm) δ 1.26 (s, 9H, $(CH_3)_3$); 7.11 (d, 1H, J = 15.3 Hz, CH_{ene}); 7.37–7.47 (*m*, 3H, CH_{Ar}); 7.57–7.66 (*m*, 3H, CH_{ene} and CH_{Ar}); 7.90 (d, 1H, J = 8.9 Hz, CH_{Ar}); 8.08 (*dd*, 1H, J = 8.9 and 2.1 Hz, CH_{Ar}); 12.69 (br s, 1H, NH). ^{13}C NMR (75 MHz, DMSO-d_6, ppm) δ 31.38 ($\underline{C}H_3)_3$); 35.50 (C_{terc}); 117.29 (C_{Ar}); 118.08 (C_{ene}); 119.59 (C_{Ar}); 121.3 (C_{Ar}); 125.97 (C_{Ar}–C_{Ar}); 128.20 (C_{Ar}–C_{Ar}); 132.03 (C_q); 132.76 (C_q); 141.10 (C_{ene}); 142.36 (C–NO_2); 152.68 (C–C_{terc}); 159.05 (C_q); 166.08 (C=O); 172.24 (C=N). $C_{20}H_{19}N_3O_3S$: 381.11 g/mol; LRMS (ESI^+): *m/z* ([M + H]$^+$) 382.1 (100%); 187.2 (1.8%); 131.2 (1.4%).

***(E)-N-(Benzo[d]thiazol-2-yl)-3-(4-chlorophenyl)acrylamide* (LQM563) –** Yield: 95%; Aspect: yellow amorphous powder; R_F: 0.72; R_T: 1.67 min; Purity: 99%; Mp: 289–290 °C. ART-FTIR (Transmittance/cm^{-1}): 3160 ν(N—H)$_s$; 1687 ν(C=O); 1625 ν(C=C_{ene}); 1091 ν(C_{Ar}=C_{Ar}); 987 ν(S—C). ^{1}H NMR (300 MHz, DMSO-d_6, ppm) δ 6.95 (d, 1H, J = 15.3 Hz, CH_{ene}); 7.31 (t, 1H, J = 7.4 Hz, CH_{Ar}); 7.44 (t, 1H, J = 7.4 Hz, CH_{Ar}); 7.52–7.58 (*m*, 2H, CH_{Ar}); 7.67–7.70 (*m*, 2H, CH_{Ar}); 7.75–7.81 (*m*, 2H, CH_{Ar} and CH_{ene}); 7.99 (d, 1H, CH_{Ar}); 12.63 (br s, 1H, NH). ^{13}C NMR (75 MHz, DMSO-d_6, ppm) δ 120.61 (C_{Ar}); 121.02 (C_{ene}); 122.20 (C_{Ar}); 124.09 (C_{Ar}); 126.64 (C_{Ar}); 129.64 (C_{Ar}–C_{Ar}); 130.29 (C_{Ar}–C_{Ar}); 132.13 (C_q); 133.59 (C_q); 135.45 (C—Cl); 142.19 (C_{ene}); 149.10 (C_q); 158.48 (C=O); 164.34 (C=N). $C_{16}H_{11}ClN_2OS$: 314.03 g/mol; LRMS (ESI^+): *m/z* ([M + H]$^+$) 315.0 (100%); 224.0 (1.2%); 151.0 (4.6%).

***(E)-3-(4-Chlorophenyl)-N-(6-fluorobenzo[d]thiazol-2-yl)acrylamide* (LQM564) –** Yield: 65%; Aspect: brown amorphous powder; R_F: 0.32; R_T: 1.41 min; Purity: 95%; Mp: 237–238 °C. ART-FTIR (Transmittance/cm^{-1}): 3085 ν(N—H)$_s$; 1692 ν(C=O); 1615 ν(C=C_{ene}); 1109 ν(C_{Ar}=C_{Ar}); 943 ν(S—C). ^{1}H NMR (300 MHz, DMSO-d_6, ppm) δ 6.94 (d, 1H, J = 15.9 Hz, CH_{ene}); 7.31 (*dd*, 1H, J = 9.0 and 2.3 Hz, CH_{Ar}); 7.52–7.58 (*m*, 2H, CH_{Ar}); 7.60 (s, 1H, CH_{Ar}); 7.67–7.70 (*m*, 2H, CH_{Ar}); 7.74–7.79 (*m*, 2H, CH_{Ar} and CH_{ene}); 12.65 (br s, 1H, NH). ^{13}C NMR (75 MHz, DMSO-d_6, ppm) δ 122.07 (C_{Ar}); 122.19 (C_{ene}); 127.80 (C_{Ar}); 129.38 (C_{Ar}); 129.65 (C_{Ar}–C_{Ar}); 130.29 (C_{Ar}–C_{Ar}); 130.39 (C—F); 133.58 (C_q); 133.67 (C_q); 135.47 (C—Cl); 142.98 (C_{ene}); 145.85 (C_q); 160.74 (C=O); 164.4 (C=N). $C_{16}H_{10}ClFN_2OS$: 332.02 g/mol; LRMS (ESI^+): *m/z* ([M + H]$^+$) 333.1 (100%); 300.0 (2.5%); 266.1 (1.02%); 164.9 (2.05%).

***(E)-3-(4-Chlorophenyl)-N-(4,6-difluorobenzo[d]thiazol-2-yl) acrylamide* (LQM565) –** Yield: 61%; Aspect: brown amorphous powder; R_F: 0.42; R_T: 1.43 min; Purity: 98%; Mp: 271–272 °C. ART-FTIR (Transmittance/cm^{-1}): 3190 ν(N—H); 1678 ν(C=O); 1628 ν(C=C_{ene}); 1012 ν(C_{Ar}=C_{Ar}); 940 ν(S—C). ^{1}H NMR (300 MHz, DMSO-d_6, ppm) δ 6.89 (d, 1H, J = 15.9 Hz, CH_{ene}); 7.36 (*dd*, 1H, J = 10.2 and 2.0 Hz, CH_{Ar}); 7.51–7.58 (*m*, 2H, CH_{Ar}); 7.63–7.69 (*m*, 2H, CH_{Ar}); 7.77–7.82 (*m*, 2H, CH_{Ar} and CH_{ene}); 12.91 (br s, 1H, NH). ^{13}C NMR (75 MHz, DMSO-d_6) δ 104.79 (C_{Ar}); 105.09 (C_{Ar}); 117.32 (C_{ene}); 120.23 (C_q); 129.64 (C_{Ar}–C_{Ar}); 130.32 (C_{Ar}–C_{Ar}); 131.35 (C_q); 133.22 (C_q); 133.48 (C—Cl); 135.55 (C_{ene}); 142.54 (C—F); 147.18 (C—F); 159.07 (C=N); 164.53 (C=O). $C_{16}H_9ClF_2N_2OS$: 350.01 g/mol; LRMS (ESI^+): *m/z* ([M + H]$^+$) 351.0 (100%); 165.0 (6.3%).

***(E)-N-(6-Chlorobenzo[d]thiazol-2-yl)-3-(4-chlorophenyl)acrylamide* (LQM566) –** Yield: 45%; Aspect: yellow amorphous powder; R_F: 0.45; R_T: 2.68 min; Purity: 98%; Dp: 298–299 °C. ART-FTIR (Transmittance/cm^{-1}): 3066 ν(N—H)$_s$; 1684 ν(C=O); 1624 ν(C=C_{ene}); 1098 ν(C_{Ar}=C_{Ar}); 988 ν(S—C). ^{1}H NMR (300 MHz, DMSO-d_6, ppm) δ 6.94 (d, 1H, J = 15.3 Hz, CH_{ene}); 7.46 (*dd*, 1H, J = 8.6 and 1.7 Hz, CH_{Ar}); 7.52–7.55 (*m*, 2H, CH_{Ar}); 7.67–7.70 (*m*, 2H, CH_{Ar}); 7.73 (s, 1H, CH_{Ar}); 7.79 (d, 1H, J = 15.4 Hz, CH_{ene}); 8.13 (d, 1H, CH_{Ar}); 12,71 (br s, 1H, NH). ^{13}C NMR (75 MHz, DMSO-d_6, ppm) δ 120.39 (C_{Ar}); 121.92 (C_{ene}); 122.23 (C_{Ar}); 126.98 (C_{Ar}); 128.12 (C_{Ar}–C_{Ar}); 129.66 (C_{Ar}–C_{Ar}); 130.32 (C_q); 133.54 (C—Cl); 133.85 (C—Cl); 135.52 (C_q); 142.43 (C_{ene}); 148.02 (C_q); 159.34 (C=O); 164.48 (C=N). $C_{16}H_{10}Cl_2N_2OS$: 347.99 g/mol; LRMS (ESI^+): *m/z* ([M + H]$^+$) 349.0 (100%); 184.9 (1.5%); 164.9 (5.1%).

***(E)-N-(4-Chlorobenzo[d]thiazol-2-yl)-3-(4-chlorophenyl)acrylamide* (LQM567) –** Yield: 89%; Aspect: beige amorphous powder; R_F: 0.37; R_T: 2.6 min; Purity: 97%; Mp: 150–151 °C. ART-FTIR (Transmittance/cm^{-1}): 3181 ν(N—H); 1692 ν(C=O); 1624 ν(C=C_{ene}); 1010 ν(C_{Ar}=C_{Ar}); 955 ν(S—C). ^{1}H NMR (300 MHz, DMSO-d_6, ppm) δ 6.93 (d, 1H, J = 15.8 Hz, CH_{ene}); 7.30 (t, 1H, J = 7.8 Hz, CH_{Ar}); 7.54 (d, 3H, J = 8.5 Hz, CH_{Ar}); 7.68 (d, 2H, J = 8.5 Hz, CH_{Ar}); 7.81 (d, 1H, J = 15.8 Hz, CH_{ene}); 7.99 (*dd*, 1H, J = 7.8 and 0.7 Hz, CH_{Ar}); 13.06 (br s, 1H, NH). ^{13}C NMR (75 MHz, DMSO-d_6, ppm) δ 120.41 (C_{ene}); 121.36 (C_{Ar}); 124.81 (C—Cl); 124.88 (C_{Ar}); 126.67 (C_{Ar}); 129.67 (C_{Ar}–C_{Ar}); 130.31 (C_{Ar}–C_{Ar}); 133.53 (C_q); 133.77 (C_q); 135.53 (C—Cl); 142.48 (C_{ene}); 146.04 (C_q); 159.77 (C=O); 164.62 (C=N). $C_{16}H_{10}Cl_2N_2OS$: 347.99 g/mol; LRMS (ESI^+): *m/z* ([M + H]$^+$) 349.0 (100%); 184.9 (2.7%); 165.0 (5.6%).

***(E)-N-(6-Bromobenzo[d]thiazol-2-yl)-3-(4-chlorophenyl)acrylamide* (LQM568) –** Yield: 75%; Aspect: yellow amorphous powder; R_F: 0.58; R_T: 3.0 min; Purity: 95%; Mp: 284–285 °C. ART-FTIR (Transmittance/cm^{-1}): 2953 ν(N—H); 1683 ν(C=O); 1624 ν(C=C_{ene}); 1056 ν(C_{Ar}=C_{Ar}); 939 ν(S—C). ^{1}H NMR (300 MHz, DMSO-d_6, ppm) δ 6.94 (d, 1H, J = 15.8 Hz, CH_{ene}); 7.32 (*dd*, 1H, J = 8.5 and 2.0 Hz, CH_{Ar}); 7.57 (d, 2H, J = 8.9 Hz, CH_{Ar}); 7.69 (d, 2H, J = 8.9 Hz, CH_{Ar}); 7.79 (d, 1H, J = 15.8 Hz, CH_{ene}); 7.87 (d, 1H, J = 2.0 Hz, CH_{Ar}); 8.27 (d, 1H, J = 2.0 Hz, CH_{Ar}); 12.68 (s, 1H, NH). ^{13}C NMR (75 MHz, DMSO-d_6, ppm) δ 115.47 (C—Br); 119.42 (C_{ene}); 122.16 (C_{Ar}); 124.24 (C_{Ar}); 128.16 (C_{Ar}–C_{Ar}); 129.11 (C_{Ar}–C_{Ar}); 130.57 (C_q); 133.91 (C_q); 134.19 (C—Cl); 143.18 (C_{ene}); 148.45 (C_q); 158.82 (C=O); 164.32 (C=N). $C_{16}H_{10}BrClN_2OS$: 391.94 g/mol; LRMS (ESI^+): *m/z* ([M + 2H]$^{2+}$) 392.99 (100%); 352.4 (2.6%); 279.1 (3.0%); 251.0 (1.2%); 164.9 (4.7%); 122.1 (0.7%).

***(E)-3-(4-Chlorophenyl)-N-(6-(trifluoromethyl)benzo[d]thiazol-2-yl)acrylamide* (LQM569)** – Yield: 42%; Aspect: brown amorphous powder; R_F: 0.75; R_T: 3.13 min; Purity: 96%; Mp: 231–232 °C. ART-FTIR (Transmittance/cm^{-1}): 3496 ν(N—H)$_s$; 1625 ν(C=O); 1614 ν(C=C_{ene}); 1094 ν(C_{Ar}=C_{Ar}); 939 ν(S—C). ^{1}H NMR (300 MHz, DMSO-d_6, ppm) δ 6.96 (d, 1H, J = 15.9 Hz, CH_{ene}); 7.52–7.55 (*m*, 2H, CH_{Ar}); 7.68–7.72 (*m*, 2H, CH_{Ar}); 7.76 (s, 1H, CH_{Ar}); 7.81 (d, 1H, J = 15.9 Hz, CH_{ene}); 7.90–7.93 (*m*, 1H, CH_{Ar}); 8.51 (s, 1H, CH_{Ar}); 12.86 (br s, 1H, NH). ^{13}C NMR (75 MHz, DMSO-d_6, ppm) δ 120.30 (C_{Ar}); 121.43 (C_{ene}); 123.44 (C_{Ar}); 123.99 (C_{Ar}); 124.42 ($\underline{C}F_3$); 129.66 (C_{Ar}–C_{Ar}); 130.35 (C_{Ar}–C_{Ar}); 131.34 (C–CF_3); 132.70 (C_q); 133.50 (C_q); 135.59 (C—Cl); 142.69 (C_{ene}); 151.87 (C_q); 161.73 (C=O); 164.69 (C=N). $C_{17}H_{10}ClF_3N_2OS$: 382.02 g/mol; LRMS (ESI^+): *m/z* ([M + H]$^+$) 383.0 (100%); 164.9 (2.3%).

***(E)-3-(4-Chlorophenyl)-N-(4-methylbenzo[d]thiazol-2-yl)acrylamide* (LQM570) –** Yield: 48%; Aspect: white amorphous powder; R_F: 0.35; R_T: 2.53 min; Purity: 98%; Mp: 210–211 °C. ART-FTIR (Transmittance/cm^{-1}): 2972 ν(N—H); 1652 ν(C=O); 1616 ν(C=C_{ene}); 1092 ν(C_{Ar}=C_{Ar}); 940 ν(S—C). ^{1}H NMR (300 MHz, DMSO-d_6, ppm) δ 2.58 (s, 3H, CH_3); 6.96 (d, 1H, J = 15.9 Hz, CH_{ene}); 7.18–7.27 (*m*, 2H, CH_{Ar}); 7.54 (d, 2H, J = 8.4 Hz, CH_{Ar}); 7.67 (d, 2H, J = 8.4 Hz, CH_{Ar}); 7.75–7.81 (*m*, 2H, CH_{Ar} and CH_{ene}); 12.73 (br s, 1H, NH). ^{13}C NMR (75 MHz, DMSO-d_6, ppm) δ 18.44 ($\underline{C}H_3$); 119.58 (C_{Ar}); 120.67 (C_{ene}); 124.02 (C_q); 127.09 (C_{Ar}); 129.65 (C_{Ar}–C_{Ar}); 130.23 (C_{Ar}–C_{Ar}); 130.28 (C_{Ar}); 131.8 (C–CH_3); 133.62 (C—Cl); 135.40 (C_q); 142.03 (C_{ene}); 148.22 (C_q);

157.69 (C=O); 164.28 (C=N). $C_{17}H_{13}ClN_2OS$: 328.04 g/mol; LRMS (ESI^+): *m/z* ($[M + H]^+$) 329.1 (100%); 165.0 (3.2%).

***(E)-3-(4-Chlorophenyl)-N-(6-methylbenzo[d]thiazol-2-yl)acrylamide* (LQM571)** – Yield: 74%; Aspect: yellow amorphous powder; R_F: 0.32; R_T: 4.01 min; Purity: 98%; Mp: 289–290 °C. ART-FTIR (Transmittance/cm^{-1}): 2920 *ν*(N—H); 1683 *ν*(C=O); 1625 *ν*(CH_{ene}); 1068 *ν* (C_{Ar}=C_{Ar}); 985 *ν*(S—C). ^{1}H NMR (300 MHz, DMSO-d_6, ppm) *δ* 2.41 (s, 3H, CH_3); 6.95 (d, 1H, *J* = 15.8 Hz, CH_{ene}); 7.25 (*dd*, 1H, *J* = 8.1 and 1.2 Hz, CH_{Ar}); 7.52–7.55 (*m*, 2H, CH_{Ar}); 7.62 (s, 1H, CH_{Ar}); 7.65–7.69 (*m*, 2H, CH_{Ar}); 7.74–7.79 (*m*, 2H, CH_{Ar}); 12.54 (s, 1H, NH). ^{13}C NMR (75 MHz, DMSO-d_6, ppm) *δ* 21.47 ($\underline{C}H_3$); 120.68 (C_{Ar}); 121.78 (C_{ene}); 124.61 (C_{Ar}); 127.95 (C_{Ar}); 129.64 (C_{Ar}–C_{Ar}); 130.25 (C_{Ar}–C_{Ar}); 132.28 (C_q); 133.55 (C_q); 133.62 ($\underline{C}$—Cl); 135.40 ($\underline{C}$–CH_3); 141.99 (C_{ene}); 147.10 (C_q); 157.60 (C=O); 164.20 (C=N). $C_{17}H_{13}ClN_2OS$: 328.04 g/mol; LRMS (ESI^+): *m/z* ($[M + H]^+$) 329.1 (100%); 165.2 (3.8%).

***(E)-3-(4-Chlorophenyl)-N-(5,6-dimethylbenzo[d]thiazol-2-yl) acrylamide* (LQM572)** – Yield: 85%; Aspect: yellow amorphous powder; R_F: 0.37; R_T: 5.28 min; Purity: 95%; Mp: 265–266 °C. ART-FTIR (Transmittance/cm^{-1}): 2983 *ν*(N—H); 1666 *ν*(C=O); 1625 *ν*(CH_{ene}); 1044 *ν*(C_{Ar}=C_{Ar}); 940 *ν*(S—C). ^{1}H NMR (300 MHz, DMSO-d_6, ppm) *δ* 2.31 (d, 6H, *J* = 2.9 Hz, $(CH_3)_2$); 6.92 (d, 1H, *J* = 15.8 Hz, CH_{ene}); 7.51–7.54 (*m*, 3H, CH_{Ar}); 7.66–7.77 (*m*, 4H, $(CH_{Ar})_3$ and CH_{ene}); 12.51 (s, 1H, NH). ^{13}C NMR (75 MHz, DMSO-d_6, ppm) *δ* 20.04 ($\underline{C}H_3$); 20.18 ($\underline{C}H_3$); 120.70 (C_{ene}); 121.37 (C_{Ar}); 121.92 (C_{Ar}); 129.50 (C_{Ar}); 129.63 (C_q); 130.11 (C_{Ar}); 130.24 (C_q); 132.98 (C_{Ar}); 133.62 ($\underline{C}$—Cl); 135.31 (C_{Ar}); 135.38 ($\underline{C}$–CH_3); 141.90 ($\underline{C}$–CH_3); 147.68 (C_{ene}); 157.53 (C_q); 159.35 (C=O); 164.10 (C=N). $C_{18}H_{15}ClN_2OS$: 342.06 g/mol; LRMS (ESI^+): *m/z* ($[M + H]^+$) 343.2 (100%); 179.2 (2.0%).

***(E)-N-(6-(tert-Butyl)benzo[d]thiazol-2-yl)-3-(4-chlorophenyl) acrylamide* (LQM573)** – Yield: 95%; Aspect: yellow amorphous powder; R_F: 0.42; R_T: 1.63 min; Purity: 95%; Mp: 227–228 °C. ART-FTIR (Transmittance/cm^{-1}): 2959 *ν*(N—H); 1685 *ν*(C=O); 1627 *ν*(CH_{ene}); 1016 *ν*(C_{Ar}=C_{Ar}); 979 *ν*(S—C). ^{1}H NMR (300 MHz, DMSO-d_6, ppm) *δ* 1.33 (s, 9H, $(CH_3)_3$); 6.94 (d, 1H, *J* = 15.8 Hz, CH_{ene}); 7.45–7.54 (*m*, 3H, CH_{Ar}); 7.66–7.69 (*m*, 3H, CH_{Ar}); 7.77 (d, 1H, *J* = 15.8 Hz, CH_{ene}); 7.99 (d, 1H, *J* = 1.7 Hz, CH_{Ar}); 12.54 (s, 1H, NH). ^{13}C NMR (75 MHz, DMSO-d_6, ppm) *δ* 31.88 (($\underline{C}H_3)_3$); 35.15 (C_{terc}); 118.26 (C_{Ar}); 120.42 (C_{ene}); 120.71 (C_{Ar}); 124.41 (C_{Ar}); 129.38 (C_{Ar}–C_{Ar}); 129.64 (C_q); 130.25 (C_{Ar}–C_{Ar}); 132.17 (C_q); 133.63 ($\underline{C}$—Cl); 135.40 (C_q); 142.01 (C_{ene}); 146.99 ($\underline{C}$–C_{terc}); 158.01 (C=O); 164.18 (C=N). $C_{20}H_{19}ClN_2OS$: 370.09 g/mol; LRMS (ESI^+): *m/z* ($[M + H]^+$) 371.2 (100%).

***(E)-3-(4-Chlorophenyl)-N-(6-methoxybenzo[d]thiazol-2-yl)acrylamide* (LQM574)** – Yield: 68%; Aspect: yellow amorphous powder; R_F: 0.78; R_T: 2.45 min; Purity: 95%; Mp: 245–246 °C. ART-FTIR (Transmittance/cm^{-1}): 2933 *ν*(N—H); 1685 *ν*(C=O); 1627 *ν*(C=C_{ene}); 1031 *ν* (C_{Ar}=C_{Ar}); 945 *ν*(S—C). ^{1}H NMR (300 MHz, DMSO-d_6, ppm) *δ* 3.80 (s, 3H, CH_3); 6.93 (d, 1H, *J* = 15.7 Hz, CH_{ene}); 7.03 (d, 1H, *J* = 8.3 Hz, CH_{Ar}); 7.52–7.58 (*m*, 3H, CH_{Ar}); 7.64–7.69 (*m*, 3H, CH_{Ar}); 7.76 (d, 1H, *J* = 15.6 Hz, CH_{ene}); 12.50 (br s, 1H, NH). ^{13}C NMR (75 MHz, DMSO-d_6, ppm) *δ* 56.09 ($O\underline{C}H_3$); 105.18 (C_{Ar}); 115.44 (C_{Ar}); 120.70 (C_{Ar}); 121.64 (C_{ene}); 129.64 (C_{Ar}–C_{Ar}); 130.24 (C_{Ar}–C_{Ar}); 133.47 (C_q); 133.65 ($\underline{C}$—Cl); 135.37 (C_q); 141.87 (C_{ene}); 143.24 (C_q); 156.41 ($\underline{C}$–OCH_3); 156.65 (C=O); 164.06 (C=N). $C_{17}H_{13}ClN_2O_2S$: 344.04 g/mol; LRMS (ESI^+): *m/z* ($[M + H]^+$) 345.1 (100%); 181.2 (1.9%).

***(E)-3-(4-Chlorophenyl)-N-(6-ethoxybenzo[d]thiazol-2-yl)acrylamide* (LQM575)** – Yield: 77%; Aspect: yellow amorphous powder; R_F: 0.32; R_T: 2.13 min; Purity: 98%; Mp: 264–265 °C. ART-FTIR (Transmittance/cm^{-1}): 2927 *ν*(N—H); 1684 *ν*(C=O); 1634 *ν*(C=C_{ene}); 1065 *ν* (C_{Ar}=C_{Ar}); 947 *ν*(S—C). ^{1}H NMR (300 MHz, DMSO-d_6, ppm) *δ* 1.34 (t, 3H, *J* = 1.3 Hz, CH_3); 4.06 (q, 2H, *J* = 6.9 Hz, CH_2); 6.93 (d, 1H, *J* = 15.9 Hz, CH_{ene}); 7.02 (*dd*, 1H, *J* = 8.8 and 2.4 Hz, CH_{Ar}); 7.52–7.57 (*m*, 3H, CH_{Ar}); 7.62 (s, 1H, CH_{Ar}); 7.65–7.69 (*m*, 2H, CH_{Ar}); 7.76 (d, 1H, *J* = 15.8 Hz, CH_{ene}); 12.49 (br s, 1H, NH). ^{13}C NMR (75 MHz, DMSO-d_6, ppm) *δ* 15.16 ($\underline{C}H_3$); 64.06 ($\underline{C}H_2$); 105.82 (C_{Ar}); 115.79 (C_{Ar}); 120.70 (C_{ene}); 121.63 (C_{Ar}); 129.38 (C_{Ar}); 129.64 (C_{Ar}); 130.24 (C_{Ar}); 130.4 (C_{Ar}); 133.46 (C_q); 133.65 (C_q); 135.37 ($\underline{C}$—Cl); 141.86 (C_{ene}); 143.15 (C_q); 155.88 ($\underline{C}$—O); 156.37 (C=O); 164.05 (C=N). $C_{18}H_{15}ClN_2O_2S$: 358.05 g/mol; LRMS (ESI^+): *m/z* ($[M + H]^+$) 359.1 (100%); 195.0 (1.6%).

***(E)-3-(4-Chlorophenyl)-N-(4-methoxybenzo[d]thiazol-2-yl)acrylamide* (LQM576)** – Yield: 55%; Aspect: yellow amorphous powder; R_F: 0.6; R_T: 2.75 min; Purity: 97%; Mp: 212–213 °C. ART-FTIR (Transmittance/cm^{-1}): 3234 *ν*(N—H); 1669 *ν*(C=O); 1625 *ν*(CH_{ene}); 1086 *ν* (C_{Ar}=C_{Ar}); 958 *ν*(S—C). ^{1}H NMR (300 MHz, DMSO-d_6, ppm) *δ* 3.92 (s, 3H, CH_3); 6.89 (d, 1H, *J* = 15.8 Hz, CH_{ene}); 7.00 (d, 1H, *J* = 7.9 Hz, CH_{Ar}); 7.26 (t, 1H, *J* = 7.9 Hz, CH_{Ar}); 7.51–7.55 (*m*, 3H, CH_{Ar}); 7.68 (d, 2H, *J* = 8.4 Hz, CH_{Ar}); 7.78 (d, 1H, CH_{ene}); 12.77 (s, 1H, NH). ^{13}C NMR (75 MHz, DMSO-d_6, ppm) *δ* 56.28 ($O\underline{C}H_3$); 108.13 (C_{Ar}); 113.99 (C_{ene}); 120.59 (C_{Ar}); 125.07 (C_{Ar}); 129.63 (C_{Ar}–C_{Ar}); 130.27 (C_{Ar}–C_{Ar}); 133.50 (C_q); 133.59 (C_q); 135.42 ($\underline{C}$—Cl); 139.00 ($\underline{C}$–OCH_3); 142.03 (C_{ene}); 152.32 (C_q); 156.91 (C=O); 164.12 (C=N). $C_{17}H_{13}ClN_2O_2S$: 344.04 g/mol; LRMS (ESI^+): *m/z* ($[M + H]^+$) 345.1 (100%); 266.2 (10.7%); 181.2 (1.9%).

***(E)-3-(4-Chlorophenyl)-N-(5,6-dimethoxybenzo[d]thiazol-2-yl) acrylamide* (LQM577)** – Yield: 85%; Aspect: yellow amorphous powder; R_F: 0.41; R_T: 1.2 min; Purity: 96%; Mp: 219–220 °C. ART-FTIR (Transmittance/cm^{-1}): 3085 *ν*(N—H); 1691 *ν*(C=O); 1614 *ν*(C=C_{ene}); 1010 *ν* (C_{Ar}=C_{Ar}); 942 *ν*(S—C). ^{1}H NMR (300 MHz, DMSO-d_6, ppm) *δ* 3.82 (d, 6H, *J* = 6.0 Hz, $(CH_3)_2$); 6.95 (d, 1H, *J* = 15.7 Hz, CH_{ene}); 7.31 (s, 1H, CH_{Ar}); 7.52–7.52 (*m*, 2H, CH_{Ar}); 7.60 (s, 1H, CH_{Ar}); 7.65–7.70 (*m*, 2H, CH_{Ar}); 7.74 (d, 1H, *J* = 15.7 Hz, CH_{ene}); 12.46 (br s, 1H, NH). ^{13}C NMR (75 MHz, DMSO-d_6, ppm) *δ* 56.19 ($O\underline{C}H_3$); 56.4 ($O\underline{C}H_3$); 103.93 (C_{Ar}); 104.14 (C_{Ar}); 120.53 (C_{ene}); 124.95 (C_q); 129.38 (C_{Ar}–C_{Ar}); 130.2 (C_{Ar}–C_{Ar}); 133.67 (C_q); 135.67 ($\underline{C}$—Cl); 141.68 (C_{ene}); 142.98 (C_q); 147.48 ($\underline{C}$–OCH_3); 149.41 ($\underline{C}$–OCH_3); 163.79 (C=O); 167.89 (C=N). $C_{18}H_{15}ClN_2O_3S$: 374.05 g/mol; LRMS (ESI^+): *m/z* ($[M + H]^+$) 375.1 (100%); 209.1 (1.7%); 167.2 (0.92%).

***(E)-3-(4-Chlorophenyl)-N-(6-hydroxybenzo[d]thiazol-2-yl)acrylamide* (LQM578)** – Yield: 95%; Aspect: yellow amorphous powder; R_F: 0.31; R_T: 0.89 min; Purity: 98%; Mp: 222–223 °C. ART-FTIR (Transmittance/cm^{-1}): 3286 *δ*(O—H); 2919 *ν*(N—H); 1685 *ν*(C=O); 1630 *ν* (C=C_{ene}); 1050 *ν*(C_{Ar}=C_{Ar}); 973 *ν*(S—C). ^{1}H NMR (300 MHz, DMSO-d_6, ppm) *δ* 7.25–7.32 (*m*, 2H, CH_{Ar} and CH_{ene}); 7.67 (s, 1H, CH_{Ar}); 7.89–7.95 (*m*, 3H, CH_{Ar}); 8.05 (d, 2H, *J* = 7.9 Hz, CH_{Ar}); 8.12 (d, 1H, CH_{ene}); 9.94 (br s, 1H, OH); 12.79 (br s, 1H, NH). ^{13}C NMR (75 MHz, DMSO-d_6, ppm) *δ* 106.96 (C_{Ar}); 115.77 (C_{Ar}); 120.79 (C_{Ar}); 121.63 (C_{ene}); 129.63 (C_{Ar}–C_{Ar}); 130.21 (C_{Ar}–C_{Ar}); 133.48 (C_q); 133.67 (C_q); 135.32 ($\underline{C}$—Cl); 141.7 (C_{ene}); 142.21 (C_q); 154.71 ($\underline{C}$–OH); 155.51 ($\underline{C}$=O); 163.93 ($\underline{C}$=N). $C_{16}H_{11}ClN_2O_2S$: 330.02 g/mol; LRMS (ESI^+): *m/z* ($[M + H]^+$) 331.1 (100%); 167.0 (3.6%).

***(E)-3-(4-Chlorophenyl)-N-(4-hydroxybenzo[d]thiazol-2-yl)acrylamide* (LQM579)** – Yield: 93%; Aspect: yellow amorphous powder; R_F: 0.32; R_T: 1.17 min; Purity: 98%; Mp: 222–223 °C. ART-FTIR (Transmittance/cm^{-1}): 3320 *δ*(O—H); 2969 *ν*(N—H); 1683 *ν*(C=O); 1625 *ν* (C=C_{ene}); 1050 *ν*(C_{Ar}=C_{Ar}); 934 *ν*(S—C). ^{1}H NMR (300 MHz, DMSO-d_6, ppm) *δ* 6.84 (d, 1H, *J* = 7.7 Hz, CH_{Ar}); 6.93 (d, 1H, *J* = 15.9 Hz, CH_{ene}); 7.11 (t, 1H, *J* = 7.8 Hz, CH_{Ar}); 7.38 (d, 1H, *J* = 7.8 Hz, CH_{Ar}); 7.54 (d, 2H, *J* = 7.9 Hz, CH_{Ar}); 7.68 (d, 2H, *J* = 8.0 Hz, CH_{Ar}); 7.77 (d, 1H, *J* = 15.9 Hz, CH_{ene}); 9.81 (br s, 1H, OH); 12.63 (br s, 1H, NH). ^{13}C NMR (75 MHz, DMSO-d_6, ppm) *δ* 111.8 (C_{Ar}); 112.31 (C_{Ar}); 120.74 (C_{ene}); 125.1 (C_{Ar}); 129.65 (C_{Ar}–C_{Ar}); 130.25 (C_{Ar}–C_{Ar}); 133.64 (C_q); 133.81 (C_q); 135.37 ($\underline{C}$—Cl); 138.48 (C_{ene}); 141.88 (C_q); 150.47 ($\underline{C}$–OH); 155.99 ($\underline{C}$=O); 164.09 ($\underline{C}$=N). $C_{16}H_{11}ClN_2O_2S$: 330.02 g/mol; LRMS (ESI^+): *m/z* ($[M + H]^+$) 331.1 (100%); 252.1 (2.4%); 167.0 (6.4%).

***(E)-3-(4-Chlorophenyl)-N-(5,6-dihydroxybenzo[d]thiazol-2-yl) acrylamide* (LQM580)** – Yield: 91%; Aspect: yellow amorphous powder; R_F: 0.31; R_T: 1.17 min; Purity: 98%; Mp: 219–220 °C. ART-FTIR (Transmittance/cm^{-1}): 3320 *δ*(O—H); 2921 *ν*(N—H); 1664 *ν*(C=O); 1620 *ν*(C=C_{ene}); 1050 *ν*(C_{Ar}=C_{Ar}); 973 *ν*(S—C). ^{1}H NMR (300 MHz, DMSO-d_6, ppm) *δ* 6.67 (d, 1H, CH_{ene}); 6.86 (s, 1H, CH_{Ar}); 6.99 (s, 1H, CH_{Ar}); 7.23–7.30 (*m*, 2H, CH_{Ar}); 7.36 (br s, 1H, OH); 7.41–7.51 (*m*, 3H, $(CH_{Ar})_2$ and CH_{ene}); 8.93 (br s, 1H, OH); 12.10 (br s, 1H, NH). ^{13}C NMR

(75 MHz, DMSO-d_6, ppm) δ 107.16 (C_{Ar}); 107.24 (C_{Ar}); 121.23 (C_{ene}); 122.98 (C_q); 129.73 (C_{Ar}); 129.97 (C_{Ar}); 130.52 (C_q); 130.75 (C—Cl); 134.06 (C_{Ar}); 135.61 (C–OH); 141.83 (C_{ene}); 144.77 (C–OH); 146.42 (C–OH); 156.28 (C_q); 163.95 (C=O); 168.24 (C=N). $C_{16}H_{11}ClN_2O_3S$: 346.02 g/mol; LRMS (ESI^+): *m/z* ([M + H]$^+$) 347.1 (100%); 165.0 (4.1%).

***(E)-3-(4-Chlorophenyl)-N-(6-nitrobenzo[d]thiazol-2-yl)acrylamide* (LQM581)** – Yield: 68%; Aspect: yellow amorphous powder; R_F: 0.52; R_T: 3.48 min; Purity: 95%; Mp: 138–139 °C. ART-FTIR (Transmittance/cm^{-1}): 2947 ν(N—H); 1685 ν(C=O); 1621 ν(CH_{ene}); 1051 ν(C_{Ar}=C_{Ar}); 912 ν(S—C). ^{1}H NMR (300 MHz, DMSO-d_6, ppm) δ 6.95 (d, 1H, J = 15.8 Hz, CH_{ene}); 7.54 (d, 2H, J = 8.4 Hz, CH_{Ar}); 7.70 (d, 2H, J = 8.4 Hz, CH_{Ar}); 7.83 (d, 1H, J = 15.8 Hz, CH_{ene}); 7.90 (d, 1H, J = 9.0 Hz, CH_{Ar}); 8.28 (*dd*, 1H, J = 8.9 and 2.4 Hz, CH_{Ar}); 9.06 (d, 1H, J = 2.4 Hz, CH_{Ar}); 13.04 (s, 1H, NH). ^{13}C NMR (75 MHz, DMSO-d_6, ppm) δ 119.53 (C_{Ar}); 120.21 (C_{ene}); 121.05 (C_{Ar}); 122.26 (C_{Ar}); 129.68 (C_{Ar}–C_{Ar}); 130.40 (C_{Ar}–C_{Ar}); 132.88 (C_q); 133.45 (C—Cl); 135.67 (C_q); 142.97 (C_{ene}); 143.42 (C–NO_2); 154.13 (C_q); 158.44 (C=O); 164.17 (C=N). $C_{16}H_{10}ClN_3O_3S$: 359.01 g/mol; LRMS (ESI^+): *m/z* ([M + H]$^+$) 360.1 (100%); 165.2 (7.3%).

4.13.6. Synthesis of mono- and dihydroxylated benzo[d]thiazol-2-phenylcyclopropanecarboxamide derivatives

In a 25 mL round-bottom flask containing 5 mL of anhydrous dichloromethane, 100 mg of the corresponding alkoxylated product at positions 4 or 6, or 5 and 6, were added. The solution was stirred and cooled to −78 °C. Then, 2 eq. (for each heteroatom in the starting molecule) of boron tribromide (BBr_3) were added dropwise. The reaction proceeded for 24 h at room temperature under an argon atmosphere. After completion of the reaction, 10 mL of distilled H_2O were added, forming a precipitate. The solid was filtered and washed with cold distilled H_2O (3 × 30 mL), yielding the purified product.

***(E)-N-(Benzo[d]thiazol-2-yl)-2-phenylcyclopropanecarboxamide* (LQM584)** – Yield: 60%; Aspect: brown crystalline powder; R_F: 0.9; R_T: 1.33 min; Purity: 97%; P_F: 216–217 °C. ART-FTIR (Transmittance/cm^{-1}): 3233 ν(N—H); 3062 ν(CH_{2cycle}); 1649 ν(C=O); 1077 ν(C_{Ar}=C_{Ar}); 972 ν(S—C). ^{1}H NMR (300 MHz, DMSO-d_6, ppm) δ 1.29–1.42 (*m*, 2H, CH_2); 2.05–2.10 (*m*, 1H, CH_{cycle}); 2.32–2.36 (*m*, 1H, CH_{cycle}); 6.98–7.02 (*m*, 3H, CH_{Ar}); 7.06–7.12 (*m*, 3H, CH_{Ar}); 7.21 (*td*, 1H, J = 1.2 and 0.8 Hz, CH_{Ar}); 7.52 (d, 1H, J = 7.9 Hz, CH_{Ar}); 7.75 (d, 1H, J = 7.5 Hz, CH_{Ar}); 12.42 (br s, 1H, NH). ^{13}C NMR (75 MHz, DMSO-d_6, ppm) δ 17.12 (CH_2); 25.96 (CH_{cycle}); 26.82 (CH_{cycle}); 120.99 (C_{Ar}); 122.13 (C_{Ar}); 123.98 (C_{Ar}); 126.57 ((C_{Ar})$_3$); 126.89 (C_{Ar}); 128.9 (C_{Ar}–C_{Ar}); 131.93 (C_q); 140.43 (C_q); 148.99 (C_q); 158.24 (C=O); 171.51 (C=N). $C_{17}H_{14}N_2OS$: 294.08 g/mol; LRMS (ESI^+): *m/z* ([M + H]$^+$) 295.1 (100%); 151.2 (3.5%).

***(E)-N-(6-Fluorobenzo[d]thiazol-2-yl)-2-phenylcyclopropanecarboxamide* (LQM585)** – Yield: 71%; Aspect: brown crystalline powder; R_F: 0.65; R_T: 1.48 min; Purity: 98%; Mp: 220–221 °C. ART-FTIR (Transmittance/cm^{-1}): 3129 ν(N—H); 3040 ν(CH_{2cycle}); 1684 ν(C=O); 1078 ν(C_{Ar}=C_{Ar}); 948 ν(S—C). ^{1}H NMR (300 MHz, DMSO-d_6, ppm) δ 1.50–1.63 (*m*, 2H, CH_2); 2.25–2.31 (*m*, 1H, CH_{cycle}); 2.53–2.57 (*m*, 1H, CH_{cycle}); 7.19–7.23 (*m*, 3H, CH_{Ar}); 7.26–7.33 (*m*, 2H, CH_{Ar}); 7.73 (*dd*, 1H, J = 8.8 and 4.7 Hz, CH_{Ar}); 7.88 (*dd*, 1H, J = 8.7 and 4.7 Hz, CH_{Ar}), 12.64 (br s, 1H, NH). ^{13}C NMR (75 MHz, DMSO-d_6, ppm) δ 17.10 (CH_2); 25.94 (CH_{cycle}); 26.84 (CH_{cycle}); 108.41 (C_{Ar}); 114.45 (C_{Ar}); 121.98 (C_{Ar}); 126.58 (C_{Ar}–C_{Ar}); 126.88 (C_{Ar}); 128.89 (C_{Ar}–C_{Ar}); 133.13 (C_q); 133.27 (C_q); 140.44 (C_q); 145.73 (C—F); 158.3 (C=O); 171.60 (C=N). $C_{17}H_{13}FN_2OS$: 312.07 g/mol; LRMS (ESI^+): *m/z* ([M + H]$^+$) 313.1 (100%); 169.2 (2.5%); 145.1 (1.6%).

***(E)-N-(4,6-Difluorobenzo[d]thiazol-2-yl)-2-phenylcyclopropanecarboxymide* (LQM586)** – Yield: 82%; Aspect: white amorphous powder; R_F: 0.52; R_T: 3.21 min; Purity: 98%; Mp: 260–261 °C. ART-FTIR (Transmittance/cm^{-1}): 3253 ν(N—H); 3064 ν(CH_{2cycle}); 1682 ν(C=O); 1085 ν(C_{Ar}=C_{Ar}); 990 ν(S—C). ^{1}H NMR (300 MHz, DMSO-d_6, ppm) δ 1.53 (*m*, 2H, CH_2); 2.22–2.27 (*m*, 1H, CH_{cycle}); 2.54–2.59 (*m*, 1H, CH_{cycle}); 7.19–7.23 (*m*, 3H, CH_{Ar}); 7.28–7.40 (*m*, 3H, CH_{Ar}); 7.79 (*dd*, 1H, J = 8.3 and 1.7 Hz, CH_{Ar}); 12.93 (br s, 1H, NH). ^{13}C NMR (75 MHz, DMSO-d_6, ppm) δ 17.25 (CH_2); 25.93 (CH_{cycle}); 27.01 (CH_{cycle}); 102.37 (C_{Ar}); 104.79 (C_{Ar}); 126.60 (C_{Ar}–C_{Ar}); 126.93 (C_{Ar}); 128.91 (C_{Ar}–C_{Ar}); 128.98 (C_{Ar}); 135.32 (C_q); 140.32 (C_{Ar}); 156.86 (C—F); 158.88 (C—F); 171.74 (C=O); 176.50 (C=N). $C_{17}H_{12}F_2N_2OS$: 330.06 g/mol; LRMS (ESI^+): *m/z* ([M + H]$^+$) 331.2 (100%); 187.1 (2.2%); 145.3 (3.0%).

***(E)-N-(6-Chlorobenzo[d]thiazol-2-yl)-2-phenylcyclopropanecarboxamide* (LQM587)** – Yield: 80%; Aspect: brown crystalline powder; R_F: 0.65; R_T: 2.11 min; Purity: 97%. Mp: 239–240 °C. ART-FTIR (Transmittance/cm^{-1}): 3152 ν(N—H); 3064 ν(CH_{2cycle}); 1689 ν(C=O); 1078 ν(C_{Ar}=C_{Ar}); 971 ν(S—C). ^{1}H NMR (300 MHz, DMSO-d_6) δ 1.51 (*m*, 2H, CH_2); 2.26–2.31 (*m*, 1H, CH_{cycle}); 2.53–2.58 (*m*, 1H, CH_{cycle}); 7.19–7.23 (*m*, 3H, CH_{Ar}); 7.28–7.33 (*m*, 2H, CH_{Ar}); 7.44 (*dd*, 1H, J = 8.5 and 2.1 Hz, CH_{Ar}); 7.72 (d, 1H, J = 8.6 Hz, CH_{Ar}); 8.11 (d, 1H, J = 2.0 Hz, CH_{Ar}); 12.71 (br s, 1H, NH). ^{13}C NMR (75 MHz, DMSO-d_6, ppm) δ 17.16 (CH_2); 25.99 (CH_{cycle}); 26.95 (CH_{cycle}); 121.88 (C_{Ar}); 122.18 (C_{Ar}); 126.59 (C_{Ar}–C_{Ar}); 126.90 (C_{Ar}–C_{Ar}); 127.99 (C—Cl); 128.90 (C_{Ar}–C_{Ar}); 133.67 (C_q); 140.40 (C_q); 147.91 (C_q); 159.12 (C=O); 171.69 (C=N). $C_{17}H_{13}ClN_2OS$: 328.04 g/mol; LRMS (ESI^+): *m/z* ([M + H]$^+$) 329.1 (100%); 185.1 (1.4%); 145.2 (1.9%).

***(E)-N-(4-Chlorobenzo[d]thiazol-2-yl)-2-phenylcylopropanecarboxamide* (LQM588)** – Yield: 78%; Aspect: white amorphous powder; R_F: 0.46; R_T: 3.31 min; Purity: 97%; Mp: 124–125 °C. ART-FTIR (Transmittance/cm^{-1}): 3542 ν(N—H); 2925 ν(CH_{2cycle}); 1668 ν(C=O); 1051 ν(C_{Ar}=C_{Ar}); 996 ν(S—C). ^{1}H NMR (300 MHz, DMSO-d_6, ppm) δ 1.52 (*m*, 2H, CH_2); 2.25–2.31 (*m*, 1H, CH_{cycle}); 2.53–2.59 (*m*, 1H, CH_{cycle}); 7.19–7.23 (*m*, 4H, CH_{Ar}); 7.26–7.33 (*m*, 4H, CH_{Ar}); 7.52 (d, 1H, J = 7.9 Hz, CH_{Ar}); 7.96 (d, 1H, J = 7.9 Hz, CH_{Ar}); 13.09 (br s, 1H, NH). ^{13}C NMR (75 MHz, DMSO-d_6, ppm) δ 17.34 (CH_2); 25.87 (CH_{cycle}); 27.00 (CH_{cycle}); 121.32 (C_{Ar}); 124.81 (C_{Ar}); 124.85 (C_{Ar}); 126.37 (C_{Ar}); 126.62 (C_{Ar}); 126.92 (C_q); 128.82 (C_{Ar}); 128.91 (C_q); 133.54 (C_q); 140.34 (C_{Ar}); 140.7 (C_q); 145.89 (C—Cl); 159.37 (C=O); 171.79 (C=N). $C_{17}H_{13}ClN_2OS$: 328.04 g/mol; LRMS (ESI^+): *m/z* ([M + H]$^+$) 329.1 (100%); 185.2 (3.5%); 145.3 (1.1%).

***(E)-N-(6-Bromobenzo[d]thiazol-2-yl)-2-phenycyclopropanecarboxamide* (LQM589)** – Yield: 78%; Aspect: brown crystalline powder; R_F: 0.92; R_T: 2.33 min; Purity: 95%; Mp: 219–220 °C. ART-FTIR (Transmittance/cm^{-1}): 3126 ν(N—H); 3086 ν(CH_{2cycle}); 1691 ν(C=O); 1084 ν(C_{Ar}=C_{Ar}); 972 ν(S—C). ^{1}H NMR (300 MHz, DMSO-d_6, ppm) δ 1.51–1.64 (*m*, 2H, CH_2); 2.26–2.31 (*m*, 1H, CH_{cycle}); 2.53–2.58 (*m*, 1H, CH_{cycle}); 7.19–7.23 (*m*, 3H, CH_{Ar}); 7.28–7.34 (*m*, 2H, CH_{Ar}); 7.55 (*dd*, 1H, J = 8.5 and 1.9 Hz, CH_{Ar}); 7.65 (d, 1H, J = 8.5 Hz, CH_{Ar}); 8.24 (s, 1H, CH_{Ar}); 12.72 (br s, 1H, NH). ^{13}C NMR (75 MHz, DMSO-d_6, ppm) δ 17.17 (CH_2); 25.97 (CH_{cycle}); 26.97 (CH_{cycle}); 115.88 (C—Br); 122.60 (C_{Ar}); 124.70 (C_{Ar}); 126.59 (C_{Ar}–C_{Ar}); 126.90 (C_{Ar}); 128.89 (C_{Ar}–C_{Ar}); 129.57 (C_q); 134.17 (C_q); 140.38 (C_{Ar}); 148.21 (C_q); 159.06 (C=O); 171.69 (C=N). $C_{17}H_{13}BrN_2OS$: 371.99 g/mol; LRMS (ESI^+): *m/z* ([M + H]$^+$) 373.0 (100%); 229.0 (1.7%); 145.2 (1.4%).

***(E)-2-Phenyl-N-(6-(trifluoromethyl)benzo[d]thiazol-2-yl)cyclopropanecarboxamide* (LQM590)** – Yield: 67%; Aspect: brown amorphous powder; R_F: 0.48; R_T: 2.35 min; Purity: 99%; Mp: 167–168 °C. ART-FTIR (Transmittance/cm^{-1}): 3362 ν(N—H); 3140 ν(CH_{2cycle}); 1694 ν(C=O); 1081 ν(C_{Ar}=C_{Ar}); 964 ν(S—C). ^{1}H NMR (300 MHz, DMSO-d_6, ppm) δ 1.53–1.66 (*m*, 2H, CH_2); 2.18–2.34 (*m*, 1H, CH_{cycle}); 2.53–2.6 (*m*, 1H, CH_{cycle}); 7.15–7.33 (*m*, 3H, CH_{Ar}); 7.42–7.55 (*m*, 2H, CH_{Ar}); 7.90 (s, 1H, CH_{Ar}); 8.09 (s, 1H, CH_{Ar}); 8.47 (s, 1H, CH_{Ar}); 12.80 (br s, 1H, NH). ^{13}C NMR (75 MHz, DMSO-d_6, ppm) δ 17.27 (CH_2); 26.07 (CH_{cycle}); 27.11 (CH_{cycle}); 117.94 (C_{Ar}); 121.34 (CF_3); 126.34 (C_{Ar}–C_{Ar}); 126.6 (C_{Ar}); 126.91 (C_{Ar}); 128.70 (C_{Ar}–C_{Ar}); 128.89 (C_q); 131.97 (C–CH_3); 132.54 (C_q); 140.36 (C_{Ar}); 151.82 (C_q); 156.32 (C=O); 172.02 (C=N). $C_{18}H_{13}F_3N_2OS$: 362.07 g/mol; LRMS (ESI^+): *m/z* ([M + H]$^+$) 363.1 (100%); 145.2 (1.8%).

***(E)-N-(4-Methylbenzo[d]thiazol-2-yl)-2-phenylcyclopropanecarboxamide* (LQM591)** – Yield: 66%; Aspect: brown crystalline powder; R_F: 0.7; R_T: 1.92 min; Purity: 97%; Mp: 110–111 °C.

ART-FTIR (Transmittance/cm^{-1}): 3500 ν(N—H); 2923 $\nu(CH_{2cycle})$; 1654 ν(C=O); 1078 $\nu(C_{Ar}=C_{Ar})$; 969 ν(S—C). ^{1}H NMR (300 MHz, DMSO-d_6, ppm) δ 1.48–1.62 (*m*, 2H, CH_2); 2.27–2.33 (*m*, 1H, CH_{cycle}); 2.55 (s, 4H, CH_3 and CH_{cycle}); 7.16–7.23 (*m*, 5H, CH_{Ar}); 7.25–7.33 (*m*, 2H, CH_{Ar}); 7.77 (d, 1H, J = 7.2 Hz, CH_{Ar}); 12.75 (br s, 1H, NH). ^{13}C NMR (75 MHz, DMSO-d_6, ppm) δ 17.15 ($\underline{C}H_2$); 18.41 (CH_3); 25.79 ($\underline{C}H_{cycle}$); 26.73 ($\underline{C}H_{cycle}$); 119.51 (C_{Ar}); 123.92 (C_q); 126.60 (C_{Ar}–C_{Ar}); 126.86 (C_{Ar}); 127.06 (C_{Ar}); 128.90 (C_{Ar}–C_{Ar}); 130.26 ($\underline{C}$–CH_3); 131.58 (C_q); 140.46 (C_{Ar}); 148.07 (C_q); 157.41 (C=O); 171.45 (C=N). $C_{18}H_{16}N_2OS$: 308.09 g/mol; LRMS (ESI$^+$): *m/z* ([M + H]$^+$) 309.1 (100%); 165.2 (2.1%).

***(E)-N-(6-Methylbenzo[d]thiazol-2-yl)-2-phenylcylopropanecarboxamide* (LQM592) –** Yield: 61%; Aspect: beige amorphous powder; R_F: 0.37; R_T: 1.71 min; Purity: 98%; Mp: 223–224 °C. ART-FTIR (Transmittance/cm^{-1}): 3125 ν(N—H); 3031 $\nu(CH_{2cycle})$; 1686 ν(C=O); 1081 $\nu(C_{Ar}=C_{Ar})$; 970 ν(S—C). ^{1}H NMR (300 MHz, DMSO-d_6, ppm) δ 1.48–1.62 (*m*, 2H, CH_2); 2.25–2.31 (*m*, 1H, CH_{cycle}); 2.40 (s, 3H, CH_3); 2.52–2.56 (*m*, 1H, CH_{cycle}); 7.19–7.24 (*m*, 4H, CH_{Ar}); 7.28–7.32 (*m*, 2H, CH_{Ar}); 7.61 (d, 1H, J = 8.1 Hz, CH_{Ar}); 7.74 (s, 1H, CH_{Ar}); 12.53 (br s, 1H, NH). ^{13}C NMR (75 MHz, DMSO-d_6, ppm) δ 17.01 ($\underline{C}H_2$); 21.42 ($\underline{C}H_3$); 25.92 ($\underline{C}H_{cycle}$); 26.73 ($\underline{C}H_{cycle}$); 120.63 (C_{Ar}); 121.72 (C_{Ar}); 126.59 (C_{Ar}–C_{Ar}); 126.86 (C_{Ar}); 127.85 (C_q); 128.88 (C_{Ar}–C_{Ar}); 132.10 (C_q); 133.41 ($\underline{C}$–CH_3); 140.48 (C_{Ar}); 146.99 (C_q); 157.38 (C=O); 171.33 (C=N). $C_{18}H_{16}N_2OS$: 308.1 g/mol; LRMS (ESI$^+$): *m/z* ([M + H]$^+$) 309.1 (100%); 165.2 (0.8%).

***(E)-N-(5,6-Dimethylbenzo[d]thiazol-2-yl)-2-phenylcylopropanecarboxamide* (LQM593) –** Yield: 84%; Aspect: purple amorphous powder; R_F: 0.48; R_T: 2.11 min; Purity: 98%; Mp: 194–195 °C. ART-FTIR (Transmittance/cm^{-1}): 3175 ν(N—H); 3065 $\nu(CH_{2cyle})$; 1685 ν(C=O); 1082 $\nu(C_{Ar}=C_{Ar})$; 982 ν(S—C). ^{1}H NMR (300 MHz, DMSO-d_6, ppm) δ 1.47–1.61 (*m*, 2H, CH_2); 2.24–2.28 (*m*, 1H, CH_{cycle}); 2.30 (s, 6H, $(CH_3)_2$); 2.52–2.55 (*m*, 1H, CH_{cycle}); 7.18–7.23 (*m*, 3H, CH_{Ar}); 7.27–7.32 (*m*, 2H, CH_{Ar}); 7.52 (s, 1H, CH_{Ar}); 7.68 (s, 1H, CH_{Ar}); 12.51 (br s, 1H, NH). ^{13}C NMR (75 MHz, DMSO-d_6, ppm) δ 16.95 ($\underline{C}H_2$); 19.98 ($\underline{C}H_3$); 20.14 ($\underline{C}H_3$); 25.9 ($\underline{C}H_{cycle}$); 26.68 ($\underline{C}H_{cycle}$); 121.37 (C_{Ar}); 121.86 (C_{Ar}); 126.59 (C_{Ar}–C_{Ar}); 126.84 (C_{Ar}); 128.88 (C_{Ar}–C_{Ar}); 129.30 (C_q); 132.79 ($\underline{C}$–CH_3); 135.17 (C_q); 140.50 ($\underline{C}$–CH_3); 147.57 (C_q); 157.32 (C=O); 171.21 (C=N). $C_{19}H_{18}N_2OS$: 322.11 g/mol; LRMS (ESI$^+$): *m/z* ([M + H]$^+$) 323.1 (100%); 179.1 (1.3%).

***(E)-N-(6-(tert-Butyl)benzo[d]thiazol-2-yl)-2-phenylcyclopropanecarboxamide* (LQM594) –** Yield: 62%; Aspect: yellow amorphous powder; R_F: 0.49; R_T: 3.58 min; Purity: 95%; Mp: 118–119 °C. ART-FTIR (Transmittance/cm^{-1}): 2958 ν(N—H); 2867 $\nu(CH_{2cycle})$; 1687 ν(C=O); 1078 $\nu(C_{Ar}=C_{Ar})$; 932 ν(S—C). ^{1}H NMR (300 MHz, DMSO-d_6, ppm) δ 1.33 (s, 9H, $(CH_3)_3$); 1.49–1.63 (*m*, 2H, CH_{2cycle}); 2.25–2.31 (*m*, 1H, CH_{cycle}); 2.53–2.57 (*m*, 1H, CH_{cycle}); 7.19–7.23 (*m*, 3H, CH_{Ar}); 7.26–7.33 (*m*, 2H, CH_{Ar}); 7.47 (*dd*, 1H, J = 8.6 and 2.0 Hz, CH_{Ar}); 7.64 (d, 1H, J = 8.4 Hz, CH_{Ar}); 7.95 (d, 1H, J = 1.7 Hz, CH_{Ar}); 12.54 (br s, 1H, NH). ^{13}C NMR (75 MHz, DMSO-d_6, ppm) δ 17.04 ($\underline{C}H_2$); 25.97 (CH_{cycle}); 26.72 (CH_{cycle}); 31.88 (($\underline{C}H_3)_3$); 35.13 (C_{terc}); 118.19 (C_{Ar}); 120.39 (C_{Ar}); 124.33 (C_{Ar}); 126.37 (C_{Ar}); 126.57 (C_{Ar}); 126.87 (C_{Ar}); 128.87 (C_{Ar}); 128.89 (C_{Ar}); 131.97 (C_q); 140.49 (C_q); 146.86 ($\underline{C}$–C_{terc}); 157.78 (C_q); 171.30 (C=O); 178.14 (C=N). $C_{21}H_{22}N_2OS$: 350.15 g/mol; LRMS (ESI$^+$): *m/z* ([M + H]$^+$) 351.2 (100%).

***(E)-N-(6-Methoxybenzo[d]thiazol-2-yl)-2-phenylcyclopropanecarboxamide* (LQM595) –** Yield: 68%; Aspect: brown crystalline powder; R_F: 0.81; R_T: 1.26 min; Purity: 95%; Mp: 178–179 °C. ART-FTIR (Transmittance/cm^{-1}): 3250 ν(N—H); 3067 $\nu(CH_{2cycle})$; 1672 ν(C=O); 1060 $\nu(C_{Ar}=C_{Ar})$; 967 ν(S—C). ^{1}H NMR (300 MHz, DMSO-d_6, ppm) δ 1.48–1.62 (*m*, 2H, CH_2); 2.24–2.29 (*m*, 1H, CH_{cycle}); 2.52–2.56 (*m*, 1H, CH_{cycle}); 3.80 (s, 3H, CH_3); 7.01 (*dd*, 1H, J = 8.7 and 2.3 Hz, CH_{Ar}); 7.18–7.23 (*m*, 3H, CH_{Ar}); 7.27–7.32 (*m*, 2H, CH_{Ar}); 7.55 (d, 1H, J = 2.2 Hz, CH_{Ar}); 7.76 (d, 1H, J = 8.8 Hz, CH_{Ar}); 12.49 (br s, 1H, NH). ^{13}C NMR (75 MHz, DMSO-d_6, ppm) δ 16.97 ($\underline{C}H_2$); 25.91 ($\underline{C}H_{cycle}$); 26.65 ($\underline{C}H_{cycle}$); 56.09 (CH_3); 105.16 (C_{Ar}); 115.34 (C_{Ar}); 121.34 (C_{Ar}); 126.57 (C_{Ar}–C_{Ar}); 126.85 (C_{Ar}); 128.89 (C_{Ar}–C_{Ar}); 133.25 (C_q); 140.51 (C_{Ar}); 143.09 (C_q); 156.23 ($\underline{C}$–OCH_3); 156.58 (C=O); 171.18 (C=N). $C_{18}H_{16}N_2O_2S$: 324.09 g/mol; LRMS (ESI$^+$): *m/z* ([M + H]$^+$) 325.1 (100%); 181.1 (2.4%).

***(E)-N-(6-Ethoxybenzo[d]thiazol-2-yl)-2-phenylcylopropanecarboxamide* (LQM596) –** Yield: 81%; Aspect: beige crystalline powder; R_F: 0.36; R_T: 1.63 min; Purity: 96%; Mp: 178–179 °C. ART-FTIR (Transmittance/cm^{-1}): 3136 ν(N—H); 3089 $\nu(CH_{2cycle})$; 1689 ν(C=O); 1044 $\nu(C_{Ar}=C_{Ar})$; 969 ν(S—C). ^{1}H NMR (300 MHz, DMSO-d_6, ppm) δ 1.34 (t, 3H, J = 6.9 Hz, CH_3); 1.47–1.62 (*m*, 2H, CH_2); 2.24–2.30 (*m*, 1H, CH_{cycle}); 2.52–2.56 (*m*, 1H, CH_{cycle}); 4.06 (q, 2H, J = 6.9 Hz, OCH_2); 7.00 (*dd*, 1H, J = 8.8 and 2.4 Hz, CH_{Ar}); 7.18–7.23 (*m*, 3H, CH_{Ar}); 7.28–7.32 (*m*, 2H, CH_{Ar}); 7.53 (d, 1H, J = 2.4 Hz, CH_{Ar}); 7.60 (d, 1H, J = 8.7 Hz, CH_{Ar}); 12.46 (br s, 1H, NH). ^{13}C NMR (75 MHz, DMSO-d_6, ppm) δ 15.16 ($\underline{C}H_3$); 16.96 ($\underline{C}H_2$); 25.88 ($\underline{C}H_{cycle}$); 26.64 ($\underline{C}H_{cycle}$); 64.07 ($O\underline{C}H_2$); 105.85 (C_{Ar}); 115.69 (C_{Ar}); 121.57 (C_{Ar}); 126.57 (C_{Ar}–C_{Ar}); 126.84 (C_q); 128.88 (C_{Ar}–C_{Ar}); 133.25 (C_q); 140.51 (C_{Ar}); 143.26 (C_q); 155.81 ($\underline{C}$–OCH_2CH_3); 156.21 (C=O); 171.17 (C=N). $C_{19}H_{18}N_2O_2S$: 338.11 g/mol; LRMS (ESI$^+$): *m/z* ([M + H]$^+$) 339.1 (100%); 195.1 (2.3%).

***(E)-N-(4-Methoxybenzo[d]thiazol-2-yl)-2-phenycyclopropanecarboxamide* (LQM597) –** Yield: 61%; Aspect: brown crystalline powder; R_F: 0.75; R_T: 1.30 min; Purity: 96%; Mp: 193–194 °C. ART-FTIR (Transmittance/cm^{-1}): 3244 ν(N—H); 3034 $\nu(CH_{2cycle})$; 1685 ν(C=O); 1042 $\nu(C_{Ar}=C_{Ar})$; 966 ν(S—C). ^{1}H NMR (300 MHz, DMSO-d_6, ppm) δ 1.50–1.62 (*m*, 2H, CH_2); 2.19–2.24 (*m*, 1H, CH_{cycle}); 2.53–2.57 (*m*, 1H, CH_{cycle}); 3.90 (s, 3H, CH_3); 6.98 (d, 1H, J = 7.0 Hz, CH_{Ar}); 7.19–7.23 (*m*, 3H, CH_{Ar}); 7.24–7.27 (*m*, 2H, CH_{Ar}); 7.51 (d, 1H, J = 7.9 Hz, CH_{Ar}); 12.75 (br s, 1H, NH). ^{13}C NMR (75 MHz, DMSO-d_6, ppm) δ 17.06 ($\underline{C}H_2$); 25.98 ($\underline{C}H_{cycle}$); 26.70 ($\underline{C}H_{cycle}$); 56.23 ($\underline{C}H_3$); 108.13 (C_{Ar}); 113.95 (C_{Ar}); 124.94 (C_{Ar}); 126.59 (C_{Ar}–C_{Ar}); 126.87 (C_{Ar}); 128.90 (C_{Ar}–C_{Ar}); 133.29 (C_{Ar}); 138.84 (C_q); 140.45 (C_q); 152.3 ($\underline{C}$–OCH_3); 156.68 (C=O); 171.25 (C=N). $C_{18}H_{16}N_2O_2S$: 324.09 g/mol; LRMS (ESI$^+$): *m/z* ([M + H]$^+$) 325.1 (100%); 181.1 (2.1%).

***(E)-N-(5,6-Dimethoxybenzo[d]thiazol-2-yl)-2-phenylcyclopropanecarboxamide* (LQM598) –** Yield: 59%; Aspect: brown crystalline powder; R_F: 0.67; R_T: 1.02 min; Purity: 98%; Mp: 184–185 °C. ART-FTIR (Transmittance/cm^{-1}): 3543 ν(N—H); 3128 $\nu(CH_{2cycle})$; 1672 ν(C=O); 1068 $\nu(C_{Ar}=C_{Ar})$; 963 ν(S—C). ^{1}H NMR (300 MHz, DMSO-d_6, ppm) δ 1.47–1.61 (*m*, 2H, CH_2); 2.25–2.31 (*m*, 1H, CH_{cycle}); 2.52–2.54 (*m*, 1H, CH_{cycle}); 3.80 (d, 6H, J = 3.6 Hz, $(CH_3)_2$); 7.18–7.23 (*m*, 3H, CH_{Ar}); 7.28–7.32 (*m*, 3H, CH_{Ar}); 7.53 (s, 1H, CH_{Ar}); 12.44 (br s, 1H, NH). ^{13}C NMR (75 MHz, DMSO-d_6, ppm) δ 16.93 ($\underline{C}H_2$); 25.87 ($\underline{C}H_{cycle}$); 26.59 ($\underline{C}H_{cycle}$); 56.19 ($\underline{C}H_3$); 56.43 ($\underline{C}H_3$); 104.02 (C_{Ar}); 104.19 (C_{Ar}); 123.33 (C_q); 126.55 (C_{Ar}–C_{Ar}); 126.84 (C_{Ar}); 128.89 (C_{Ar}–C_{Ar}); 140.54 (C_q); 142.99 (C_q); 147.38 ($\underline{C}$–OCH_3); 149.34 ($\underline{C}$–OCH_3); 156.74 (C=O); 170.92 (C=N). $C_{19}H_{18}N_2O_3S$: 354.1 g/mol; LRMS (ESI$^+$): *m/z* ([M + H]$^+$) 355.1 (100%).

***(E)-N-(6-Hydroxybenzo[d]thiazol-2-yl)-2-phenylcyclopropanecarboxamide* (LQM599) –** Yield: 98%; Aspect: yellow amorphous powder; R_F: 0.65; R_T: 0.79 min; Purity: 98%; Mp: 161–162 °C. ART-FTIR (Transmittance/cm^{-1}): 3179 δ(O—H); 2965 ν (N—H); 2852 $\nu(CH_{2cycle})$; 1675 ν(C=O); 1196 $\nu(C_{Ar}=C_{Ar})$; 957 ν(S—C). ^{1}H NMR (300 MHz, DMSO-d_6, ppm) δ 3.00–3.28 (*m*, 4H, CH_2 and $(CH_{cycle})_2$); 6.17 (s, 1H, OH); 7.21 (*dd*, 1H, J = 8.7 and 2.4 Hz, CH_{Ar}); 7.63–7.67 (*m*, 3H, CH_{Ar}); 7.69 (s, 1H, CH_{Ar}); 7.72–7.77 (*m*, 2H, CH_{Ar}); 7.83 (d, 1H, J = 8.8 Hz, CH_{Ar}); 9.95 (br s, 1H, NH). ^{13}C NMR (75 MHz, DMSO-d_6, ppm) δ 28.51 ($\underline{C}H_{cycle}$); 30.08 ($\underline{C}H_{cycle}$); 62.60 ($\underline{C}H_2$); 106.97 (C_{Ar}); 115.69 (C_{Ar}); 122.06 (C_{Ar}); 125.83 (C_{Ar}–C_{Ar}); 127.71 (C_{Ar}–C_{Ar}); 129.14 (C_{Ar}); 133.37 (C_q); 141.68 (C_q); 142.04 (C_q); 153.61 ($\underline{C}$–OH); 154.85 (C=O); 174.99 (C=N). $C_{17}H_{14}N_2O_2S$: 310.08 g/mol; LRMS (ESI$^+$): *m/z* ([M + H]$^+$) 311.1 (100%).

***(E)-N-(4-Hydroxybenzo[d]thiazol-2-yl)-2-phenylcyclopropanecarboxamide* (LQM600) –** Yield: 88%; Aspect: yellow amorphous powder; R_F: 0.61; R_T: 0.92 min; Purity: 96%; Mp: 243–244 °C. ART-FTIR (Transmittance/cm^{-1}): 3429 δ(O—H); 3029 ν (N—H); 2968 $\nu(CH_{2cycle})$; 1710 ν(C=O); 1087 $\nu(C_{Ar}=C_{Ar})$; 937 ν(S—C). ^{1}H NMR (300 MHz, DMSO-d_6, ppm) δ 2.57–2.87 (*m*, 4H, CH_2 and

(CH_{cycle})$_2$); 5.87 (s, 1H, OH); 6.78 (*dd*, 1H, J = 7.8 and 0.7 Hz, CH_{Ar}); 7.09 (t, 1H, J = 7.9 Hz, CH_{Ar}); 7.21–7.27 (*m*, 3H, CH_{Ar}); 7.31–7.37 (*m*, 3H, CH_{Ar}); 9.71 (br s, 1H, NH). ^{13}C NMR (75 MHz, DMSO-d_6, ppm) δ 28.51 ($\underline{C}H_{cycle}$); 30.13 ($\underline{C}H_{cycle}$); 62.46 ($\underline{C}H_2$); 111.86 (C_{Ar}); 112.26 (C_{Ar}); 125.44 (C_{Ar}); 126.04 (C_{Ar}–C_{Ar}); 127.76 (C_{Ar}); 129.10 (C_{Ar}–C_{Ar}); 133.58 (C_q); 137.86 (C_q); 141.87 (C_q); 150.53 ($\underline{C}$–OH); 153.97 (C=O); 175.11 (C=N). $C_{17}H_{14}N_2O_2S$: 310.08 g/mol; LRMS (ESI$^+$): *m/z* ([M + H]$^+$) 311.1 (100%).

***(E)-N-(5,6-Dihydroxybenzo[d]thiazol-2-yl)-2-phenylcyclopropanecarboxamide* (LQM601) –** Yield: 99%; Aspect: yellow amorphous powder; R_F: 0.63; R_T: 0.66 min; Purity: 96%; Mp: 288–289 °C. ART-FTIR (Transmittance/cm^{-1}): 3187 δ(O—H); 1671 ν(C=O); 1058 ν(C_{Ar}=C_{Ar}); 923 ν(S—C). ^{1}H NMR (300 MHz, DMSO-d_6, ppm) δ 2.54–2.84 (*m*, 4H, CH_2 and (CH_{cycle})$_2$); 5.74–5.79 (*m*, 2H, (OH)$_2$); 6.93 (s, 1H, CH_{Ar}); 7.21–7.25 (*m*, 4H, CH_{Ar}); 7.30–7.35 (*m*, 3H, (CH_{Ar})$_2$ and NH). ^{13}C NMR (75 MHz, DMSO-d_6, ppm) δ 28.50 ($\underline{C}H_{cycle}$); 30.07 ($\underline{C}H_{cycle}$); 62.52 ($\underline{C}H_2$); 106.79 (C_{Ar}); 107.30 (C_{Ar}); 122.42 (C_{Ar}); 125.85 (C_{Ar}–C_{Ar}); 127.69 (C_q); 129.11 (C_{Ar}–C_{Ar}); 141.95 (C_q); 142.14 ($\underline{C}$–OH); 144.53 ($\underline{C}$–OH); 145.98 (C_q); 154.07 (C=O); 174.62 (C=N). $C_{17}H_{14}N_2O_3S$: 326.07 g/mol; LRMS (ESI$^+$): *m/z* ([M + H]$^+$) 327.1 (100%).

***(E)-N-(6-Nitrobenzo[d]thiazol-2-yl)-2-phenylcyclopropanecarboxamide* (LQM602)** – Yield: 52%; Aspect: yellow amorphous powder; R_F: 0.61; R_T: 1.48 min; Purity: 95%; Mp: 240–241 °C. ART-FTIR (Transmittance/cm^{-1}): 3350 ν(N—H); 3068 ν(CH_2); 1690 ν(C=O); 1047 ν(C_{Ar}=C_{Ar}); 940 ν(S—C). ^{1}H NMR (300 MHz, DMSO-d_6, ppm) δ 1.55–1.67 (*m*, 2H, CH_2); 2.29–2.35 (*m*, 1H, CH_{cycle}); 2.55–2.62 (*m*, 1H, CH_{cycle}); 7.20–7.23 (*m*, 3H, CH_{Ar}); 7.28–7.33 (*m*, 2H, CH_{Ar}); 7.87 (d, 1H, J = 8.9 Hz, CH_{Ar}); 8.26 (*dd*, 1H, J = 8.8 and 2.2 Hz, CH_{Ar}); 9.03 (d, 1H, J = 2.2 Hz, CH_{Ar}); 13.03 (br s, 1H, NH). ^{13}C NMR (75 MHz, DMSO-d_6, ppm) δ 17.41 ($\underline{C}H_2$); 26.05 ($\underline{C}H_{cycle}$); 27.36 ($\underline{C}H_{cycle}$); 119.46 (C_{Ar}); 121.03 (C_{Ar}); 122.22 (C_{Ar}); 126.63 (C_{Ar}–C_{Ar}); 126.96 (C_{Ar}); 128.90 (C_{Ar}–C_{Ar}); 132.72 (C_q); 140.25 (C_q); 143.42 (C–NO_2); 153.97 (C_q); 163.75 (C=N); 172.19 (C=O). $C_{17}H_{13}N_3O_3S$: 339.07 g/mol; LRMS (ESI$^+$): *m/z* ([M + H]$^+$) 340.1 (100%); 196.0 (1.6%); 145.2 (3.1%).

4.13.7. Coupling of 4-(p-tolyl)-2-aminothiazole to cinnamic acids and trans-phenylcyclopropanecarboxylic acid

The synthesis of derivatives **(LQM603–606)** followed the same procedures used for the non-halogenated 2-aminobenzo[*d*]thiazole derivatives with the corresponding carboxylic acids. However, the purification was different: after completion of the reaction, the product was washed with saturated $NaHCO_3$ solution (3 × 10 mL) and distilled H_2O (3 × 25 mL), followed by recrystallization in ethanol:distilled water (2:1), yielding the purified compound [70].

***(E)-N-(4-(p-Toluyl)thiazol-2-yl)cinnamamide* (LQM603) –** Yield: 71%; Aspect: orange amorphous powder; R_F: 0.48; R_T: 2.07 min; Purity: 95%; Mp: 154–155 °C. ART-FTIR (Transmittance/cm^{-1}): 3025 ν(N—H); 1696 ν(C=O); 1675 ν(C=C_{ene}); 1084 ν(C_{Ar}=C_{Ar}); 913 ν(S—C). ^{1}H NMR (300 MHz, DMSO-d_6, ppm) δ 2.32 (s, 3H, CH_3); 6.95 (d, 1H, J = 15.8 Hz, CH_{ene}); 7.24 (d, 2H, J = 8.0 Hz, CH_{Ar}); 7.45–7.49 (*m*, 3H, CH_{Ar}); 7.58 (s, 1H, CH_{thio}); 7.64 (*dd*, 2H, J = 7.5 and 1.5 Hz, CH_{Ar}); 7.74 (d, 1H, J = 15.8 Hz, CH_{ene}); 7.80 (d, 2H, J = 8.1 Hz, CH_{Ar}); 12.49 (br s, 1H, NH). ^{13}C NMR (75 MHz, DMSO-d_6, ppm) δ 21.77 (CH_3); 108.63 (C_{thio}); 120.55 (C_{ene}); 126.61 (C_{Ar}); 128.98 (C_{Ar}–C_{Ar}); 129.17 (C_{Ar}); 129.88 (C_{Ar}); 130.08 (C_{Ar}–C_{Ar}); 130.29 (C_q); 131.33 ($\underline{C}$–CH_3); 132.62 (C_{Ar}); 135.27 (C_q); 138.10 (C_{Ar}); 143.17 (C_{ene}); 150.17 (C_q); 158.86 (C=N); 164.36 (C=O). $C_{19}H_{16}N_2OS$: 320.1 g/mol; LRMS (ESI$^+$): *m/z* ([M + H]$^+$) 321.1 (100%); 191.1 (1.3%).

***(E)-3-(4-(tert-Butyl)phenyl)-N-(4-(p-toluyl)thiazol-2-yl)acrylamide* (LQM604) –** Yield: 70%; Aspect: orange amorphous powder; R_F: 0.58; R_T: 1.29 min; Purity: 95%; Mp: 167–168 °C. ART-FTIR (Transmittance/cm^{-1}): 2962 ν(N—H); 1708 ν(C=O); 1674 ν(C=C_{ene}); 1085 ν(C_{Ar}=C_{Ar}); 979 ν(S—C). ^{1}H NMR (300 MHz, DMSO-d_6) δ 1.29 (s, 12H, CH_3 and (CH_3)$_3$); 6.90 (d, 1H, J = 15.8 Hz, CH_{ene}); 7.24 (d, 2H, J = 8.0 Hz, CH_{Ar}); 7.47–7.50 (*m*, 2H, CH_{Ar}); 7.68–7.73 (*m*, 3H, CH_{Ar} and CH_{thio}); 7.78–7.81 (*m*, 2H, CH_{Ar}); 8.05 (d, 1H, J = 15.8 Hz, CH_{ene}); 12.44 (br s, 1H, NH). ^{13}C NMR (75 MHz, DMSO-d_6, ppm) δ 21.26 (CH_3); 31.35 (($\underline{C}H_3$)$_3$); 35.02 (C_{tert}); 110.21 (C_{thio}); 119.46 (C_{ene}); 124.69 (C_{Ar}); 126.15 (C_{Ar}–C_{Ar}); 126.37 (C_{Ar}); 128.31 (C_{Ar}); 128.48 (C_{Ar}–C_{Ar}); 129.77 (C_q); 131.97 ($\underline{C}$–CH_3); 137.56 (C_{Ar}); 144.24 (C_q); 149.63 (C_{Ar}); 153.53 (C_{ene}); 153.74 (C_q); 158.39 (C=N); 163.98 (C=O). $C_{23}H_{24}N_2OS$: 376.16 g/mol; LRMS (ESI$^+$): *m/z* ([M + H]$^+$) 377.2 (100%).

***(E)-3-(4-Chlorophenyl)-N-(4-(p-toluyl)thiazol-2-yl)acrylamide* (LQM605) –** Yield: 75%; Aspect: brown amorphous powder; R_F: 0.43; R_T: 1.41 min; Purity: 99%; Mp: 194–195 °C. ART-FTIR (Transmittance/cm^{-1}): 3263 ν(N—H); 1708 ν(C=O); 1691 ν(C=C_{ene}); 1087 ν(C_{Ar}=C_{Ar}); 979 ν(S—C). ^{1}H NMR (300 MHz, DMSO-d_6, ppm) δ 2.32 (s, 3H, CH_3); 7.24 (d, 1H, J = 8.0 Hz, CH_{ene}); 7.52–7.61 (*m*, 3H, CH_{Ar}); 7.65–7.70 (*m*, 4H, CH_{Ar}); 7.75 (s, 1H, CH_{thio}); 7.80 (d, 2H, J = 8.0 Hz, CH_{ene} and CH_{Ar}); 12.53 (br s, 1H, NH). ^{13}C NMR (75 MHz, DMSO-d_6, ppm) δ 21.49 ($\underline{C}H_3$); 108.23 (C_{thio}); 120.53 (C_{ene}); 120.75 (C_{Ar}); 125.02 (C_{Ar}); 126.09 (C_{Ar}); 127.86 (C_{Ar}); 128.26 (C_{Ar}); 129.38 (C_{Ar}); 129.64 (C_{Ar}); 130.15 (C_{Ar}); 130.41 (C_q); 132.07 ($\underline{C}$–CH_3); 133.67 (C_q); 135.16 ($\underline{C}$—Cl); 142.99 (C_{ene}); 158.29 (C_q); 163.65 ($\underline{C}$=O); 167.89 ($\underline{C}$=N). $C_{19}H_{15}ClN_2OS$: 354.06 g/mol; LRMS (ESI$^+$): *m/z* ([M + H]$^+$) 355.1 (100%).

***(E)-2-Phenyl-N-(4-(p-toluyl)thiazol-2-yl)cyclepropanecarboxamide* (LQM606) –** Yield: 65%; Aspect: brown powder; R_F: 0.95; R_T: 2.35 min; Purity: 98%; Mp: 195–196 °C. ART-FTIR (Transmittance/cm^{-1}): 3293 ν(N—H); 3066 ν(CH2); 1664 ν(C=O); 1082 ν(C_{Ar}=C_{Ar}); 957 ν(S—C). ^{1}H NMR (300 MHz, DMSO-d_6, ppm) δ 1.45–1.59 (*m*, 2H, CH_2); 2.23–2.29 (*m*, 1H, CH_{cycle}); 2.31 (s, 3H, CH_3); 2.51–2.53 (*m*, 1H, CH_{cycle}); 7.18–7.23 (*m*, 5H, CH_{Ar}); 7.28–7.32 (*m*, 2H, CH_{Ar}); 7.52 (s, 1H, CH_{thio}); 7.77 (d, 2H, J = 8.2 Hz, CH_{Ar}); 12.53 (br s, 1H, NH). ^{13}C NMR (75 MHz, DMSO-d_6, ppm) δ 16.81 ($\underline{C}H_2$); 21.25 (CH_3); 25.67 ($\underline{C}H_{cycle}$); 26.42 ($\underline{C}H_{cycle}$); 107.59 (C_{thio}); 126.06 (C_{Ar}); 126.58 (C_{Ar}–C_{Ar}); 126.81 (C_{Ar}–C_{Ar}); 128.88 (C_{Ar}–C_{Ar}); 129.74 (C_{Ar}–C_{Ar}); 132.10 (C_q); 137.52 ($\underline{C}$–CH_3); 140.58 (C_q); 149.32 (C_q); 158.21 (C=N); 170.73 (C=O). $C_{20}H_{18}N_2OS$: 334.11 g/mol; LRMS (ESI$^+$): *m/z* ([M + H]$^+$) 335.2 (100%).

4.14. In silico binding mode studies

Molecular dynamics (MD) simulations were performed to evaluate the dynamic behavior and conformational stability of the protein–ligand complexes formed with compounds 84 and 92. The previously prepared structures of these complexes were subjected to the MD protocol using the Desmond module, available in the Maestro® suite v.2023.1 (academic license from D. E. Shaw Research, https://www.deshawresearch.com/resources.html). Initially, the complexes were preprocessed using the Protein Preparation Wizard module, and the protonation states of the residues were adjusted to a physiological pH of 7.4 through the PROPKA module, with a convergence threshold of 0.3 Å for heavy atoms. The system was solvated with the TIP3P water model, placed inside an orthorhombic simulation box, with the addition of anions and cations as needed for neutralization. Next, energy minimization was performed using the OPLS_2005 force field. The system was then equilibrated under NPT conditions at 300 K and 1 bar. Production simulations were run for 100 ns, with trajectory recording every 100 ps, totaling 1000 frames per system. Throughout the simulation, root mean square deviation (RMSD) values of the protein and ligand, root mean square fluctuations (RMSF), and interaction fractions between the compounds and protein residues were monitored. These analyses were carried out using integrated tools in Maestro®, enabling the evaluation of the structural stability of the complexes under conditions simulating physiological environments. Interaction diagrams were also generated to visualize the persistence and types of intermolecular interactions over the simulation, such as hydrogen bonds, hydrophobic interactions, ionic interactions, π–π, and π–cation interactions. The stability of these interactions was considered indicative of the affinity and complementarity between the ligands and the binding site. Finally, binding free energy calculations were conducted using the Prime/MM-GBSA module,

employing the 10 most stable frames from the trajectories to determine the average binding energy of compounds **LQM560** and **LQM601** with the target protein according to the following equation:

$\Delta G_{bind} = \Delta E_{MM} + \Delta G_{solv} - \Delta G_{SA}$

In which, $\Delta E_{MM} = E_{Complex} - (E_{Protein} + E_{Ligand})$; $\Delta G_{Solv} = \Delta G_{SolvComplex} - (\Delta G_{SolvProtein} + \Delta G_{SolvLig})$; then, $\Delta G_{SA} = \Delta G_{SAComplex} - (\Delta G_{SAProtein} + \Delta G_{SALigand})$. Additionally, the terms *Solv* = solvation energy; *SA* = surface area associated energy; *E* = energy minimized states of the protein-ligand complex.

CRediT authorship contribution statement

Wadja Feitosa dos Santos Silva: Writing – review & editing, Writing – original draft, Methodology. **Shweta Choudhary:** Writing – original draft, Methodology, Investigation. **Isadora Hart Cavalcante:** Writing – original draft, Methodology, Investigation. **Tanuj Handa:** Writing – original draft, Methodology, Investigation. **Leandro Rocha Silva:** Writing – original draft, Methodology, Investigation. **Manuele Figueiredo da Silva:** Writing – original draft, Methodology, Investigation. **Mirely Vitória Farias da Silva:** Writing – original draft, Software, Methodology, Investigation. **Rayane Martins Botelho:** Writing – original draft, Methodology, Investigation. **Peng Zhan:** Writing – review & editing, Writing – original draft. **Franciso Jaime Bezerra Mendonça-Júnior:** Writing – original draft, Supervision, Funding acquisition. **João Xavier Araújo-Júnior:** Writing – original draft, Supervision. **Tanja Schirmeister:** Supervision, Methodology, Investigation. **Alexandre Urban Borbely:** Writing – original draft, Supervision, Methodology, Investigation, Conceptualization. **Shailly Tomar:** Writing – review & editing, Writing – original draft, Supervision, Software, Methodology, Investigation, Conceptualization. **Edeildo Ferreira da Silva-Júnior:** Writing – review & editing, Writing – original draft, Supervision, Project administration, Methodology, Investigation, Funding acquisition, Conceptualization.

Funding

This research received financial support from a partnership involving the Deutschen Akademischen Austauschdienst (DAAD) and the Brazilian National Council for Scientific and Technological Development (CNPq), registered under the code: 290318/2017-3 (protocol number: 8963482463546497), *via* the public call number 04/2017. Also, Silva-Júnior, E.F. and Mendonça-Júnior, F.J.B. thank for their CNPq grants (numbers: #306323/2022-2 and #316996/2023-8, respectively). Moreover, this study was funded in part by Paraíba State Research Foundation – FAPESQ-PB, through PRONEX program, grant number: #030/2023. The authors thank to the Fundação de Amparo à Pesquisa do Estado de Alagoas (FAPEAL), grant numbers E:60030.0000000161/2022; E:60030.0000001720/2022, Coordination for the Improvement of Higher Education Personnel (CAPES, finance code 001), and Funding Authority for Studies and Projects (FINEP).

Declaration of competing interest

The authors declare that they have no known competing financial interests or personal relationships that could have appeared to influence the work reported in this paper.

Acknowledgements

The corresponding author, Edeildo F. da Silva-Júnior, sincerely thanks all members of the "ArbeitsKreis (AK)-Schirmeister" for welcoming me to their research team at the Johannes Gutenberg University (JGU) of Mainz, Germany. They were all extremely kind to me during my doctoral period abroad. I am deeply grateful to Prof. Tanja Schirmeister, who taught me so much during this time. I also thank the other members of the group, especially Marvin Schwickert, Sascha Jung, Kevin Schwickert, Sabine Mëhrlein, and Hannah Maus, for their collaboration and the valuable knowledge they shared with me. Additionally, the authors thank to the financial support agencies. Also, the authors thank the Shawn Research Group (https://www.deshawresearch.com/index.html) for making the Desmond software academically available.

Appendix A. Supplementary data

Supplementary data to this article can be found online at https://doi.org/10.1016/j.rechem.2026.103414.

Data availability

No data was used for the research described in the article.

References

[1] C.E. Scatularo, O.A. Ballesteros, C. Saldarriaga, I. Mendoza, F. Wyss, A.S. Liprandi, A. Munera, M.C. Liendro, A. Baranchuk, Zika & heart: A systematic review, Trends Cardiovasc. Med. 32 (2022) 52–58, https://doi.org/10.1016/j.tcm.2020.11.003.
[2] V.P. Chavda, A. Kumar, R. Banerjee, N. Das, Ayurvedic and other herbal remedies for dengue: an update, Clin. Complement. Med. Pharmacol. 2 (2022) 100024, https://doi.org/10.1016/j.ccmp.2022.100024.
[3] M.S. Mustafa, V. Rasotgi, S. Jain, V. Gupta, Discovery of fifth serotype of dengue virus (DENV-5): a new public health dilemma in dengue control, Med. J. Armed Forces India 71 (2015) 67–70, https://doi.org/10.1016/j.mjafi.2014.09.011.
[4] O. Saeed, A. Asif, Dengue virus disease; the origins, in: Dengue Virus Dis., Elsevier, 2020, pp. 9–16, https://doi.org/10.1016/B978-0-12-818270-3.00002-3.
[5] B.H. Kok, H.T. Lim, C.P. Lim, N.S. Lai, C.Y. Leow, C.H. Leow, Dengue virus infection – a review of pathogenesis, vaccines, diagnosis and therapy, Virus Res. 324 (2023) 199018, https://doi.org/10.1016/j.virusres.2022.199018.
[6] Pan American Health Organization, Dengue Epidemiological Situation in the Region of the Americas - Epidemiological Week 27, 2025, 2025.
[7] Q. Jing, M. Wang, Dengue epidemiology, Glob. Heal. J. 3 (2019) 37–45, https://doi.org/10.1016/j.glohj.2019.06.002.
[8] E. Vyhmeister, G. Provan, B. Doyle, B. Bourke, G.G. Castane, L. Reyes-Bozo, Comparison of time series and mechanistic models of vector-borne diseases, Spat. Spatiotemporal. Epidemiol. 41 (2022) 100478, https://doi.org/10.1016/j.sste.2022.100478.
[9] D.P. Tchouassi, S.B. Agha, J. Villinger, R. Sang, B. Torto, The distinctive bionomics of *Aedes aegypti* populations in Africa, Curr. Opin. Insect Sci. 54 (2022) 100986, https://doi.org/10.1016/j.cois.2022.100986.
[10] PAHO, Zika: analysis by country, Pan Am. Heal. Organ. (2025). https://www.paho.org/en/arbo-portal/zika-data-and-analysis/zika-analysis-country (accessed August 2, 2025).
[11] R.V. da Cunha, K.S. Trinta, Chikungunya virus: clinical aspects and treatment - a review, Mem. Inst. Oswaldo Cruz 112 (2017) 523–531, https://doi.org/10.1590/0074-02760170044.
[12] PAHO, Chikungunya: analysis by country, Pan Am. Heal. Organ. (2025). https://www.paho.org/en/arbo-portal/chikungunya-data-and-analysis/chikungunya-analysis-country (accessed August 12, 2025).
[13] C. De'Sean Mears, K. Tabata, T. Ariizumi, B.M. Hang'ombe, Y. Qiu, H. Harima, M. Kajihara, W.W. Hall, M. Sasaki, H. Sawa, Y. Orba, Mosquito-borne alphaviruses in Zambia: isolation and characterization of Eilat and Sindbis viruses, Virus Res. 358 (2025) 199604, https://doi.org/10.1016/j.virusres.2025.199604.
[14] S. Kurkela, Sindbis Virus (Togaviridae), in: Encycl. Virol., Elsevier, 2021, pp. 837–842, https://doi.org/10.1016/B978-0-12-814515-9.00048-5.
[15] S. Adouchief, T. Smura, J. Sane, O. Vapalahti, S. Kurkela, Sindbis virus as a human pathogen-epidemiology, clinical picture and pathogenesis, Rev. Med. Virol. 26 (2016) 221–241, https://doi.org/10.1002/rmv.1876.
[16] S. Harding, S. Sewgobind, N. Johnson, JMM Profile: Sindbis virus, a cause of febrile illness and arthralgia, J. Med. Microbiol. 72 (2023), https://doi.org/10.1099/jmm.0.001674.
[17] J. Neyts, Challenges in combating arboviral infections, Nat. Commun. 15 (2024) 3350, https://doi.org/10.1038/s41467-024-47161-3.
[18] M.W. Starolis, O. Perez, E.A. Powell, Clinical features and laboratory diagnosis of emerging arthropod-transmitted viruses, J. Clin. Virol. 132 (2020) 104651, https://doi.org/10.1016/j.jcv.2020.104651.
[19] A. Piantadosi, S. Kanjilal, Diagnostic approach for Arboviral infections in the United States, J. Clin. Microbiol. 58 (2020), https://doi.org/10.1128/JCM.01926-19.
[20] J. Zephyr, D.N. Rao, C. Johnson, A.M. Shaqra, E.A. Nalivaika, A. Jordan, N. Kurt Yilmaz, A. Ali, C.A. Schiffer, Allosteric quinoxaline-based inhibitors of the flavivirus NS2B/NS3 protease, Bioorg. Chem. 131 (2023) 106269, https://doi.org/10.1016/j.bioorg.2022.106269.
[21] S. Voss, C. Nitsche, Inhibitors of the Zika virus protease NS2B-NS3, Bioorg. Med. Chem. Lett. 30 (2020) 126965, https://doi.org/10.1016/j.bmcl.2020.126965.

[22] E.F. Silva-Júnior, J.X. Araújo-Júnior, Peptide derivatives as inhibitors of NS2B-NS3 protease from Dengue, West Nile, and Zika flaviviruses, Bioorg. Med. Chem. 27 (2019) 3963–3978, https://doi.org/10.1016/j.bmc.2019.07.038.
[23] B.D. Lindenbach, C.M. Rice, Molecular biology of flaviviruses, in: M.J. Roossinck (Ed.), Adv. Virus Res. Viruses Clim. Chang., 59th ed., Elsevier B.V, Amsterdam, 2003, pp. 23–61, https://doi.org/10.1016/S0065-3527(03)59002-9.
[24] B. Millies, F. von Hammerstein, A. Gellert, S. Hammerschmidt, F. Barthels, U. Göppel, M. Immerheiser, F. Elgner, N. Jung, M. Basic, C. Kersten, W. Kiefer, J. Bodem, E. Hildt, M. Windbergs, U.A. Hellmich, T. Schirmeister, Proline-based allosteric inhibitors of Zika and Dengue virus NS2B/NS3 proteases, J. Med. Chem. 62 (2019) 11359–11382, https://doi.org/10.1021/acs.jmedchem.9b01697.
[25] I.J. dos S. Nascimento, P.F.S. da Santos-Júnior, T.M. de Aquino, J.X. de Araújo-Júnior, E.F. da Silva-Júnior, Insights on dengue and Zika NS5 RNA-dependent RNA polymerase (RdRp) inhibitors, Eur. J. Med. Chem. 224 (2021) 113698, https://doi.org/10.1016/j.ejmech.2021.113698.
[26] M. de M. Silva, T.S. Macedo, H.M.P. Teixeira, D.R.M. Moreira, M.B.P. Soares, A. L. Ana, V. de L. Serafim, F.J.B. Mendonça-Júnior, M. do Carmo A. de Lima, R.O. de Moura, E.F. da Silva-Júnior, J.X. de Araújo-Júnior, M.D. Maria, E. de O. O. Nascimento, T.M.S. Maciel, T.M. de Aquino, I.M. Figueiredo, J.C.C. Santos, Correlation between DNA/HSA-interactions and antimalarial activity of acridine derivatives: proposing a possible mechanism of action, J. Photochem. Photobiol. B Biol. 189 (2018) 165–175, https://doi.org/10.1016/j.jphotobiol.2018.10.016.
[27] É.E.S. da Rodrigues, H. Maus, S.J. Hammerschmidt, J.X. Araújo-Júnior, T. Schirmeister, E.F. da Silva-Júnior, A new furin-based peptidomimetic as an inhibitor of NSB2-NS3 protease from Zika virus (ZIKV), in: Proc. 7th Int. Electron. Conf. Med. Chem., MDPI, Basel, Switzerland, 2021, p. 11431, https://doi.org/10.3390/ECMC2021-11431.
[28] É.E. da S. Rodrigues, H. Maus, S.J. Hammerschmidt, A. Ruggieri, E.C. Santos, Ê. J. Bassi, L. Anderson, P.G.V. Aquino, J.X. Araújo-Júnior, F. Wei, X. Liu, P. Zhan, T. Schirmeister, E.F. Silva-Júnior, The medicinal chemistry of Zika virus, in: S. I. Ahmad (Ed.), Hum. Viruses Dis. Treat. Vaccines New Insights, 1st ed., Springer International Publishing, Cham, 2021, pp. 233–295, https://doi.org/10.1007/978-3-030-71165-8_13.
[29] H. Wu, S. Bock, M. Snitko, T. Berger, T. Weidner, S. Holloway, M. Kanitz, W. E. Diederich, H. Steuber, C. Walter, D. Hofmann, B. Weißbrich, R. Spannaus, E. G. Acosta, R. Bartenschlager, B. Engels, T. Schirmeister, J. Bodem, Novel dengue virus NS2B/NS3 protease inhibitors, Antimicrob. Agents Chemother. 59 (2015) 1100–1109, https://doi.org/10.1128/AAC.03543-14.
[30] H. Maus, F. Barthels, S.J. Hammerschmidt, K. Kopp, B. Millies, A. Gellert, A. Ruggieri, T. Schirmeister, SAR of novel benzothiazoles targeting an allosteric pocket of DENV and ZIKV NS2B/NS3 proteases, Bioorg. Med. Chem. 47 (2021) 116392, https://doi.org/10.1016/j.bmc.2021.116392.
[31] G.G. Vilela, W.F. dos S. Silva, V. de M. Batista, L.R. Silva, H. Maus, S. J. Hammerschmidt, C.A.C.B. Costa, O.F. da S. Moura, J.D. de Freitas, G.L. Coelho, J. de A. Brandão, L. Anderson, Ê.J. Bassi, J. Xavier de Araújo-Júnior, T. Schirmeister, E.F. da Silva-Júnior, Fragment-based design of α-cyanoacrylates and α-cyanoacrylamides targeting Dengue and Zika NS2B/NS3 proteases, New J. Chem. (2022), https://doi.org/10.1039/D2NJ01983C.
[32] P. Kumar, D. Kumar, R. Giri, Targeting the nsp2 cysteine protease of chikungunya virus using FDA approved library and selected cysteine protease inhibitors, Pathogens 8 (2019) 128, https://doi.org/10.3390/pathogens8030128.
[33] B. Muthu Ramalingam, H.J. Oh, J.D. Sears, C.-H. Chen, A. Vala, S. Liu, K.M. Talbot, M.A. Hossain, P.J. Brown, S. Houliston, J. Garcia Perez, F. Li, M.G. Amare, P. Halfmann, J.L. Smith, A.J. Hirsch, C.H. Arrowsmith, L. Halabelian, A. Vargason, R.M. Couñago, J.J. Arnold, C.E. Cameron, N.J. Moorman, M.T. Heise, T.M. Willson, Enantioselective chemical probe for chikungunya nsp2 helicase with antialphaviral activity, ACS Infect. Dis. (2025), https://doi.org/10.1021/acsinfecdis.5c00351.
[34] M. Mastalipour, I. Gering, M.A. Coronado, J.E.H. González, D. Willbold, R. J. Eberle, Novel peptide inhibitor for the chikungunya virus nsP2 protease: identification and characterization, Curr. Res. Microb. Sci. 8 (2025) 100376, https://doi.org/10.1016/j.crmicr.2025.100376.
[35] M. Mastalipour, M.A. Coronado, J.E.H. González, D. Willbold, R.J. Eberle, Inhibition of Chikungunya Virus nsP2 Protease in Vitro by Pantinin-1 Isolated from Scorpion Venom, 2025, https://doi.org/10.1101/2025.06.29.662183.
[36] J.P. Oliveira Lima, C.H. Alexandre Roberto, M. Nunes da Rocha, V. Moreira de Oliveira, R.M. Freire, R. Santos-Oliveira, E.S. Marinho, P. de Lima Neto, P. B. Almeida Fechine, Phenol and chromone compounds for in silico inhibition of nsP2 and nsP3 of chikungunya virus, Pharm. Sci. Adv. (2025) 100084, https://doi.org/10.1016/j.pscia.2025.100084.
[37] P.K. Das, A. Merits, A. Lulla, Functional cross-talk between distant domains of chikungunya virus non-structural protein 2 is decisive for its RNA-modulating activity, J. Biol. Chem. 289 (2014) 5635–5653, https://doi.org/10.1074/jbc.M113.503433.
[38] S. Wang, S. Mahalingam, A. Merits, Alphavirus nsP2: a multifunctional regulator of viral replication and promising target for anti-alphavirus therapies, Rev. Med. Virol. 35 (2025), https://doi.org/10.1002/rmv.70030.
[39] S. Kumar, A. Kumar, P. Mamidi, A. Tiwari, S. Kumar, A. Mayavannan, S. Mudulli, A.K. Singh, B.B. Subudhi, S. Chattopadhyay, Chikungunya virus nsP1 interacts directly with nsP2 and modulates its ATPase activity, Sci. Rep. 8 (2018) 1–14, https://doi.org/10.1038/s41598-018-19295-0.
[40] C.D. Meshram, T. Lukash, A.T. Phillips, I. Akhrymuk, E.I. Frolova, I. Frolov, Lack of nsP2-specific nuclear functions attenuates chikungunya virus replication both in vitro and in vivo, Virology 534 (2019) 14–24, https://doi.org/10.1016/j.virol.2019.05.016.
[41] I. Frolov, N. Garmashova, S. Atasheva, E.I. Frolova, Random insertion mutagenesis of Sindbis virus nonstructural protein 2 and selection of variants incapable of downregulating cellular transcription, J. Virol. 83 (2009) 9031–9044, https://doi.org/10.1128/JVI.00850-09.
[42] G.F.S. Passos, M.G.M. Gomes, T.M. de Aquino, J.X. de Araújo-Júnior, S.J.M. de Souza, J.P.M. Cavalcante, E.C. dos Santos, È.J. Bassi, E.F. da Silva-Júnior, Computer-aided design, synthesis, and antiviral evaluation of novel acrylamides as potential inhibitors of E3-E2-E1 glycoproteins complex from Chikungunya virus, Pharmaceuticals 13 (2020) 141, https://doi.org/10.3390/ph13070141.
[43] B. Millies, F. von Hammerstein, F. Barthels, U. Goppel, U.A. Hellmich, T. Schirmeister, New Nanomolar Inhibitors of NS2B/NS3-Protease of Zika- and Dengue-Virus, in: 20, JungChemikerForum Frühjahrssymposium, Konstanz, 2018.
[44] B.G. de Souza, S. Choudhary, G.G. Vilela, G.F.S. Passos, C.A.C.B. Costa, J.D. de Freitas, G.L. Coelho, J. de A. Brandão, L. Anderson, È.J. Bassi, J.X. de Araújo-Júnior, S. Tomar, E.F. da Silva-Júnior, Design, synthesis, antiviral evaluation, and In silico studies of acrylamides targeting nsP2 from Chikungunya virus, Eur. J. Med. Chem. 258 (2023) 115572, https://doi.org/10.1016/j.ejmech.2023.115572.
[45] W.H. Perkin, XXVIII.—On some hydrocarbons obtained from the homologues of cinnamic acid; and on anethol and its homologues, J. Chem. Soc. 32 (1877) 660–674, https://doi.org/10.1039/JS8773200660.
[46] J.F.J. Dippy, R.M. Evans, The nature of the catalyst in the Perkin condensation, J. Org. Chem. 15 (1950) 451–456, https://doi.org/10.1021/jo01149a001.
[47] G. Trapani, M. Franco, A. Latrofa, A. Reho, G. Liso, Synthesis, in vitro and in vivo cytotoxicity, and prediction of the intestinal absorption of substituted 2-ethoxycarbonyl-imidazo[2,1-b]benzothiazoles, Eur. J. Pharm. Sci. 14 (2001) 209–216, https://doi.org/10.1016/S0928-0987(01)00173-7.
[48] D. Babinski, O. Soltani, D.E. Frantz, Stereoselective synthesis of acetoacetate-derived enol triflates, Org. Lett. 10 (2008) 2901–2904, https://doi.org/10.1021/ol8010002.
[49] D.E. Frantz, D.G. Weaver, J.P. Carey, M.H. Kress, U.H. Dolling, Practical synthesis of aryl triflates under aqueous conditions, Org. Lett. 4 (2002) 4717–4718, https://doi.org/10.1021/ol027154z.
[50] F. Olimpieri, A. Volonterio, M. Zanda, Three-component, one-pot sequential synthesis of 1,3-disubstituted 5-arylhydantoins, Synlett 2008 (2008) 3016–3020, https://doi.org/10.1055/s-0028-1087352.
[51] T. Chew, R. Noyce, S.E. Collins, M.H. Hancock, K.L. Mossman, Characterization of the interferon regulatory factor 3-mediated antiviral response in a cell line deficient for IFN production, Mol. Immunol. 46 (2009) 393–399, https://doi.org/10.1016/j.molimm.2008.10.010.
[52] N. Kumar, R. Santhoshkumar, M.M. Venkataswamy, Chikungunya virus infection in human microglial C20 cells induces mitochondria-mediated apoptosis, Front. Cell. Infect. Microbiol. 14 (2024) 1–11, https://doi.org/10.3389/fcimb.2024.1380736.
[53] M.P. Papa, L.M. Meuren, S.V.A. Coelho, C.G. de O. Lucas, Y.M. Mustafá, F. Lemos Matassoli, P.P. Silveira, P.S. Frost, P. Pezzuto, M.R. Ribeiro, A. Tanuri, M. L. Nogueira, L. Campanati, M.T. Bozza, H.A. Paula Neto, P.M. Pimentel-Coelho, C. P. Figueiredo, R.S. de Aguiar, L.B. de Arruda, Zika virus infects, activates, and crosses brain microvascular endothelial cells, without barrier disruption, Front. Microbiol. 8 (2017) 1–17, https://doi.org/10.3389/fmicb.2017.02557.
[54] L.A. Moser, B.T. Boylan, F.R. Moreira, L.J. Myers, E.L. Svenson, N.B. Fedorova, B. E. Pickett, K.A. Bernard, Growth and adaptation of Zika virus in mammalian and mosquito cells, PLoS Negl. Trop. Dis. 12 (2018) e0006880, https://doi.org/10.1371/journal.pntd.0006880.
[55] C. Steuer, K.H. Heinonen, L. Kattner, C.D. Klein, Optimization of assay conditions fo r dengue virus protease: effect of various polyols and nonionic detergents, J. Biomol. Screen. 14 (2009) 1102–1108, https://doi.org/10.1177/1087057109344115.
[56] S. Ludewig, M. Kossner, M. Schiller, K. Baumann, T. Schirmeister, Enzyme kinetics and hit validation in fluorimetric protease assays, Curr. Top. Med. Chem. 10 (2010) 368–382, https://doi.org/10.2174/156802610790725498.
[57] G.P. Maier, C.M. Bernt, A. Butler, Catechol oxidation: considerations in the design of wet adhesive materials, Biomater. Sci. 6 (2018) 332–339, https://doi.org/10.1039/C7BM00884H.
[58] H. Singh, R. Mudgal, M. Narwal, R. Kaur, V.A. Singh, A. Malik, M. Chaudhary, S. Tomar, Chikungunya virus inhibition by peptidomimetic inhibitors targeting virus-specific cysteine protease, Biochimie 149 (2018) 51–61, https://doi.org/10.1016/j.biochi.2018.04.004.
[59] R. Mudgal, C. Bharadwaj, A. Dubey, S. Choudhary, P. Nagarajan, M. Aggarwal, Y. Ratra, S. Basak, S. Tomar, Selective estrogen receptor modulators limit alphavirus infection by targeting the viral capping enzyme nsP1, Antimicrob. Agents Chemother. 66 (2022), https://doi.org/10.1128/aac.01943-21.
[60] T. Mosmann, Rapid colorimetric assay for cellular growth and survival: application to proliferation and cytotoxicity assays, J. Immunol. Methods 65 (1983) 55–63, https://doi.org/10.1016/0022-1759(83)90303-4.
[61] W. Azevedo de Brito, M. Gomes Dantas, F. Andrade Nogueira, E. Ferreira da Silva-Júnior, J. Xavier de Araújo-Júnior, T. Aquino, Ê. Adélia Nogueira Ribeiro, L. da Silva Solon, C. Soares Aragão, A. Barreto Gomes, Development and validation of HPLC-DAD and UHPLC-DAD methods for the simultaneous determination of guanylhydrazone derivatives employing a factorial design, Molecules 22 (2017) 1394, https://doi.org/10.3390/molecules22091394.
[62] K. Yakoub, S. Jung, C. Sattler, H. Damerow, J. Weber, A. Kretzschmann, A. S. Cankaya, M. Piel, F. Rösch, A.S. Haugaard, B. Frølund, T. Schirmeister, H. Lüddens, Structure–function evaluation of imidazopyridine derivatives selective for δ-subunit-containing γ-aminobutyric acid type A (GABA A) receptors, J. Med. Chem. 61 (2018) 1951–1968, https://doi.org/10.1021/acs.jmedchem.7b01484.
[63] M.V.O.D.O. Cardoso, L.R.P. De Siqueira, E.B. Da Silva, L.B. Costa, M.Z. Hernandes, M.M. Rabello, V.R.A. Pereira, M.C.A.B. Castro, P.V. Bernhardt, A.C.L. Leite, M. Veríssimo, D.O. Cardoso, L. Rabelo, P. De Siqueira, E. Barbosa, L. Bandeira,

M. Zaldini, D. Rodrigo, M. Carolina, A. Brelaz, P.V. Bernhardt, A. Cristina, L. Leite, M.V.O.D.O. Cardoso, L.R.P. De Siqueira, E.B. Da Silva, L.B. Costa, M.Z. Hernandes, M.M. Rabello, V.R.A. Pereira, M.C.A.B. Castro, P.V. Bernhardt, A.C.L. Leite, R. S. Ferreira, L.F. Da Cruz, D.R. Magalhães Moreira, V.R.A. Pereira, M.C.A.B. De Castro, P.V. Bernhardt, A.C.L. Leite, 2-Pyridyl thiazoles as novel anti- *Trypanosoma cruzi* agents: structural design, synthesis and pharmacological evaluation, Eur. J. Med. Chem. 86 (2014) 48–59, https://doi.org/10.1016/j.ejmech.2014.08.012.

[64] D.R. Magalhaes-Moreira, A.D.T. De Oliveira, P.A. Teixeira De Moraes Gomes, C. A. De Simone, F.S. Villela, R.S. Ferreira, A.C. Da Silva, T.A.R. Dos Santos, M.C. A. Brelaz De Castro, V.R.A. Pereira, A.C.L. Leite, D.R. Magalhaes Moreira, A.D. T. De Oliveira, P.A. Teixeira De Moraes Gomes, C.A. De Simone, F.S. Villela, R. S. Ferreira, A.C. Da Silva, T.A.R. Dos Santos, M.C.A. Brelaz De Castro, V.R. A. Pereira, A.C.L. Leite, Conformational restriction of aryl thiosemicarbazones produces potent and selective anti-*Trypanosoma cruzi* compounds which induce apoptotic parasite death, Eur. J. Med. Chem. 75 (2014) 467–478, https://doi.org/10.1016/j.ejmech.2014.02.001.

[65] E.P. Martin Badertscher, Philippe Bühlmann, Structure Determination of Organic Compounds, Springer Berlin Heidelberg, Berlin, Heidelberg, 2009, https://doi.org/10.1007/978-3-540-93810-1.

[66] Neil E. Jacobsen, NMR Data Interpretation Explained, 2016.

[67] E.F. Silva-Júnior, E.P.S. Silva, P.H.B. França, J.P.N. Silva, E.O. Barreto, E.B. Silva, R.S. Ferreira, C.C. Gatto, D.R.M. Moreira, J.L. Siqueira-Neto, F.J.B. Mendonça-Júnior, M.C.A. Lima, J.H. Bortoluzzi, M.T. Scotti, L. Scotti, M.R. Meneghetti, T. M. Aquino, J.X. Araújo-Júnior, Design, synthesis, molecular docking and biological evaluation of thiophen-2-iminothiazolidine derivatives for use against *Trypanosoma cruzi*, Bioorg. Med. Chem. 24 (2016) 4228–4240, https://doi.org/10.1016/j.bmc.2016.07.013.

[68] Y. Luo, Y. Zhu, K. Ran, Z. Liu, N. Wang, Q. Feng, J. Zeng, L. Zhang, B. He, T. Ye, S. Zhu, X. Qiu, L. Yu, Synthesis and biological evaluation of N-(4-phenylthiazol-2-yl)cinnamamide derivatives as novel potential anti-tumor agents, Medchemcomm 6 (2015) 1036–1042, https://doi.org/10.1039/C4MD00573B.

[69] P. Jimonet, F. Audiau, M. Barreau, J.-C. Blanchard, A. Boireau, Y. Bour, M.-A. Coléno, A. Doble, G. Doerflinger, C. Do Huu, M.-H. Donat, J.M. Duchesne, P. Ganil, C. Guérémy, E. Honoré, B. Just, R. Kerphirique, S. Gontier, P. Hubert, P. M. Laduron, J. Le Blevec, M. Meunier, J.-M. Miquet, C. Nemecek, M. Pasquet, O. Piot, J. Pratt, J. Rataud, M. Reibaud, J.-M. Stutzmann, S. Mignani, Riluzole Series. Synthesis and in vivo "antiglutamate" activity of 6-substituted-2-benzothiazolamines and 3-substituted-2-imino-benzothiazolines, J. Med. Chem. 42 (1999) 2828–2843, https://doi.org/10.1021/jm980202u.

[70] W.-T. Zhang, J.-L. Ruan, P.-F. Wu, F.-C. Jiang, L. Zhang, W. Fang, X.-L. Chen, Y. Wang, B.-S. Cao, G.-Y. Chen, Y.-J. Zhu, J. Gu, J.-G. Chen, Design, synthesis, and cytoprotective effect of 2-aminothiazole analogues as potent poly(ADP-ribose) polymerase-1 inhibitors, J. Med. Chem. 52 (2009) 718–725, https://doi.org/10.1021/jm800902t.